8-2020

Tumor-derived exosomes drive immunosuppressive macrophages in a pre-metastatic niche through NF-Kβ dependent glycolytic metabolic reprogramming.

Samantha M. Morrissey
University of Louisville

TUMOR-DERIVED EXOSOMES DRIVE IMMUNOSUPPRESSIVE MACROPHAGES IN A PRE-METASTATIC NICHE THROUGH NF-KB DEPENDENT GLYCOLYTIC METABOLIC REPROGRAMMING

By

Samantha M. Morrissey
B.A., University of Pennsylvania, 2013

A Dissertation
Submitted to the Faculty of the
School of Medicine of the University of Louisville
In Partial Fulfillment of the Requirements
for the Degree of

Doctor of Philosophy in Microbiology and Immunology

Department of Microbiology and Immunology
University of Louisville
Louisville, KY

August 2020

TUMOR-DERIVED EXOSOMES DRIVE IMMUNOSUPPRESSIVE MACROPHAGES IN A PRE-METASTATIC NICHE THROUGH NF-KB DEPENDENT GLYCOLYTIC METABOLIC REPROGRAMMING

By

Samantha M. Morrissey
B.A., University of Pennsylvania, 2013

A Dissertation Approved On

June 16, 2020

By the Following Dissertation Committee

_____

Jun Yan, M.D., Ph.D.

_____

Esma Yolcu, Ph.D.

_____

Haribabu Bodduluri, Ph.D.

_____

Haval Shirwan, Ph.D.

_____

Huang-ge Zhang, Ph.D.

DEDICATION

“All your dreams can come true if you have the courage to pursue them.”- Walt Disney

ACKNOWLEDGMENTS

I want to thank my mentor, Dr. Jun Yan, for helping me grow into an independent, passionate scientist. Thank you for all the opportunities you have afforded me over the past four years. I consider it a great privilege and honor to have worked in your lab.

I want to thank my thesis committee, who have provided invaluable advice throughout my doctoral work. I could not have asked for a better and wiser group of minds.

I want to thank my Mom and Dad, two of the most caring and selfless people I know. Your unwavering faith in my ability to succeed has gotten me to where I am today. Thank you for all that you have sacrificed to make my dreams come true.

I want to thank my friends and family, who have supported me throughout every step of my education. Thank you keeping me sane through all the ups and downs of scientific exploration.

I want to thank all of the members of the Yan lab that I have had the privilege to work with and learn from. You made the Yan lab such a pleasant and enjoyable place, no matter the hour. I look forward to the opportunity of seeing many of you again if my travels take me to China.

ABSTRACT

TUMOR-DERIVED EXOSOMES DRIVE IMMUNOSUPPRESSIVE MACROPHAGES IN A PRE-METASTATIC NICHE THROUGH NF-KB DEPENDENT GLYCOLYTIC METABOLIC REPROGRAMMING

Samantha M. Morrissey

June 16, 2020

The formation of a pre-metastatic niche is a fundamental requirement for primary tumor metastasis. One of the defining characteristics of a pre-metastatic niche is infiltration of immunosuppressive macrophages. However, how these macrophages acquire their immunosuppressive phenotype remains largely unexplored. Here, we demonstrate that tumor-derived exosomes (TDE) polarize macrophages towards an immunosuppressive phenotype characterized by increased PD-L1 expression through NF-kB-dependent metabolic reprogramming in mice and humans. While NF-κB has previously been shown to act as a direct transcription factor for PD-L1, we report a novel mechanism where TDE-induced NF-κB activation drives PD-L1 expression by augmenting the glycolytic capacity of macrophages through two separate pathways. First, NF-κB increases glucose uptake into macrophages via a HIF-1α/GLUT-1-dependent mechanism. Secondly, elevated NOS2-dependent nitric oxide inhibits mitochondrial oxidative phosphorylation resulting in an increased conversion of pyruvate to lactate. Lactate then feeds back on NF-κB further increasing PD-L1 expression. Analysis of metastasis

negative draining lymph nodes of non-small cell lung cancer patients revealed that macrophage PD-L1 expression positively correlates with expression levels of GLUT-1 and exosomal release genes YKT6 and TSG101 from primary tumors. Collectively, our study provides a novel mechanism by which macrophages within a pre-metastatic niche acquire their immunosuppressive phenotype and identifies an important link between exosomes, metabolism, and metastasis.

TABLE OF CONTENTS

LIST OF TABLES

LIST OF FIGURES

1. OVERVIEW

1.1 Overview of Innate and Adaptive Immunity

The human immune system has developed as a result of an amalgamation of traits over hundreds of millions of years from both vertebrate and non-vertebrate animals[1, 2]. These traits consist of a variety of different cellular responses that protect the host from invading pathogens. Over time, this conglomerate has been stratified into the three main branches of immunological defense: physical barriers, innate immunity, and adaptive immunity[3]. Each facet of the human immune system has distinctive properties that make up its respective defense mechanism.

The first and largest barrier to infection is the skin[1]. It along with various mucus membranes constitute the physical barriers separating host from pathogen. Keratinized skin cells from a tough outer layer that can only be breached by physical damage resulting from wounds, burns, and surgical procedures. The mucus membranes that line the respiratory, gastrointestinal, and urogenital tracts are designed with specialized fluid layers consisting of glycoproteins, proteoglycans, and enzymes that trap and expel pathogens from the body[1]. Should the various physical barriers become breached, the second line of defense, the innate immune system is mobilized into action.

Once a pathogen, like bacteria, has surpassed the external defenses and entered the body, it is first recognized by a variety of effector mechanisms known as the innate immune system[1]. The hallmark sign of activation of the innate immune system is

inflammation. Inflammation is characterized by warmth, pain, redness, and swelling[1]. Mechanistically, inflammation results from activation of the resident effector cells called macrophages. Macrophages are the mature form of circulating monocytes that localize to particular areas of the body that are most susceptible to invading pathogens. Deposition of small proteins, called complement, on the surface of invading pathogens mark and attract macrophages to promote clearance of the pathogen through a process called phagocytosis or "cellular eating"[4]. The surface of macrophages is lined with specialized receptors, toll-like-receptors, (TLRs) that are specifically designed to recognize different types of microbial products. Activation of macrophages through TLR signaling results in transcription of a variety of inflammatory cytokines that amplify the immune response. These mediators include interleukin-6 (IL-6), interleukin-1β (IL-1β), and tumor-necrosis factor-α (TNFα) and often are responsible for driving the clinical symptoms associated with infection: fever, increased C-reactive protein, and neutrophilia[1]. However, while this response is rapid and robust, it is often not enough to limit the course of infection and a secondary, more specialized, system is needed to ultimately clear the pathogen.

The final arm of the human immune system is the adaptive immune system and it is responsible for immunological memory, the premise upon which vaccination is built[1]. The two main mediators of adaptive immunity are B cells and T cells[3]. Any molecule or macromolecule that is capable of being bound by a T-cell receptor (TCR) or B-cell receptor (BCR) is known as an antigen. The particular part of antigen that is recognized by the TCR or BCR is an epitope. T cell and B cell receptors consist of two separate parts, the constant region and the variable region. The variable region contains the site that binds specific pathogen associated epitopes. The ability for TCRs and BCRs to bind to the limitless number of pathogen-associated epitopes is conferred by a process

known as somatic recombination. Within this process, numerous combinations of gene segments are rearranged allowing for a pool of cells with different receptor specificities, called clones. Elimination of clones that are specific for host cell epitopes is achieved through a process known as clonal selection[5]. T-cell clones that recognize antigen complexed with the self-glycoprotein called major histocompatibility complex (MHC) are positively selected for in the thymus. $CD8^+$ T cells recognize antigen presented via MHC Class I while $CD4^+$ T cells recognize MHC Class II. Following positive selection, clones that recognize self-peptides in the context of MHC I and MHC II are eliminated via apoptosis or programmed cell death. Errors in this process are considered to be one potential mechanism by which autoimmune disease develops[6]. B cells go through a similar process as T cells for selection. However, upon pathogen infection, they have an additional mechanism for diversification, somatic hypermutation. Introduction of nucleotide substitutions in the heavy and light chains of B cell receptors produces antibodies that bind pathogens more tightly allowing for more specified pathogen clearance. A certain subset of these specific antibody producing cells will go on to become plasma cells.

In addition to phagocytosis and production of cytokines, another role for macrophages in innate immunity is presentation of antigen to T cells thus classifying them as antigen-presenting cells (APCs)[1]. Macrophages and other APCs, such dendritic cells, load antigens into their MHCs at the site of infection and travel to the local secondary lymphoid structure, often the draining lymph node, where they present antigen to the resident T cells. A small number of T cells with TCRs specific to the loaded antigen are activated and clonal expansion of these cells results in in pool of effector T cells. Activated cytotoxic $CD8^+$ T cells hone to the site of infection via particular cytokine gradients and kill the invading pathogen. Conversely $CD4^+$ T cells, or

helper T cells, in the lymph node interact via a surface receptor called CD40-ligand (CD40L) with antigen specific B cells, releasing the necessary cytokines (IL-4, IL-5, IL-6) for B cell proliferation and differentiation[1].

Overall, the process of innate and adaptive immune activation takes roughly two weeks which is the normal duration of the common cold[7]. However, reinfection with the same pathogen in the future will result in a robust reactivation of specific memory T and B cells from the primary infection allowing for rapid identification and clearance of the pathogen[8]. It is this mechanism of long-lasting immunity that has allowed for successful eradication of diseases like smallpox from the population[9].

1.2 Immune landscape of cancer

The immune system has developed over hundreds of millions of years to fight foreign invading pathogens like fungi, bacteria, and viruses[2]. However, not all disease causing pathogens are extrinsic to the host. One disease in particular that has developed synonymously within the host is cancer. Unlike foreign pathogens that look very different from self in the eyes of the immune system, cancerous cells are native cells that proliferate uncontrollably as a result of genetic mutation causing disruption to normal physiology and ultimately disease[1]. Because cancer has co-evolved with the immune system, it has effectively developed a variety of mechanisms that mitigate the majority of attacks mounted by both the innate and adaptive immune systems.

The interplay between the immune system and the development of cancerous neoplasms is called immunosurveillance[10]. It was first put forth by Dr. Paul Ehrlich in 1909, that the immune system must be responsible for suppressing growth of carcinomas or else they would occur at a far greater rate. Technological advancements over past two decades in particular have allowed for further investigation into this

dynamic and complex relationship. From these studies, the “Three E Paradigm” of cancer immunoediting was born[10]. This hypothesis is based on the notion of three phases of tumor progression with regards to immunologic surveillance- elimination, equilibrium, and escape.

The first phase of immunosurveillance, elimination, harkens back to Ehrlich’s original concept of immune mediated oncological suppression. The human body is exposed to hundreds of carcinogens on almost a daily basis that are capable of causing genetic mutation[11]. However, due to the process of elimination, the majority of mutated cells are cleared prior to tumor formation[12]. In the elimination phase, both innate and adaptive immune cells are mobilized to identify potentially cancer cells. These “danger signals” which can be readily recognized by the innate immune system include increased production of uric acid, and generation of proinflammatory responses from expression of TLR ligands and heat shock proteins[12]. Studies using mice deficient in the recombination activating gene (RAG) which is responsible for TCR and BCR diversification, saw dramatic increases in tumor burden as compared to original wild type hosts pointing towards a regulatory role for B cells and T cells in cancer progression[12].

While engagement of the host immune system with tumor cells has been shown to limit the emergence of fully developed neoplasms, it is also responsible for shaping the tumor’s immunological phenotype. Namely, within the elimination phase, tumor cells that are susceptible to immunoregulation are selected against, while those that are resistant to immunological elimination are positively selected for. This selection pressure is what brings the tumor cells to the second phase of immunoediting-equilibrium[10, 12]. While a significant portion of tumor cells are culled out by the immune system, those that remain pose a significant threat due to their inherent resistance to immune targeting. These cells often result from genetic instability within the primary tumor allowing for stochastic generation of clones that display increased resilience in the face of

immunological selection pressure[1]. Clinically, the idea of cancer equilibrium becomes apparent in case of transmission of cancer from donor to recipient in organ transplant[13]. Grossly, the organ appears cancer-free, however, following transmission into an immunocompromised recipient, the dormant cancer cells that were held in check by the immunocompetent donor overpower the fledgling immune system of transplant recipient leading to the last stage of immunoediting- escape[14].

Tumor escape is defined as uncontrolled proliferation and progression unrestrained by immune pressure[10]. During the escape phase tumors become clinically apparent. It is thought that both genetic and epigenetic modifications of the tumor cells are responsible for conferring mechanisms that circumvent both the innate and adaptive branches of the immune system. Therefore, the focus in the field over the past 30 years or so has been to elucidate the types of resistance mechanisms the tumor cells generate in order to develop new therapeutics against them[15]. This pursuit has birthed an entire new arm of immunological research called immunotherapy[16].

1.3 Immunotherapy and the forefront of the cancer crusade

The concept of immunotherapy, or using the immune system as a therapeutic against cancer, was first put forth by Dr. William B. Coley beginning in 1891[17]. He believed that administration of bacterial toxins into patients with non-resectable tumors would galvanize the immune system into orchestrating increased surveillance and elimination. During forty years of practice, Coley treated over 1000 bone and soft-tissue sarcoma patients with his toxins achieving varying successful outcomes[18]. Unfortunately, widespread criticism in the field combined with the advent of radiotherapy and chemotherapy caused the use of Coley's Toxins to fall out of favor. However, Coley had

started the burgeoning field of immunotherapy that a century later would be the forefront of the immunological crusade against cancer.

Up until recently the three main pillars of cancer treatment were surgery, radiation, and chemotherapy[19]. However, major advances in the field of immunotherapy, particularly with immune checkpoint inhibitors and adoptive cell therapies, are changing the norm. In 2018, James Allison and Tasuku Honjo were awarded the Nobel Prize in Physiology or Medicine for their discovery and use of immune checkpoint molecules, cytotoxic T-lymphocyte associated protein-4 (CTLA-4) and Programmed Death-1 (PD-1), respectively for cancer immunotherapy[20]. These proteins each expressed on the surface of T cells are mechanisms to control errant T cell responses following infection/activation. However, cancer cells coopted this system to protect themselves, causing blunting of the infiltrating cytotoxic T cells responses in tumors[21]. The development and utilization of blocking antibodies that interfere with this process have demonstrated remarkable efficacy in the clinic[22]. To date, anti-CTLA-4 and anti-PD-1 monoclonal antibody treatments have been FDA approved as first line treatments for melanoma and non-small lung cancer in addition to receiving approval as adjunct therapies for numerous types of cancer including kidney, liver, bladder, esophageal, head and neck squamous cell, colorectal and uterine cancer[23]. Immunotherapy has brought the 5-year survival rate for melanomas patients up to an astonishing 98%[24]. However, that figure dramatically drops to only 23% for metastatic melanoma. Therefore, gaining a better understanding of the mechanisms of primary tumor metastasis and immunotherapy resistance is of paramount importance to increase overall survival rates of patients with metastatic cancer.

1.4 Scope of Dissertation Study

The work herein deals with two mechanisms of primary tumor metastasis, pre-metastatic niche formation and immunometabolism. The first set of studies, described in Chapter 2, detail the role small nanoparticles called exosomes released from the primary tumor play in priming a distant tissue for tumor metastasis. Specifically, this work provides insight into exosomes' influence on the phenotype and functionality of macrophages within a pre-metastatic niche. The second set of studies, presented in Chapter 3, focuses on the mechanism by which exosomes polarize tissue resident macrophages towards the immunosuppressive phenotype detailed in Chapter 2. These studies reveal a novel connection between exosomes, glycolytic metabolism, and lactate that drives increased expression of the immune checkpoint molecule, programmed death ligand- 1 (PD-L1) on macrophages in a pre-metastatic niche. Overall, this study aims to better characterize mechanisms of metastasis in effort to identify novel targets to help increase the efficacy of immunotherapies and improve outcomes for patients with metastatic cancer.

2. TUMOR DERIVED EXOSOMES DRIVE PD-L1 EXPRESSION IN TISSUE RESIDENT MACROPHAGES

2.1 INTRODUCTION

2.1.1 Non-small cell lung cancer

Lung cancer, particularly non-small cell lung cancer (NSCLC), is the most common form of cancer worldwide in men and the third most common in women [25]. NSCLC is a group of cancers that include the adenocarcinoma, squamous cell, and large cell subtypes[26]. Adenocarcinoma lesions are often found on the outer lobes of the lung and are comprised of mutated mucus secreting cells. Squamous cell carcinoma lesions, as their name implies, start in the squamous epithelial cells that line the lung bronchi. These tumors are often found more medially in the lung. Both adenocarcinoma and squamous cell carcinoma are associated with a history of smoking[27]. Large cell carcinoma is less common than the other two and can be found in any part of the lung. It often grows faster and larger than the other two subtypes making it more difficult to treat.

Because the lung is a highly perfused organ, it is one of the most common sites of metastasis for a variety of primary cancer types including bladder, breast, colon, and kidney among others[28]. The symptoms of metastatic cancer to the lung are similar to that of primary lung cancer and include persistent cough, hemoptysis, dyspnea, and sudden weight loss[27]. Metastatic lung cancer occurs in 20% to 54% of all solid tumor cancer patients depending on the original tumor type [29]. Despite advances in current therapies,

metastasis remains a major challenge with poor five-year survival outcomes for a majority of patients [30]. The FDA has approved the use of pembrolizumab (anti-PD-1) in patients with metastatic NSCLC patients whose primary tumors had ≥50% expression of PD-L1 in addition to patients that have Stage III non-resectable NSCLC[31]. Combination treatment with immunotherapy agents like Pembrolizumab have increased the median progression free survival rates for patients with later stages cancers to approximately 8.8 months, almost a 50% improvement over sole treatment with platinum-based chemotherapy[32]. However, only roughly 20% of patients achieve a sustained response to the therapy[33]. Therefore, it is critical to delineate which factors are driving immunotherapy resistance.

2.1.2 Pre-metastatic niche formation

The theory behind primary tumor metastasis began in 1889 with Stephen Paget's Seed and Soil hypothesis which likens the ability of tumors to metastasize to seeds falling on congenial soil[34]. He believed that metastasis was not a random phenomenon solely dependent on the anatomical structure of the vascular system and that certain factors had to prime the secondary tissue to permit tumor cells to grow. The process through with a secondary tissue undergoes remodeling for the purpose of preparing for tumor cell implantation is pre-metastatic niche formation. Accumulating evidence suggests that cancer metastasis is a temporal and spatial process that starts with the formation of a favorable local environment within a distant tissue[35].

One of the first events that is necessary for tumor metastasis is the epithelial to mesenchymal transition (EMT) of primary tumor cells[36]. Within this process, tumor cells downregulate surface epithelial markers and upregulate mesenchymal markers that confer a more stem-like, migratory phenotype. Following this transformation, the next

rate-limiting step of metastasis is intravasation of the tumor cells into circulation. Intravasation is a low-fidelity process with only 0.01% of intravasating tumor cells successfully forming metastatic lesions[36]. Once through the vessel wall and into the bloodstream, it is thought that circulating tumor cells associate with platelets as an additive layer of protection from immune surveillance[37]. For the circulating tumor cells that survive the inhospitable environment of circulation, successful extravasation, modulation of the endothelial barrier and transendothelial migration are necessary for tissue invasion and colonization[38]. These processes are thought to be mediated by a variety of intrinsic tumor associated factors as well as extrinsic factors secreted by endothelial cells, platelets, and other infiltrating immune subtypes.

While primary tumor cells are undergoing EMT, intravasation and extravasation, a series of molecular and cellular changes are happening in parallel to secondary tissues to create a pre-metastatic niche. There are six enabling characteristics of a pre-metastatic niche that prepare and permit circulating tumor cells to engraft and grow. These characteristics include: inflammation, angiogenesis/vascular permeability, lymphangiogenesis, organotropism, reprogramming, and immunosuppression[35].

2.1.3 Immunosuppressive cell types within a pre-metastatic niche

One of the defining characteristics of a primary tumor and its subsequent metastatic niche is immunosuppression. Elimination of localized immune responses is necessary and critical for tumor growth. There are a variety of factors that contribute to the immunosuppressive phenotype including decreased oxygen saturation, accumulation of immune dampening metabolites, and infiltration of regulatory immune cells[39]. Under normal physiological conditions, regulatory immune cells exist to limit and control immune cell activation during host/pathogen responses in order to prevent the

development of autoimmunity following resolution of the infection[40]. However, primary tumors hijack this system and release chemokines and cytokines as a defensive strategy to cause abnormal accumulation of immunosuppressive cells within the tissue. The four main classes of regulatory/suppressive immune cells are myeloid derived suppressor cells (MDSCs), $T_{regulatory}$ cells (T_{regs}), tumor associated neutrophils (TAN) and tumor associated macrophages (TAMs)[35, 41]. These classes of cells have been found around the invasive margin of highly fibrotic lesions like pancreatic ductal adenocarcinoma tumors and are speculated to prevent infiltration of cytotoxic lymphocytes resulting in what is called an infiltrated-excluded tumor immune microenvironment (TIME)[42]. In other types of TIME, such as the infiltrated-inflamed, the immune regulatory cells along with the cytotoxic lymphocytes highly penetrate into the core of the tumor[42]. Increased expression of immune checkpoint molecules, PD-1 on lymphocytes and PD-L1 on tumor cells, often still construes an immunosuppressive phenotype despite the marked influx of immune cells.

While attention has been paid to the other types of immune regulatory cells within the pre-metastatic niche, the most notable and well characterized is the TAM. TAMs are considered to be a subset of M2-like polarized macrophages that can be identified by increases in Arginase-1 expression, IL-10 production, and mitochondria dependent oxidative phosphorylation[43]. Functionally, they are poor antigen presenting cells, have decreased phagocytic capabilities, and produce lower levels of nitric oxide[43]. Multiple murine models of cancer have shown the presence of TAMs, particularly yolk sac derived TAMs, increase the proliferative capacity of tumor cells[42]. Conversely, depletion of macrophages in both breast and colon cancer models significantly decreased the number of metastatic nodules indicating a strong role for macrophages in promoting tumor metastasis [44, 45]. Interestingly, in terms of immune checkpoint blockade therapy, it

has been shown that PD-L1 expression on antigen presenting cells, like macrophages, is necessary for successful treatment with both anti-PD-1 and anti-PD-L1 monoclonal antibodies[46]. These results suggest that immunosuppressive macrophages might play a greater role in restraining T-cell activation than previously considered. Therefore, it is important to determine what factors drive PD-L1 expression on macrophages in the context of cancer.

2.1.4 Exosomes

Exosomes are small nanoparticles, 30-150 nm in diameter, that are released via exocytosis from the surface of both normal and tumor cells alike. Specifically, exosomes arise from the inward budding of vesicles in the late endosome to form a multivesicular body (MVB)[47]. Fusion of the MVB with the plasma membrane releases the exosomes extracellularly. Numerous proteins are involved in this process including RAB27, YKT6, and TSG101[47]. The cargo packaged into the exosomes prior to their release is very heterogenous including a wide assortment of RNA, DNA, proteins, microRNAs, metabolites, and other biologically active molecules derived from their parent cell. Interestingly, following release, exosomes often hone to particular highly vascularized tissues like the lung and liver based on their surface integrin profiles and the integrin profiles of their parental cell of origin [48]. This organotrospism, or affinity of certain substances for particular tissues or organs, is believed to contribute to exosomes overall pro-tumorigenic phenotype[35].

Given their abundance and propensity to be found in bodily fluids, exosomes are being targeted clinically as potential biomarkers for cancer [49, 50]. To date, exosomes have been isolated from a variety of bodily fluids including bile, blood, breast milk, urine, cerebrospinal fluid, and saliva[51]. The total concentration of exosomes isolated from the

plasma of head and neck squamous cell carcinoma patients positively correlates with active disease status and clinical stage suggesting a pathogenic nature [52]. There has been an increasing focus on how TDE contribute to the complex intracellular communications within the tumor microenvironment[53] . It has been shown that TDE and their associated miRNAs are capable of modulating tumor progression via secretion of pro-inflammatory cytokines, promotion of angiogenesis, TLR-3 driven neutrophil infiltration, and recruitment of myeloid-derived suppressor cells (MDSCs) [54, 55, 56, 57]. Similarly, exosomal factors including miRNAs have been associated with promoting pre-metastatic niche formation in various cancers [41]. In ovarian cancer, which has one of highest rates of tumor metastasis within the abdominal cavity, TDE have been shown to induce pre-metastatic niche formation through IL-6 and Fas ligand mediated mechanisms of tumor cell escape[50]. Conversely, depletion of exosome secretion via genetic manipulation or pharmacological inhibition has been shown to decrease metastatic burden and increase overall survival in a variety of tumor-bearing mice[58, 59, 60]. Given the close association with tumor proliferation and growth, it is important to further elucidate the pro-tumoral characteristics of exosomes, particularly with regard to immune checkpoint therapy.

2.1.5. Exosomes and PD-L1

Accumulating evidence suggests that exosomes are a significant source of extra-tumoral PD-L1 and may be one mechanism contributing to PD-1 Ab treatment resistance. Exosomes acquire their PD-L1 expression from endocytosis of parent cell surface PD-L1 [60 61 62]. Utilization of this characteristic has allowed for the isolation of exosomes from the supernatants of various tumor cell line cultures and human plasma through binding of surface PD-L1 to immobilized biotinylated PD-1 antibodies [62, 63, 64].

Different tumor cell lines or types of cancer have fluctuating amounts of PD-L1 packaged into secreted exosomes. Metastatic melanoma cell lines were found to secrete exosomes with higher PD-L1 expression compared to primary cell lines [62]. Exosomes extracted from the plasma of stage IV metastatic melanoma patients revealed increased exosomal PD-L1 expression compared to healthy donors [62]. Furthermore, increased exosomal PD-L1 expression level has been found to positively correlate with increasing tumor size, higher disease activity, and overall clinical stage in a variety of cancers[58, 62, 65, 66]. Interestingly, soluble PD-L1 in the plasma of head and neck squamous cell carcinoma (HNSCC) patients did not correlate with clinical pathological parameters, further suggesting exosomal PD-L1 imparts a specific phenotype in cancer [65].

As a secreted component from primary tumors, exosomes have been credited to possess a wide assortment of pre-metastatic niche enhancing characteristics [41]. However, thus far, the majority of these pro-tumoral characteristics have been found to be mediated by intracellular mRNA, miRNA, and protein cargo contained within the exosomes [41, 67]. Conversely, exosomal PD-L1 which is localized to the surface has been associated with tumor progression in a variety of cancers including melanoma, breast cancer, HNSCC, and glioblastoma [58, 62, 65, 66]. Specifically, patients with metastatic melanoma had significantly higher levels of exosomal PD-L1 than healthy donors [62]. In breast cancer, PD-L1/exosome co-localization increased with advancing tumor grade from Grade I/I-II to Grade II-III/III [58]. PD-L1 expression on exosomes correlated with glioblastoma tumor volumes and with clinical stage and level of nodal involvement in HNSCC [65, 66]. In addition, exosome PD-L1 expression negatively correlated with postoperative survival time in pancreatic ductal adenocarcinoma patients [68].

The high level of correlation between exosomal PD-L1 expression and advanced tumor staging suggests that PD-L1 on exosomes is responsible in some capacity for

augmenting tumor growth and metastasis. Previous studies in a variety of mouse models have shown that exogenous administration of tumor-derived exosomes increases metastatic potential and overall tumor burden of primary tumors [69, 70]. However, only recently has this tumor promoting phenotype specifically been linked to exosomal PD-L1 expression[71]. Treatment of PD-L1KO breast, prostate, and colorectal cell lines with PD-L1 expressing exosomes restored tumor growth capabilities in a dose dependent manner [58 60]. Multiple studies have shown that in *vitro* co-culture of PD-L1$^{+/high}$ exosomes with T cells results in inhibition of T cell activation [65 66 58 61].

Labeling of exosomes from a variety of tumor models revealed that mainly phagocytic cells, over lymphocytes, uptake exosomes in their local microenvironment. CD14^{+} monocytes from glioblastoma patients compared to healthy controls demonstrated increased uptake of labeled exosomes from glioblastoma stem cells [72]. Additionally, CD14^{+} cells resected directly from glioblastoma multiform patient samples showed increased PD-L1 expression compared to these in the peripheral blood from healthy donors. Similarly, mice receiving a single injection of labeled E0771 breast cancer derived exosomes showed the highest exosome signal in F4/80^{+}CD11b^{+} macrophages in the lungs [70]. However, the exact mechanisms behind the increased PD-L1 expression and whether it contributes to pre-metastatic niche formation remains to be elucidated and therefore is the topic of this dissertation.

2.1.6 Summary and Findings

In this study, we investigated whether tumor-derived exosomes (TDE) contribute to macrophage mediated pre-metastatic niche formation and if so, by what signaling mechanism do TDE induce this polarization towards an immunosuppressive phenotype. We found that exogenous administration of TDE increased expression of metastasis-

associated markers in naive mice and increased the metastatic burden in the lungs of subcutaneous tumor-bearing mice. TDE specifically drive *de novo* synthesis of PD-L1 in macrophages. The increased PD-L1 expression curtailed immune responses through inhibition of effector T cell functions in both mice and humans. We further reveled that PD-L1 expression on macrophages from metastasis negative draining lymph nodes of non-small cell lung cancer patients positively correlates with exosomal release genes YKT6 and TSG101 from primary tumors. Taken together, our findings support the idea that TDE drive primary tumor metastasis through polarization of tissue resident macrophages towards an immunosuppressive phenotype characterized by increased PD-L1 expression.

2.2 MATERIALS AND METHODS

2.2.1 Mice

C57BL/6, MyD88$^{-/-}$, TLR2$^{-/-}$, TLR4$^{-/-}$, TLR6$^{-/-}$ TLR7$^{-/-}$, OT-I and OT-II mice were purchased from commercially available vendors. TLR9$^{-/-}$ mice were purchased from Oriental Yeast Co. (Japan). LysM-cre;Raptor$^{fl/fl}$ and LysM-cre;Rictor$^{fl/fl}$ mice were generated by crossing LysM$^{Cre/wt}$ with Raptor$^{fl/fl}$ or Rictor$^{fl/fl}$ mice both which were purchased from Jackson Laboratory (Bar Harbor, ME). Raptor$^{fl/fl}$ and Rictor$^{fl/fl}$ mice were used as controls. All animals were housed and treated in accordance with institutional guidelines and approved by the Institutional Animal Care and Use Committee at the University of Louisville, Louisville, KY.

2.2.2 Cell culture and cell lines

The authenticated human adenocarcinoma cell line A549, murine lung adenocarcinoma (LLC), colon carcinoma (MC38), and melanoma (B16-F10) cell lines were obtained from American Type Culture Collection (ATCC). The murine breast cancer cell line 4T-1 was kindly provided by Dr. Nejat Egilmez, Department of Microbiology and Immunology, University of Louisville. The control MLE-12 cell line was provided by Dr. Haribabu Bodduluri and the human HBEC cell line provided by Dr. Geoffrey Clark. All cell lines were cultured in DMEM supplemented with 10% FBS (Atlanta Biologicals), and 1% Penicillin-Streptomycin Solution (Corning). For exosome isolation studies, cells were cultured in appropriate medium with 10% exosome-free FBS (Thermo-Fisher Scientific, Waltham, MA).

RAB27KO 4T-1 cell line was generated using CRISPR/CAS9 technology. Briefly, cells were transfected with Rab27a sgRNA CRISPR All-in-One-Lentivirus set (Applied Biological Materials (abm), Vancouver, Canada) at a MOI of 10. Cells were also transfected with Scrambled sgRNA CRISPR/Cas9 All-in-One Lentivirus to serve as a control. Properly transfected cells were selected for using puromycin antibiotic selection. Genomic cleavage was detected using the CRISPR Genomic Cleavage Detection Kit and standard protocol (abm, cat. No. G932). The following sgRNA sequence was used: sg1Rab27 CCA CCT GCA GTT ATG GGA CA

2.2.3 Exosome purification and characterization

Supernatants were obtained from cancerous cell lines (LLC, 4T-1, MC38, B16-F10, and A549) and non-cancerous epithelial cell lines (MLE-12 and HBEC) grown to 80% confluence over a 48 hour period in the appropriate growth media. For *in vivo* exosome isolation, primary tumors were excised, mechanically separated and enzymatically digested (collagenase (5g/L), Hyaluronidase(0.4g/L), DNAse I (0.15g/L)) for 35 minutes with rotation at 37°C. Cells were then cultured in complete DMEM as specified for cell lines. Exosomes were prepared as previously described [73, 74]. Briefly, the cell supernatants were spun once each at 2,000 x g and 10,000 x g. The supernatant was decanted and then carefully layered on top of 8mL of 30% sucrose prior to beging spun at 100,000 x g for 90 minutes. The supernatant was removed and the sucrose fraction containing the exosomes was washed with PBS and spun again at 100,000 x g for 90 minutes. Exosomes were collected using 150ul of PBS. Exosomes were then run through qEV 35nm single use columns (Izon Biosciences, Boston, MA) for further purification. Samples were run on a NanoSight NS300 to confirm exosome isolation via size verification. The total exosomal protein concentrations were determined by using the BCA Protein Assay kit (Thermo Fisher

Scientific, Santa Clara, CA). Finally, an Exo-check Antibody Array (Systems Bioscience, Palo Alto CA) was used to confirm proper surface marker expression profile for exosomes.

2.2.4 Isolation of Peritoneal Macrophages

Peritoneal macrophages were harvested by peritoneal lavage as previously described [75]. Briefly, cold 3% FBS was injected into the peritoneal cavity and extracted after gentle agitation. The peritoneal cell suspension was centrifuged at 1600 r.p.m. After centrifugation, cells were resuspended in complete RPMI-1640 supplemented with 10% FBS (Atlanta Biologicals), and 1% Penicillin-Streptomycin Solution (Corning). Unless otherwise noted, cells were plated at a density of $5.0x10^5$ cells/well in a 24 well plate. Cells were incubated at 37°C for 2 hours to allow macrophages to adhere to the plate. Floating cells were removed by two subsequent washes with PBS. For cell sorting, peritoneal macrophages were stained with Fixable Viability Dye and F4/80/FITC antibody (Biolegend) at 4°C for 30 min in the dark. Samples were then washed and resuspended in MACS running buffer. The samples were sorted on a FACS Aria gated on singlets followed by live, $F4/80^+$. Cells were immediately plated for use in subsequent experiments.

2.2.5 *In Vitro* Peritoneal Macrophage Culture

Peritoneal macrophages were treated with MLE-12 Exo or LLC exo (40µg/mL) for 16 hours. After incubation, supernatant was removed and cells were washed briefly with PBS. Cells were harvested by adding 500µL Cell Stripper (Corning) and incubated for 1 minute at 37°C. RPMI-1640 was added to quench the reaction and cells were gently removed by scraping. For NF-κB experiments, macrophages were pre-treated with 0.2

μg/mL BAY-11-7082 for 1 hour at 37°C. Cells were then washed with PBS and then treated with exosomal stimulation as normal. For the HMGB-1 studies, cells were stimulated with 10μg/mL recombinant murine HMGB-1 (Cat# 764006, Biolegend) for 16 hours.

2.2.6 Murine T cell proliferation assay

Splenocytes from Ova-transgenic-I (OT-I) and Ova-transgenic-II (OT-II) mice were labeled with 5(6)-carboxyfluorescein diacetate succinimidyl ester (CFSE cell trace, Thermo Fisher) at a concentration of 1 μM/mL according to manufacturer's instructions. Briefly, CFSE labelled cells were co-cultured with macrophages pre-treated with 40ug/mL exosomes (48 hours) at a 1:15 ratio. Macrophages were washed prior to T-cell addition to remove residual exosomes. OVA antigen was added at a final concentration of 25 μg/mL (OT-I) or 200 μg/mL (OT-II) for 48 or 72 hours, respectively. Blocking α-PD-1 antibody (40μg/mL, 60μg/mL) for OT-I and OT-II was added to culture along with OVA. Following culture cells were surfaced stained with CD4/APC and CD8/APC for 20 min. Cells were then fixed (Fixation Buffer, Biolegend) and permeabilized (Intracellular Staining Perm Wash Buffer, Biolgend) prior to overnight intracellular staining with IFN-γ.

2.2.7 Quantitative PCR

Total RNA was extracted using TRizol (Invitrogen) and isolated according to manufacturer's instructions. cDNA was generated using the iScript cDNA Synthesis Kit (Bio-Rad). mRNA expression analysis was carried out using iQ SYBR Green (Bio-Rad). RNA concentration was quantified using NanoDrop RNA 6000 nano-assays and analyzed using the CFX Connect PCR Machine (Bio-Rad). See Table S2 for the primer sequences.

2.2.8 Cytokine and ELISA measurement

Supernatant was isolated from culture conditions, centrifuged at 6000rpm for 5 minutes to remove cellular debris and transferred to a new Eppendorf tube for storage at -20°C till use. Cytokine array was performed using the Proteome Profile Mouse Cytokine Array Panel A (R&D Systems Inc, Minneapolis, MN) according to the manufacturer's instructions. ELISA MAX IL-6 and IL-10 kits (Biolegend) were used according to manufacturer's instructions.

2.2.9 Western blot

$F4/80^{+}$ cells were sorted using FACS Aria and the stimulated according to experimental design. Macrophage proteins were separated using SDSPAGE 10% Tris-HCl gels and transferred onto PVDF membranes (Millipore, Cat# IPVH00010). The blots were blocked with 5% BSA at room temperature for 1 hour and incubated overnight at 4°C with listed primary antibodies, followed by incubation with HRP-conjugated secondary antibodies (GE Healthcare) at room temperature for 1 hour. The membrane blots were developed with Amersham ECL Prime Western Blotting Detection Reagent (GE Healthcare, Cat # RPN2232) and detected through Medical Film Processor (Konica Minolta Medical & Graphic, Inc. Model: SRX-101A). We used Precision Plus Protein™ Kaleidoscope™ Prestained Protein Standards as a standard protein marker (Bio-Rad, Cat# 1610375)

Primary antibody list

Antibody Name	Vendor	Catalog Number
Phospho-NF-κB p65 (Ser536) (93H1)	Cell Signaling Technology	3033
NF-κB p65 (D14E12)	Cell Signaling Technology	8242
PD-L1	R&D Systems	AF1019
B-Actin	Sigma	A5316
HMGB-1	Cell Signaling Technology	6893S

2.2.10 Immunofluorescence staining

To detect exosome uptake in F4/80^{+} peritoneal macrophages, cells were cultured with GFP^{+} LLC exosomes (40μg/mL) for a one or two hour incubation on glass cover slips pre-coated with poly-L lysine. Slides were incubated overnight with rat anti-mouse F4/80 (1:100). Lung samples from *in vivo* experiments were frozen in OCT and stored at -80°C. Sections of lung approximately 8 μm were fixed with cold acetone for 15 minutes followed by 30 minutes of air drying. Slides were then blocked using 20% FBS in PBS for 1 h. Primary Ab staining occurred overnight at 4°C in humidified staining container with antibodies to PD-L1 (1:100), CD11b (1:100), and F4/80 (1:100).

2.2.11 *In vivo* Syngeneic Tumor Metastasis Model

LLC ($0.5x10^6$, in 100μl PBS) or Rab27$^{-/-}$/SCRAM 4T-1 ($1.2x10^6$, in 100μl PBS) cells were injected subcutaneously into the flanks of C57BL/6 mice or orthotopically in the mammary glands of BALB/c mice, respectively. The mice were euthanized when the tumor diameter reached 10mm. Lung tissue was isolated and weighed prior to

enzymatic digestion (collagenase (5g/L), Hyaluronidase(0.4g/L), DNAse I (0.15g/L)) for 35 minutes with rotation at 37°C. Following digestion, RBC's were lysed using ACK and resuspended in RPMI-1640 as a single cell suspension. Lung tissue was also fixed in OCT for hematoxylin and eosin staining or for confocal microscopic analysis.

2.2.12 Exosome-mediated Metastasis Model

The experiment was designed as previously described [76]. Briefly, 8-10 week old C57BL/6 mice were subcutaneously injected in the flank with GFP^+ LLC ($0.85x10^6$, 100µl PBS) cells. Seven days post-injection, LLC exosomes or control MLE-12 exosomes (10µg in 100µl PBS) were injected intravenously every three days for three weeks. Lung tissue samples were frozen in OCT at -80°C. Lung tissue was enzymatically digested (collagenase (5g/L), Hyaluronidase(0.4g/L), DNAse I (0.15g/L)) for 35 minutes with rotation at 37°C. Whole lung cells ($5x10^6$) were frozen in TRIzol for RNA extraction. Similarly, 8-10 week old C57BL/6 mice were injected i.v. with LLC exosomes (10µg, in 100µl PBS) every 2 days for 2 weeks prior to lung acquisition and analysis via RT-PCR for metastasis-associated markers.

2.2.13 *In vivo* tracking of fluorescently labeled exosomes

Purified exosomes were labeled according to the previous protocol [70]. Briefly, exosomes were incubated for 10 minutes with Vybrant DiI (ThermoFisher, 1:1000 dilution). Excess dye was removed by washing in 20mL of PBS at 100,000 x g (90 minutes) to generate final DiI labeled exosomes. Exosomes were then intravenously injected into C57BL/6 mice (40 µg in 100µl PBS) and lung, bone marrow, and spleen were isolated 24 hours later and assessed for uptake via Flow cytometry.

2.2.14 Human Samples

Samples were obtained as approved by the University of Louisville Institutional Review Board. Draining LN were obtained from lung transplant donors during lung resection and from cancer patients during tumor resection and/or biopsy. Patient information was summarized in Table S1. PBMCs were obtained from healthy donors. Informed consent was obtained from all donors prior to sample collection. For flow cytometry analysis, cells were stained with Fixable Viability Dye/APC-Cy7, CD14/PE, CD45/Alexa Fluor 700, CD16/FITC, CD11b/ Biotin, PD-L1/Pe-Cy7, CD66b/PE Dazzle, CD68/Percp, HLA-DR/APC, CD33/BV605, CD63/BV650, CD206/BV421, TIM-3/Biotin, CD8/PE, CD45RO/FITC, CD3/PerCP, CD103/PE/Dazzle 594, γδ TCR/APC, PD-1/PE-Cy7, CD4/BV60, CD69/BV650, CD45RA/BV421. Table S3 provided a full antibody list. Cells from patient dLN samples were sorted for YKT6 RT-PCR analysis using CD45-PE on a FACS Aria. Data was analyzed using Cytobank software to generate viSNE plots.

2.2.15 *In vitro* Human suppression assay

The human T cell suppression assay was performed according to the previously published protocol [77]. Briefly, donor PBMCs were sorted on a BD FACsAria for $CD14^+$ or $CD3^+$ expression. The $CD14^+$ cells were plated in a 96-well U-bottom plate ($0.5x10^5$ cells/well) and stimulated with 40 μg/mL of HBEC or A549 exosomes for 48 hours. The 96 U-bottom plate had previously been coated with anti-human CD3 Abs (clone:OKT3) (1 μg/mL) in 100μL PBS at 37°C for 4 hours. The $CD3^+$ T cells were then labeled with 1 μM of the fluorescent dye 5,6-carboxyfluorescein diacetate succinimidyl ester (CFSE, Invitrogen), according to the manufacturer's instructions. Wells were gently washed

twice with PBS before the addition of cells. CFSE-labeled responders ($1.0x10^5$ cells /well) were mixed with previously stimulated $CD14^+$ cells in a 1:2 ratio and co-cultured for 4 days in the complete cell culture media. The CFSE signal was analyzed by flow cytometry on gated on both CD4+ and CD8+ lymphocytes.

To measure the IFN-γ production, $1.0x10^5$ autologous sorted $CD3^+$ T cells stimulated with plate-bound anti-human CD3 Ab were co-incubated with previously stimulated $CD14^+$ subsets in a 1:2 ratio for 48 hours in 96 well U-bottom plate. BD GolgiStop and BD GolgiPlug were added into the cell cultures during the last 12 hours. Surface stained cells were fixed with Fixation Buffer (Biolegend) for 20 minutes. The fixed cells were permeabilized with Intracellular Staining Perm Wash Buffer (Biolegend) and then stained with the anti-human IFN-γ (Biolegend, clone: 4S.B3). The percent of intracellular IFN-γ positive $CD4^+$ and $CD8^+$ T cells was analyzed by flow cytometry.

2.2.16 *In vitro* human culture

A549 exosomes or HBEC exosomes were added (40μg/mL) to previously sorted $CD14^+$ myeloid cells ($0.5x10^5$, 48 well plate) and stimulated for 16 hours. TLR2 blocking antibody (TLR2 Monoclonal Antibody (TL2.1), eBioscience) was added at 40μg/mL to sorted $CD14^+$ cells for 30 min at RT before stimulation with 40μg/mL of A549 exosomes. Sorted $CD14^+$ cells were stimulated with recombinant human HMGB-1 (4μg/mL and 10μg/mL, Cat# 1690-HMB, R&D Systems, Minneapolis, MN) for 16 hours.

2.2.17 Statistical analysis

All results were repeated in at least three independent experiments, and data from one representative experiment was shown. All statistical analyses were performed using GraphPad PRISM software unless otherwise noted (version 8.0, Irvine, CA, USA). All experiments that compared two conditions used unpaired Student's *t* tests. Those that compared three or more conditions used a one-way ANOVA with multiple comparisons. A value of $p < 0.05$ (two-sided) was considered statistically significant. Data are represented as mean ± SEM.

2.2.18 PCA analysis

To collectively assess the relationships of myeloid and T cell markers of human samples screened in this study in the context of disease status, we conducted Principal Component Analysis (PCA) using estimated cell marker percentages in each of the 9 NSCLC and 10 HD samples. Within the R statistical environment (https://www.r-project.org/), PCA was performed using the prcomp() function, with the "scale" parameter set to "TRUE". The PCA plot was generated using the R package "factoextra", including 95% confidence ellipses. To assess the statistical association of the first principal component and disease status, linear regression was conducted using the R lm() function, in which disease status of each NSCLC and HD subject was treated as the dependent variable and the first principle component scores were treated as the independent variable.

2.2.19 TCGA Nodal Status Analysis

RNA-seq data was downloaded from TCGA for several cancer types. The cases with nodal status were kept. Deseq 2 was run on the raw counts between cases with nodal status N0 and all other nodal status (N1,N2,N3). Plots were made with Deseq2's function

plotCounts with counts normalized by the library size. The p value reported was adjusted to correct for false positives due to multiple testing.

2.3 RESULTS

2.3.1 Exosomal characterization and trafficking

Exosomes were isolated from the supernatants of the murine lung adenocarcinoma cell line, Lewis Lung Carcinoma (LLC) [73]. Size confirmation of exosome isolates demonstrated particles averaging 185nm, which is slightly larger than the previously reported size range of 20-150 nm[73] (Figure 1A). Protein array analysis confirmed surface expression of known exosome markers including CD63, CD81, Annexin 5 (ANXA5), and TSG101 (Figure 1B).

To confirm uptake of exosomes by $CD11b^+$ macrophages in the lung, we injected DiI-labeled exosomes intravenously into WT mice. We then harvested lung, spleen, and bone marrow to look at exosome uptake and distribution. Looking specifically at the $CD11b^+$ $F4/80^+$ compartment, we found that lung $CD11b^+$ cells had the highest uptake compared to those harvested from spleen and bone marrow (Figure 1C).

2.3.2 The effect of TDE on macrophages in a pre-metastatic niche

We intravenously injected non-GFP LLC or control mouse lung epithelial cell (MLE-12) exosomes into wild type (WT) mice that 7 days prior had been subcutaneously injected with LLC-GFP tumor cells (Figure 2A). While mice treated with the MLE-12 exosomes showed no difference compared to untreated tumor-bearing mice, LLC exosome treated mice had an increased number of micro-metastases as assessed by the percentage of $LLC\text{-}GFP^+$ cells in the lung (Figure 2B). Fluorescent microscopy analysis confirmed these results (Figure 2C). Further confocal analysis of the lung tissues demonstrated increased PD-L1 co-expression with both CD11b and F4/80 in LLC exosome-treated mice suggesting that the exogenously administered TDE were preferentially driving PD-L1 expression on myeloid cells within the lung (Figure 2D).

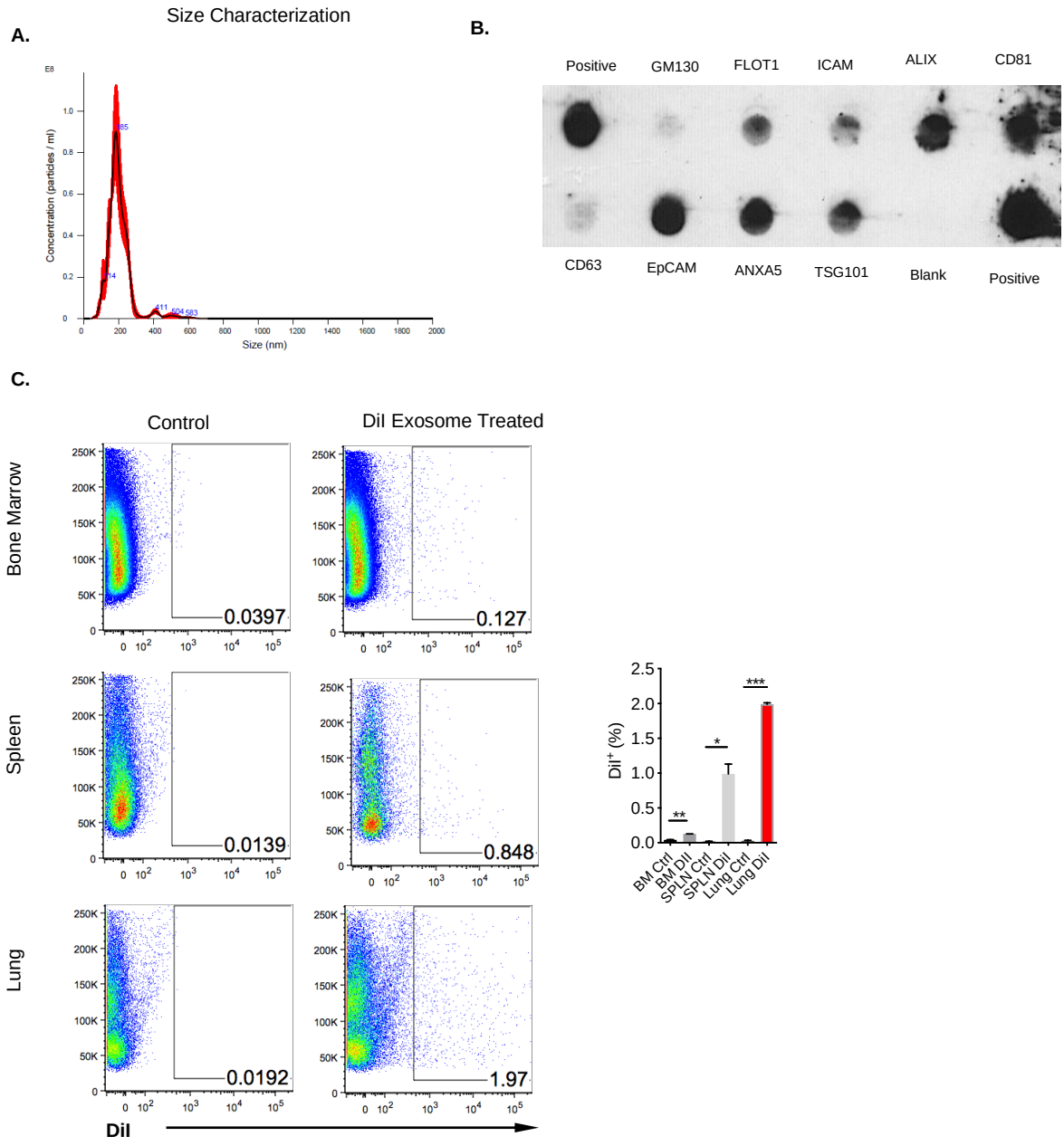

Figure 1. Exosome Isolation and Uptake. **(A)** Size characterization of exosome centrifugation isolate using Nanosight NS300. Representative plot for n=3 independent experiments **(B)** Exo-check antibody array to confirm proper isolation of LLC exosomes via ultracentrifugation of culture supernatants. *GM-130*: cis-golgi-matrix protein (monitor cellular contamination), *TSG101*: Tumor susceptibility gene, *ANXA5*: Annexin A5, *EpCAM*: epithelial cell adhesion molecule, *CD63*:LAMP-3, *CD81*, *ALIX*: programmed death 6-interacting protein, *ICAM1*- intracellular adhesion molecule 1, *FLOT1*: flotillin 1, *positive*: control for HRP detection. Representative WB for n=3 independent experiments with similar results. **(C)** *In vivo* injection of DiI labeled LLC exosome (40 µg/mouse) to determine biodistribution among bone marrow (top), spleen (middle), and lung (bottom). n=3. The data are shown as mean ± SEM. *p<0.05, **p<0.01, ***p<0.001, (unpaired student's t test).

To determine the effect exosomes alone have on priming a metastatic site, we intravenously injected WT mice with LLC exosomes for two weeks. LLC exosome treatment significantly increased expression levels of known metastasis markers, MMP9, S100a8, and S100a9 (Figure 3A), which have been associated with increased tumor cell invasion, migration, and colonization at the metastatic site [54].

2.3.3 TDE polarize macrophages towards an immunosuppressive phenotype

Similar to the *in vivo* myeloid phenotype, F4/80$^+$ peritoneal macrophages treated *in vitro* with TDE showed an increase in surface PD-L1 expression as compared with control MLE-12 exosomes or macrophages alone (Figure 3B). LLC exosome treatment also increased expression of activation marker, CD80, as compared to controls (Figure 3C). Stimulation with exosomes isolated directly from subcutaneous LLC tumors also demonstrated increased PD-L1 expression thus eliminating the possibility that the phenotype was an *in vitro* artifact from cell line culture (Figure 3D)[78]. Additionally, to emphasize this phenotype is not only limited to lung adenocarcinoma, peritoneal macrophages were treated with exosomes isolated from 4-T1 breast cancer, MC38 colon cancer, and B16F10 melanoma cell lines all of which demonstrated increased PD-L1 expression (Figure 3E). Confocal analysis of F4/80$^+$ peritoneal macrophages confirmed increased uptake of FITC$^+$ LLC exosomes over time (Figure 4A).

However, the question remained as to whether exosomal uptake was increasing endogenous production of PD-L1 by the macrophages or whether the macrophages were acquiring the PD-L1 from the exosomes. Western blot analysis confirmed that LLC exosomes do express PD-L1, similar to previously reports (Figure 4B)[62, 66, 72]. However, RT-PCR analysis of macrophages treated with LLC exosomes demonstrated a

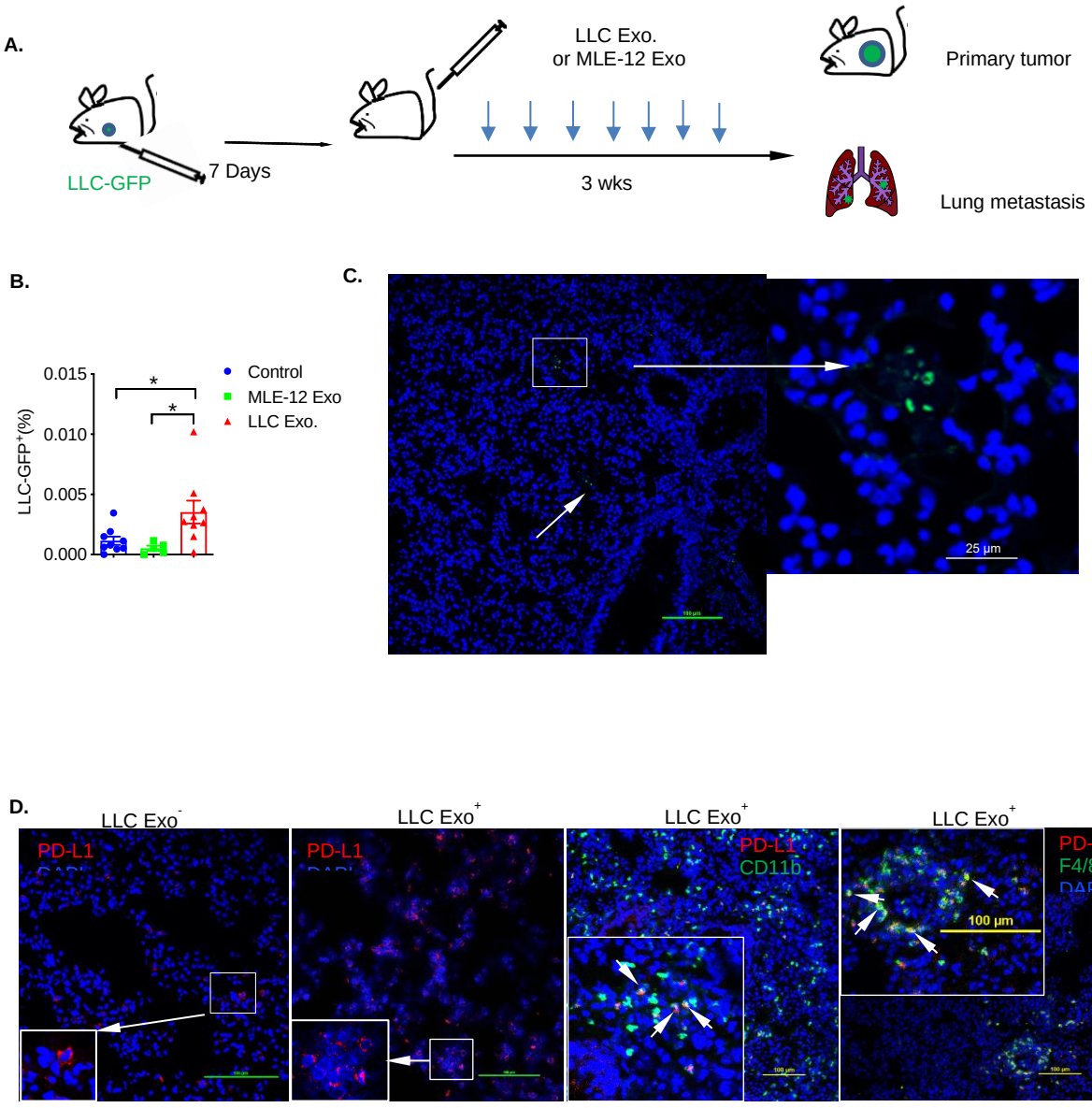

Figure 2. The effect of TDE on macrophages in a pre-metastatic niche. **(A)** Schematic for experimental design (B-D). **(B)** Micro-metastatic burden was quantified by LLC-GFP% in the lungs of subcutaneous GFP-LLC tumor-bearing mice treated i.v. with 10 µg/mL MLE-12 or LLC exosomes every three days for 3 weeks (ctrl n=6, MLE-12 Exo. n=5, LLC Exo. n=6). **(C)** Confocal microscopic analysis of lung GFP$^+$ micro-metastases from primary subcutaneous LLC tumor-bearing mice. **(D)** Confocal microscopic analysis of PD-L1 expression in LLC Exo$^-$ or LLC Exo$^+$ treated lungs (left) and PD-L1 co-expression with CD11b and F4/80 in LLC Exo$^+$ mice (right). Scale bar, 100µM. The data are shown as mean ± SEM. *p<0.05, (one-way ANOVA with multiple comparisons).

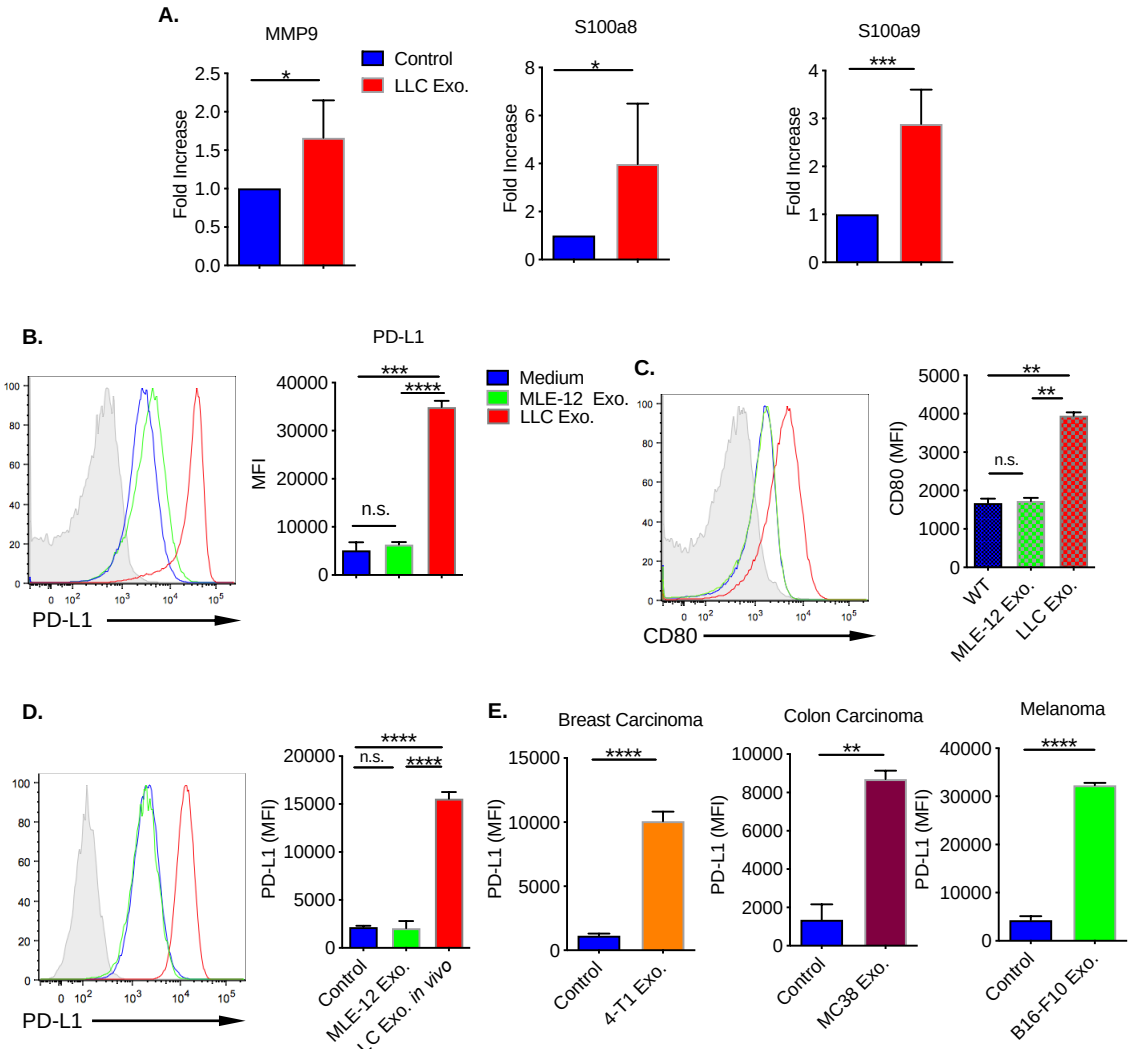

Figure 3. TDE stimulation drives PD-L1 expression in macrophages. **(A)** Metastasis-associated marker gene expression in the lungs of WT mice treated i.v. with LLC exosomes every 2 days for two weeks compared WT control. The data are normalized to WT gene expression level. n=4 control, n=8 LLC Exo. **(B)** Expression of PD-L1 by flow cytometry in peritoneal macrophages stimulated with MLE-12 exo. or LLC Exo. (40µg/mL) for 16 hours. Representative histograms and summarized MFI are shown. MFI= mean fluorescent intensity. n=3 per group. ***p<0.001, ****p<0.001, one-way ANOVA with multiple comparisons. **(C)** Expression of CD80 in peritoneal macrophages stimulated with 40µg/mL MLE-12 exo. or LLC Exo. for 16 hours. MFI= mean fluorescent intensity. n=3 per group., **p<0.01 one-way ANOVA with multiple comparisons. **(D)** Expression of PD-L1 in peritoneal macrophages treated with exosomes isolated from subcutaneous LLC tumors compared to MLE-12 controls. Tumors were excised from the flank, digested, and cultured *in vitro* for ultracentrifugation exosome isolation**.** n=4 mice per group**.** ****p<0.001, one-way ANOVA with multiple comparisons. **(E)** PD-L1 expression in peritoneal macrophages treated with exosomes (40µg/mL) from Breast cancer (4-T1), Colon cancer (MC38), and Melanoma (B16-F10) cell lines. n=3 per group. The data are shown as mean ± SEM. *p<0.05, **p<0.01, ***p<0.001, ****p<0.001 (unpaired student's t test).

significant increase in PD-L1 mRNA expression indicating that *de novo* synthesis of PD-L1 is likely a greater source of PD-L1 (Figure 4C). Taken together, these data suggest that TDE are taken up selectively by F4/80^{+} macrophages, resulting in increased endogenous production of PD-L1 both *in vitro* and *in vivo*, and promote primary tumor progression and metastasis in the lung.

We next explored if TDE stimulation impacts the functionality of macrophages. We first performed a cytokine array on the supernatants from the 16 hour macrophage culture (Figure 5A). As compared to macrophages alone, as well as macrophages stimulated by MLE-12 exosomes, the TDE stimulated macrophages displayed prominent increases in the secretion of TNFα, TIMP-1, MCP-1, IL-10, IL-6, IL-1ra, G-CSF, and CXCL1. Notably, all cell supernatants were negative for IFN-γ thus eliminating this as a potential mechanism for PD-L1 upregulation[79]. ELISA analysis also confirmed increased IL-6 and IL-10 production, two cytokines that are hallmarks of cancer-related inflammation (Figure 5B) [80]. The immunosuppressive phenotype was further characterized by increased arginase-1(Arg-1) and vascular endothelial growth factor (VEGF) expression (Figure 5C). However, a dramatic increase in iNOS production was also noted, supporting the emerging notion that macrophages within the tumor microenvironment often display a mixed M1/M2 phenotype[56].

To further examine the impact of TDE-induced macrophages on effector T cell function, we pre-treated peritoneal macrophages with control MLE-12 or LLC exosomes prior to co-culture with OVA transgenic T cells. As depicted in Figure 6A, CD8^{+} T cells displayed a dramatic decrease in both cell proliferation as well as IFN-γ production when co-cultured with TDE-polarized macrophages. This phenotype was largely rescued when neutralizing α-PD-1 was added suggesting that the PD-L1 expression on macrophages

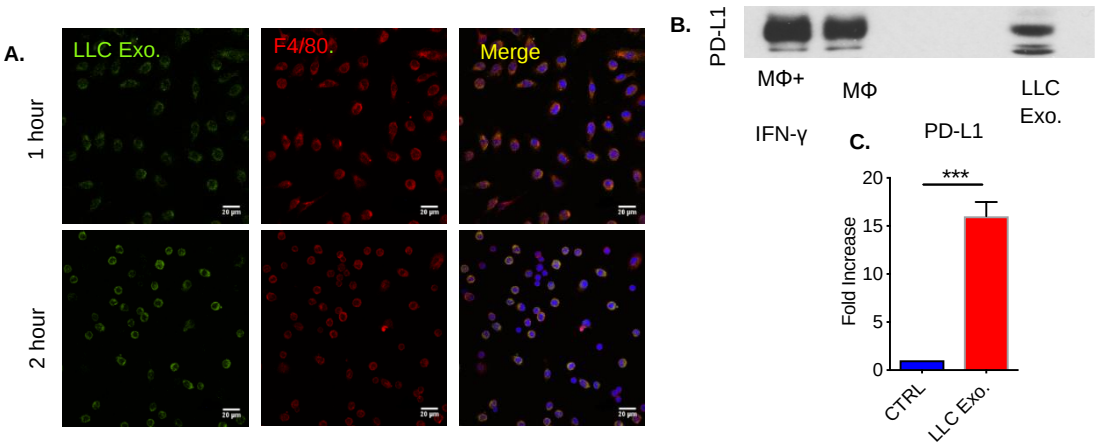

Figure 4. TDE drive *de novo* production of PD-L1. **(A)** Confocal microscopic analysis of GFP⁺ LLC exosome uptake expression in F4/80⁺ peritoneal macrophages treated for indicated period of time. Scale bars, 20μm. **(B)** Representative WB analysis of PD-L1 expression in macrophages stimulated with IFN-γ, macrophages alone, and LLC exosomes. **(C)** The mRNA expression of PD-L1 in peritoneal macrophages following 6 hour LLC exo. stimulation. Data was normalized to control expression level. The data are shown as mean ± SEM. ***p<0.001 (unpaired student's t test).

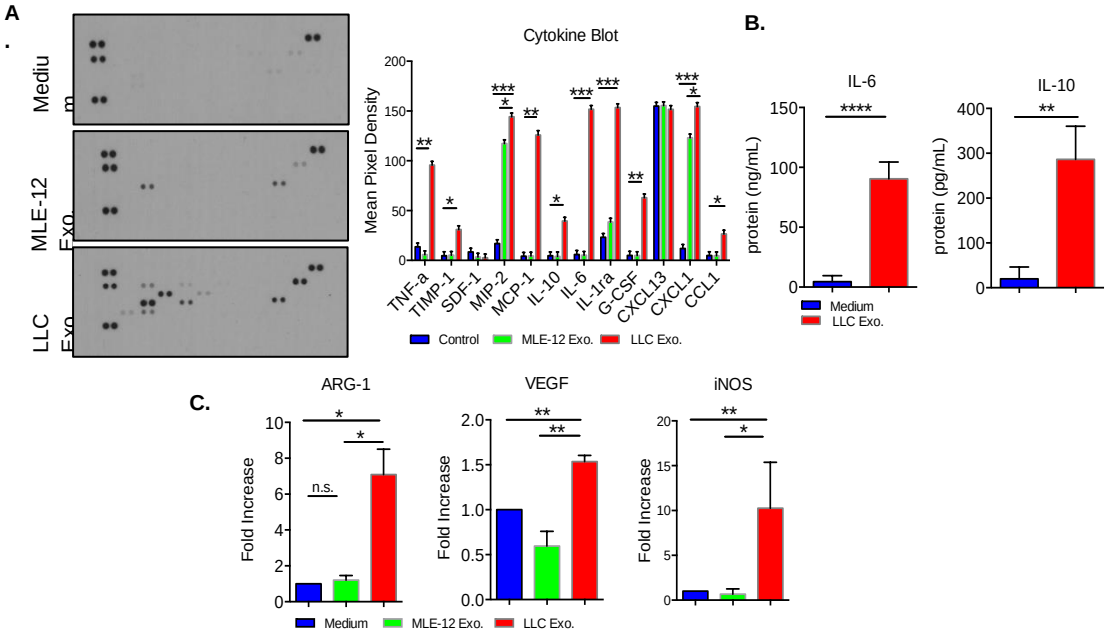

Figure 5 TDE polarize macrophages towards an immunosuppressive phenotype. **(A)** Representative cytokine array panels of supernatants taken from 16 hour culture of peritoneal macrophages stimulated with media alone (top), MLE-12 exosomes (middle), or LLC exosomes (bottom). Representative plots and summarized mean pixel density of each protein are shown (n=3). **(B)** IL-6 and IL-10 concentration detected by ELISA from supernatants of 16 hour peritoneal macrophages stimulated with or without LLC exosomes (40μg/mL). **p<0.01, ****p<0.001 (unpaired student's t test). **(C)** The mRNA expression levels of Arginase-1 (Arg-1), vascular endothelial growth factor (VEGF), and inducible nitric oxide (iNOS) in peritoneal macrophages treated alone or with 40 μg/mL MLE-12 or LLC exosomes for 6 hours. n=3. The data are shown as mean ± SEM. *p<0.05, **p<0.01, ***p<0.001, ****p<0.001 (one-way ANOVA with multiple comparisons).

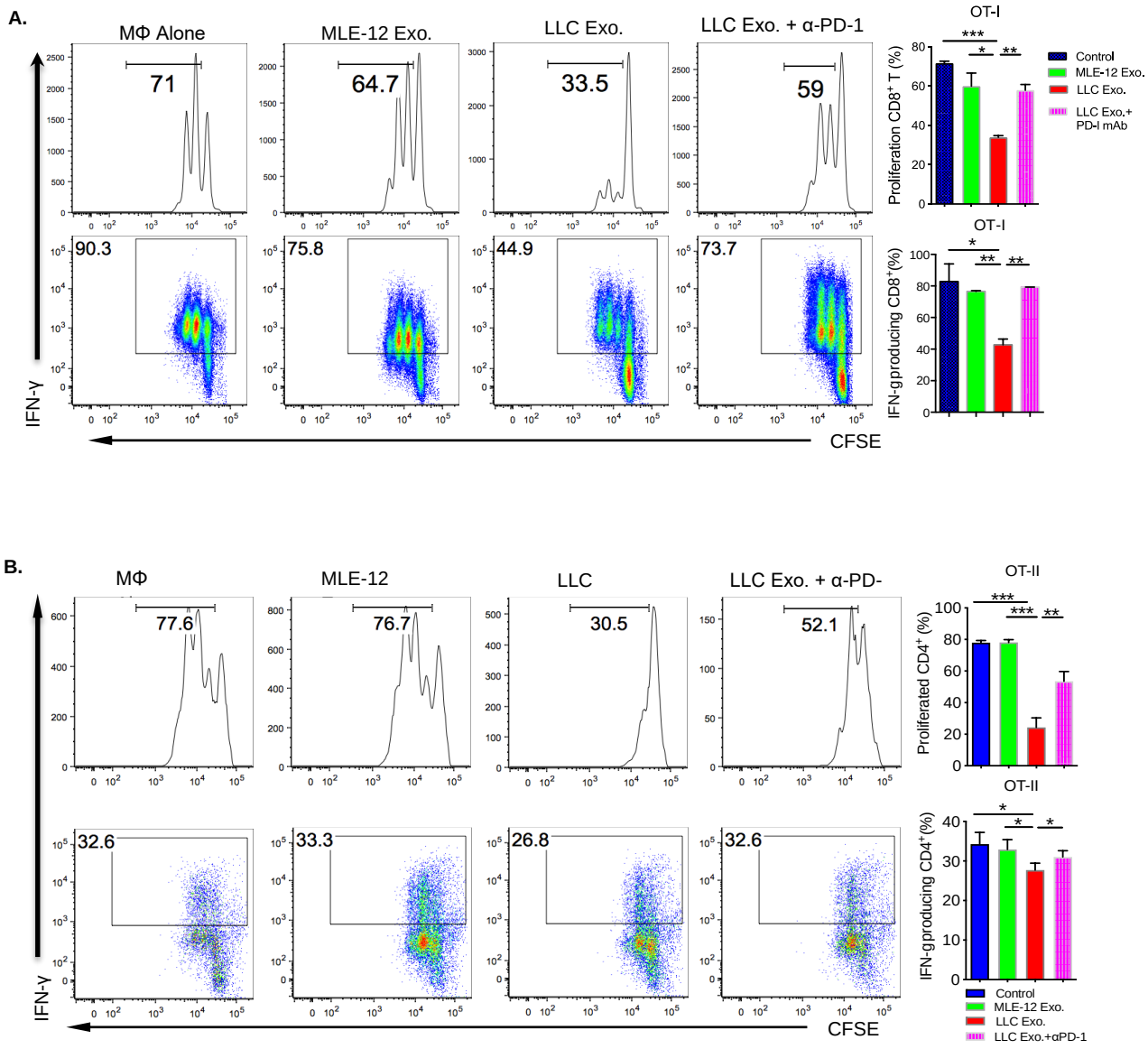

Figure 6. TDE restrain T cell effector functioning. **(A)** LLC exosome polarized peritoneal macrophages suppress OT-I T-cell proliferation (top) and IFN-γ production (bottom) in a PD-L1 dependent manner. Peritoneal macrophages were polarized with MLE-12 or LLC exosomes (40 μg/mL) for 48 hours prior to co-culture with purified OVA-specific CD8 T cells in the presence of OVA (25 μg/mL) for two days with or without α-PD-1 (40 μg/mL). Representative histograms and summarized data are shown (n=3). **(B)** LLC exosome polarized peritoneal macrophages suppress OT-II T-cell proliferation (top) and IFN-γ production (bottom) in a PD-L1 dependent manner. Representative histograms and summarized data are shown (n=3). The data are shown as mean ± SEM. *p<0.05, **p<0.01, ***p<0.001, (one-way ANOVA with multiple comparisons).

is, at least in part, causing functional inhibition of effector T cells. A similar phenotype was seen with $CD4^+$ T cells (Figure 6B).

2.3.4 TDE mediate PD-L1 expression through TLR2 and NF-κB

Toll-like receptors (TLRs) play an important role in innate immunity and are often found on sentinel immune cells such as macrophages and dendritic cells. Using mice deficient in the TLR adaptor protein MyD88, we found that the increased PD-L1 expression following LLC exosome stimulation was completely abrogated in $MyD88^{-/-}$ macrophages (Figure 7A). To identify which specific TLR pathway was involved, peritoneal macrophages from TLR2-, TLR4-, TLR6-, TLR7-, and TLR9-deficient mice were stimulated with TDE. As seen in Figure 7B, TLR2-deficient macrophages specifically lost the increased PD-L1 expression, while all other TLR-deficient mice showed normal PD-L1 expression following TDE stimulation.

To solidify the finding that TLR2 ligation is necessary for exosomes to mediate their effect on macrophages and promote pre-metastatic niche formation, we repeated our initial *in vivo* LLC-GFP subcutaneous tumor model using $TLR2^{-/-}$ mice. There was no difference in LLC-GFP% in the lungs of the TDE-treated group compared to the controls in $TLR2^{-/-}$ mice (Figure 7C). Furthermore, when compared to WT, the LLC-GFP% was overall significantly reduced in the $TLR2^{-/-}$ mice (Figure 7D). Confocal microscopy analysis showed no obvious tumor foci in the lungs of TDE treated $TLR2^{-/-}$ mice (Figure 7E). Collectively, these results indicate that signaling through TLR2 is required for TDE to mediate upregulated PD-L1 expression on macrophages and influence the progression of primary tumor metastasis to the lung.

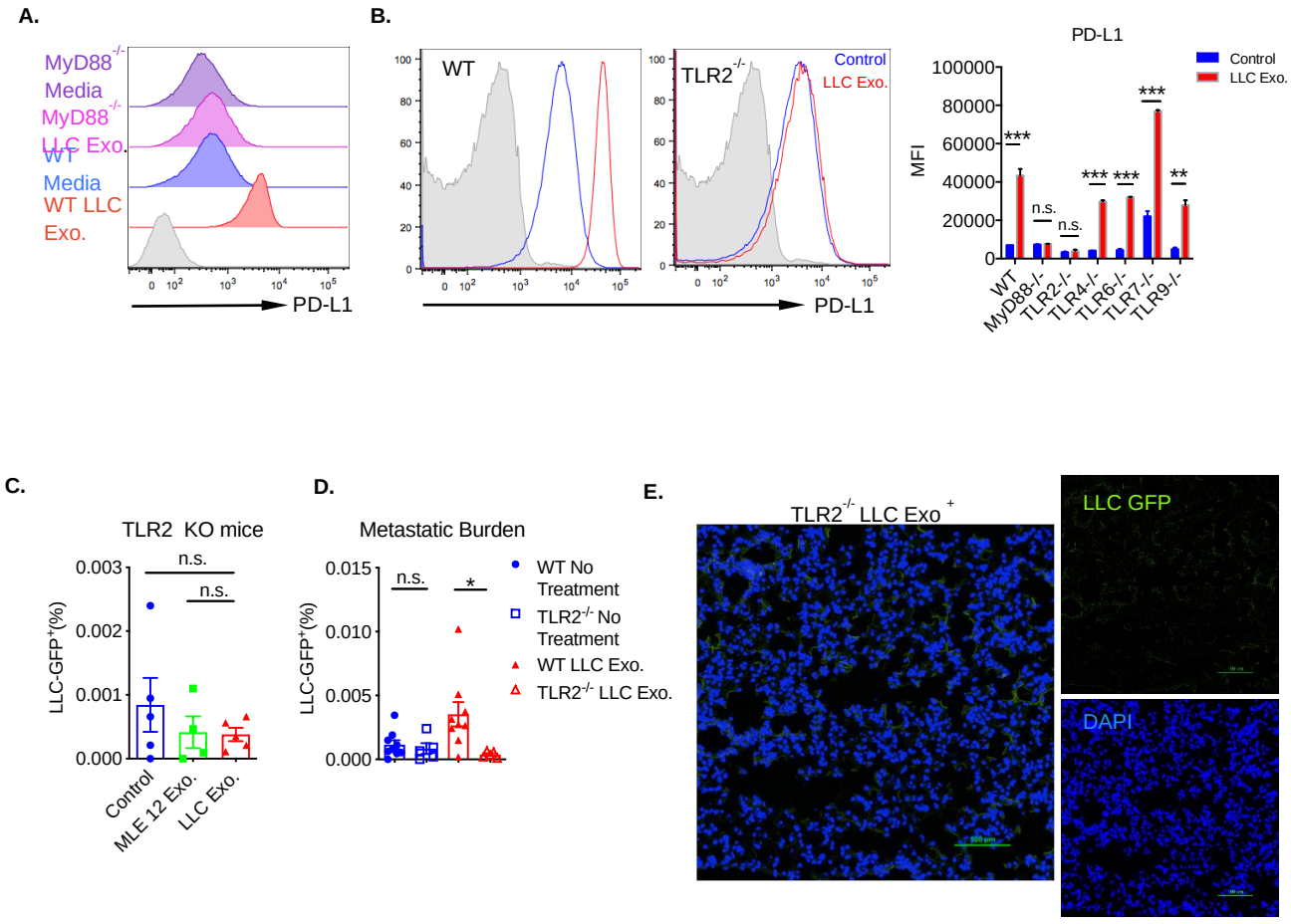

Figure 7. TDE mediate PD-L1 expression through TLR2 (A) The expression of PD-L1 on WT or MyD88$^{-/-}$ peritoneal macrophages that were stimulated with or without LLC exosomes (40 µg/mL) for 16 hours assessed by flow cytometry. **(B)** Expression of PD-L1 assessed by flow cytometry in WT or TLR2$^{-/-}$ peritoneal macrophages following stimulation with LLC exosomes (40 µg/mL) for 16 hours (left). Macrophages from TLR4$^{-/-}$, TLR6$^{-/-}$, TLR7$^{-/-}$, and TLR9$^{-/-}$ showed normal PD-L1 expression compared to WT control following TDE stimulation indicating those pathways are not involved in LLC exosome signaling (right). n=3 mice per group. **(C)** Summary of GFP^{+} micrometastases in the lungs of TLR2$^{-/-}$ mice that had previously been injected subcutaneously with GFP-LLC tumor cells (1.0x10^{6}) and then treated i.v. with 10 µg/mL MLE-12 or LLC exosomes every three days for 3 weeks Control n=5, MLE-12 Exo n= 4, LLC Exo n= 5 mice per group. **(D)** Comparison of GFP^{+} micrometastases between WT and TLR2$^{-/-}$ LLC Exo treated mice. n= 5 mice per group. **(E)** Confocal analysis of GFP^{+} micrometastases in the lungs of TLR2$^{-/-}$ mice. The data are shown as mean ± SEM. *p<0.05, **p<0.01, ***p<0.001, (one-way ANOVA with multiple comparisons).

Previous studies have linked increased PD-L1 expression to activation of the NF-κB pathway [81] and TLR2 is well-known to activate the NF-kB pathway. To probe whether exosomal stimulation activates the NF-κB cascade downstream of TLR2, we performedWestern blot analysis in macrophages stimulated with control or TDE. Stimulation with LLC exosomes, but not control MLE-12 exosomes, increased phosphorylation of NF-kBp65 (Figure 8A). In addition, inhibition of NF-κB with BAY-11-7082 (BAY) reduced PD-L1 expression in macrophages as assessed by flow cytometric assay (Figure 8B). These results were further confirmed by RT-PCR analysis (Figure 8C). Another prominent signaling pathway previously reported to affect PD-L1 expression is the mechanistic/mammalian target of rapamycin (mTOR) pathway [82]. LLC exosome stimulation of macrophages deficient in the adaptor protein Raptor or Rictor for the mTOR complex 1 (mTORC1) or mTORC2 resulted in unaltered levels of PD-L1 expression (Figure 8D), suggesting that this pathway is not involved in PD-L1 upregulation on macrophages induced by TDE.

2.3.5 Exosomal HMGB-1 activates TLR-2

Having demonstrated TLR2 as the receptor through which TDE signal, we next determined which specific exosomal factor activates TLR2. One known ligand for TLR2 that has been shown to positively correlate with NSCLC lymph node metastasis is high-mobility group box-1 (HMGB-1) [83]. Overexpression of HMGB-1 has been demonstrated in many types of cancer [83, 84, 85]. Indeed, LLC whole cell lysate and TDE indicated significant expression of HMGB-1 (Figure 9A). Stimulation of peritoneal macrophages with recombinant murine (rm)HMGB-1 resulted in increased PD-L1 expression (Figure 9B). Conversely, stimulation of MyD88$^{-/-}$ (Figure 9C) or TLR2$^{-/-}$ (Figure 9D) peritoneal macrophages with rmHMGB-1 exhibited no change in PD-L1 expression. shRNA

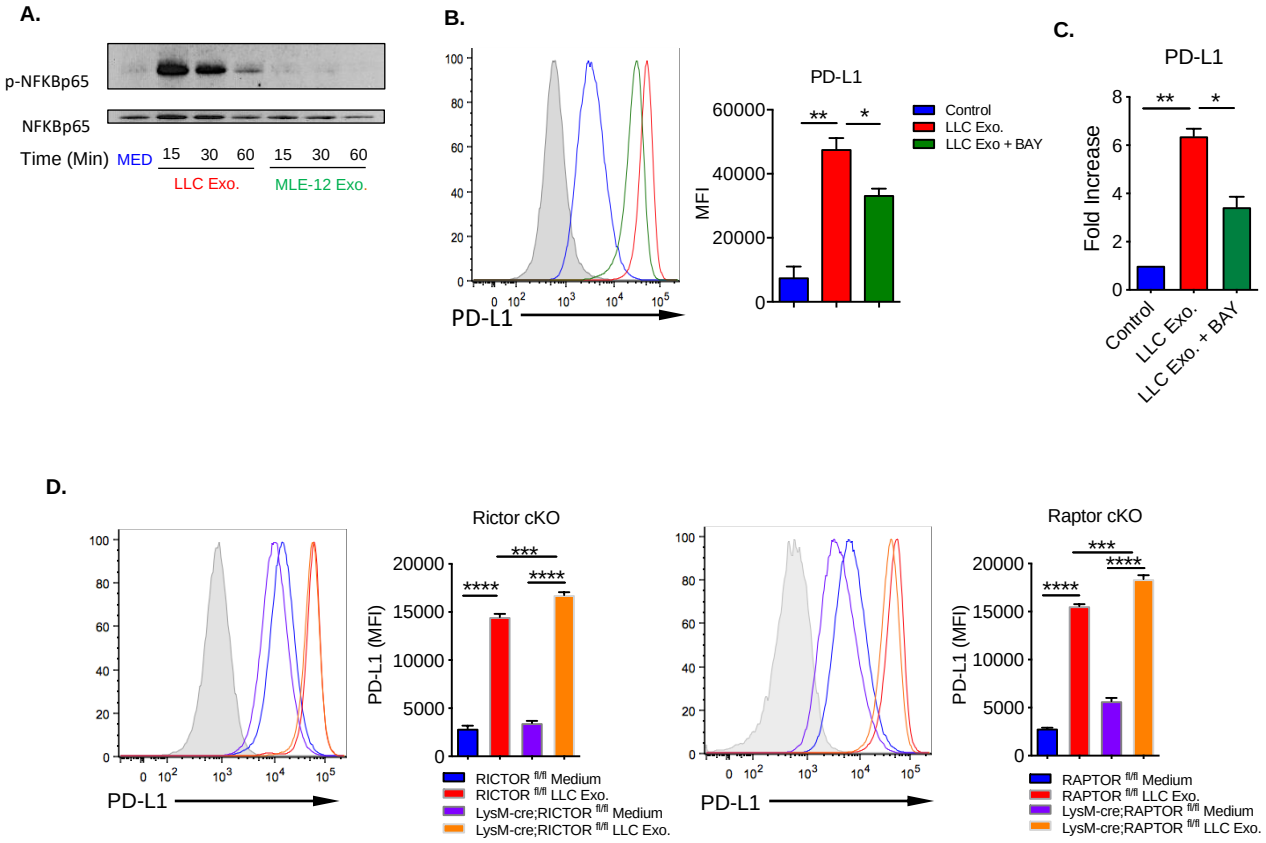

Figure 8. TDE drives PD-L1 expression through NF-κB **(A)** Activation of NF-κB signaling cascade in peritoneal macrophages following stimulation with MLE-12 or LLC exosomes (40 μg/mL) at indicated time determined by WB analysis. **(B)** Peritoneal macrophages were pre-treated with the NF-κB inhibitor, BAY-11-7082 (0.2μg/mL) for 1 hour prior to 16 hour stimulation with LLC exosomes (40 μg/mL). PD-L1 expression was assessed by flow cytometry. Data was normalized to the control. n=3. **(C)** The mRNA expression level of PD-L1 in peritoneal macrophages pre-treated with the NF-κB inhibitor, BAY-11-7082 (0.2μg/mL) for 1 hour prior to 6 hour LLC exo. stimulation. n=3. **(D)** PD-L1 expression in LysM-cre;Rictor$^{fl/fl}$ (left) and LysM-cre;Raptor$^{fl/fl}$ (right) peritoneal macrophages compared to Rictor$^{fl/fl}$, Raptor$^{fl/fl}$ controls following 16 hour stimulation with LLC exosomes. (n=3 per group). The data are shown as mean ± SEM. *p<0.05, **p<0.01, ***p<0.001, ****p<0.0001 (one-way ANOVA with multiple comparisons).

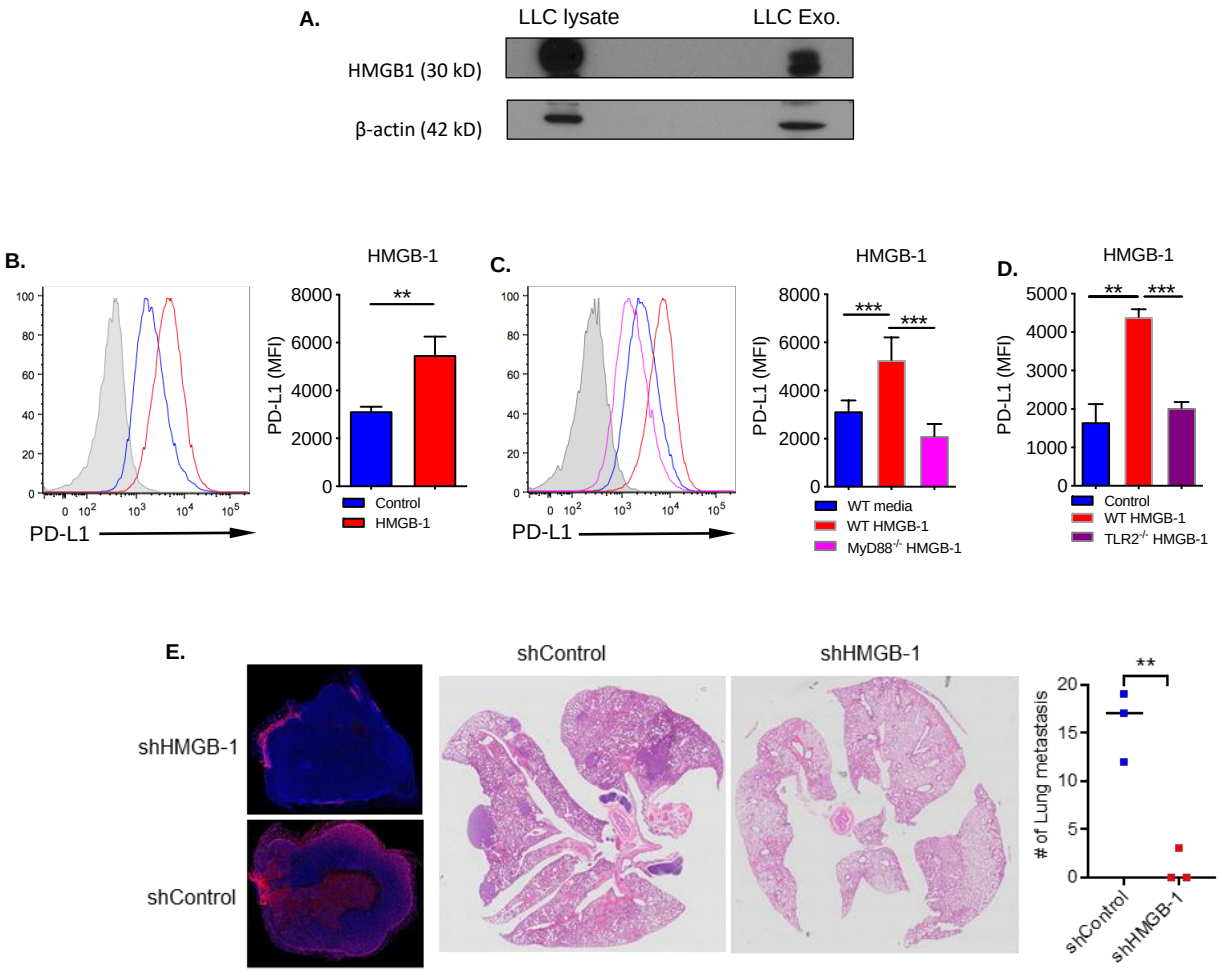

Figure 9. HMGB-1 on TDE induces TLR2 mediated PD-L1 expression (A) Representative WB analysis of HMGB-1 expression in LLC whole cell lysate and LLC exosomes**. (B)** PD-L1 expression in peritoneal macrophages stimulated with murine HMGB-1 (rmHMGB-1) for 16 hours. Representative histograms and summarized MFI data are shown. n=5. **(C)** Comparison of PD-L1 expression between WT and MyD88$^{-/-}$ peritoneal macrophages following stimulation with rmHMGB-1. Representative histograms and summarized MFI are shown. n=4 per group. ***p<0.001 (one-way ANOVA with multiple comparisons). **(D)** PD-L1 expression in TLR2$^{-/-}$ peritoneal macrophages compared to control following LLC exo. stimulation for 16 hours. Summarized MFI data is shown. n=3. **p<0.01, ***p<0.001 (one-way ANOVA with multiple comparisons). **(E)** Expression of HMGB-1 in either shControl or shHMGB-1 primary 4T1 subcutaneous tumors (left), H&E staining of lung (middle) and summarized number of metastatic tumor nodules (right) in the lungs of shControl or shHMGB-1 tumor-bearing mice. The data are shown as mean ± SEM. **p<0.01 (unpaired student's t test).

knockdown of HMGB-1 in 4T-1 breast cancer cells decreased overall expression of HMGB-1 in primary tumor and accordingly decreased the number of metastatic nodules in the lung (Figure 9E). Taken together, these data suggest that tumor-derived exosomal HMGB-1 is at least one factor responsible for mediating TLR2 dependent PD-L1 upregulation and subsequent tumor metastasis.

2.3.6 TDE drive PD-L1 expression *in vivo*

We next examined how the TDE driven phenotype impacts the immune landscaping of a pre-metastatic niche *in vivo*. We particularly focused on the lungs of WT mice that had previously been injected subcutaneously with LLC cells. H&E staining confirmed the lungs were negative for overt primary tumor metastasis at end point (Figure 10A). Analysis of the interstitial (IM:$CD11b^{+}/F4/80^{+}$) and the alveolar (AM:$CD11b^{low/-}/F4/80^{+}$) macrophage populations (Figure 10B) showed that the IM population dramatically increased in the tumor-bearing mice while the AM population remained largely unchanged compared to the control. Furthermore, the IMs demonstrated increased PD-L1 expression within this pre-metastatic tumor environment whereas the AMs showed no change. Other noticeable effects within the lung included a decrease in monocytes ($CD11b^{+}Ly6C^{+}$) and an increase in MDSCs ($CD11b^{+}Gr\text{-}1^{+}$) in tumor-bearing mice (Figure 10C).

Next, we aimed to demonstrate that TDE, specifically, are responsible for mediating the increased PD-L1 expression in the IM compartment allowing for priming of lung cancer metastasis. In order to address this question, we used CRISPR/CAS-9 technology to edit RAB27a gene expression in 4T-1 breast carcinoma. Rab27a is a critical regulatory protein necessary for exosome secretion from the plasma membrane [86]. Given that breast cancer, particularly triple-negative breast cancer, often metastasizes to the lungs, a triple negative primary 4T-1 orthotopic breast cancer with

metastasis to the lung served as a clinically relevant model. Western blot analysis showed about a 50% reduction in Rab27a expression following transfection (Figure 11A). There was no difference in overall primary tumor burden between the scrambled (SCRAM) control and the Rab27$^{-/-}$ cells (Figure 11B). However, the lung resident CCR2^{-} IM population that expanded the most in the exosome competent tumor was significantly diminished in RAB27$^{-/-}$ tumors (Figure 11C). Moreover, depletion of RAB27 specifically decreased PD-L1 expression in the CCR2^{-} IM compartment and left the CCR2^{+} unchanged (Figure 11D). These data suggest that TDE specifically impact the tissue resident interstitial macrophages rather than the recruited bone marrow-derived macrophages to drive PD-L1 expression in the pre-metastatic niche. The AM compartment displayed no change following RAB27 depletion (Figure 11E).

The collective immune landscape in the lung following RAB27 depletion demonstrated an overall more active immune profile. Specifically, there was a decrease in the percentage of immunosuppressive MDSCs (Figure 12A) and analysis of the T-cell compartment within the lung demonstrated an increase in percentage of CD8^{+} T cells (Figure 12B) with a trending decrease in exhaustion marker PD-1 expression (Figure 12C). Conversely, the overall percentage of CD4^{+} T cells in the Rab27$^{-/-}$ tumor-bearing mice was unchanged but there was a significant decrease in PD-1 expression (Figure 12D). These results together indicate that circulating exosomes from primary tumors are capable of infiltrating in the lung and increasing the expression of PD-L1 on the tissue resident interstitial macrophage population, inducing an exhausted T cell phenotype and further recruiting immunosuppressive MDSCs to the pre-metastatic site.

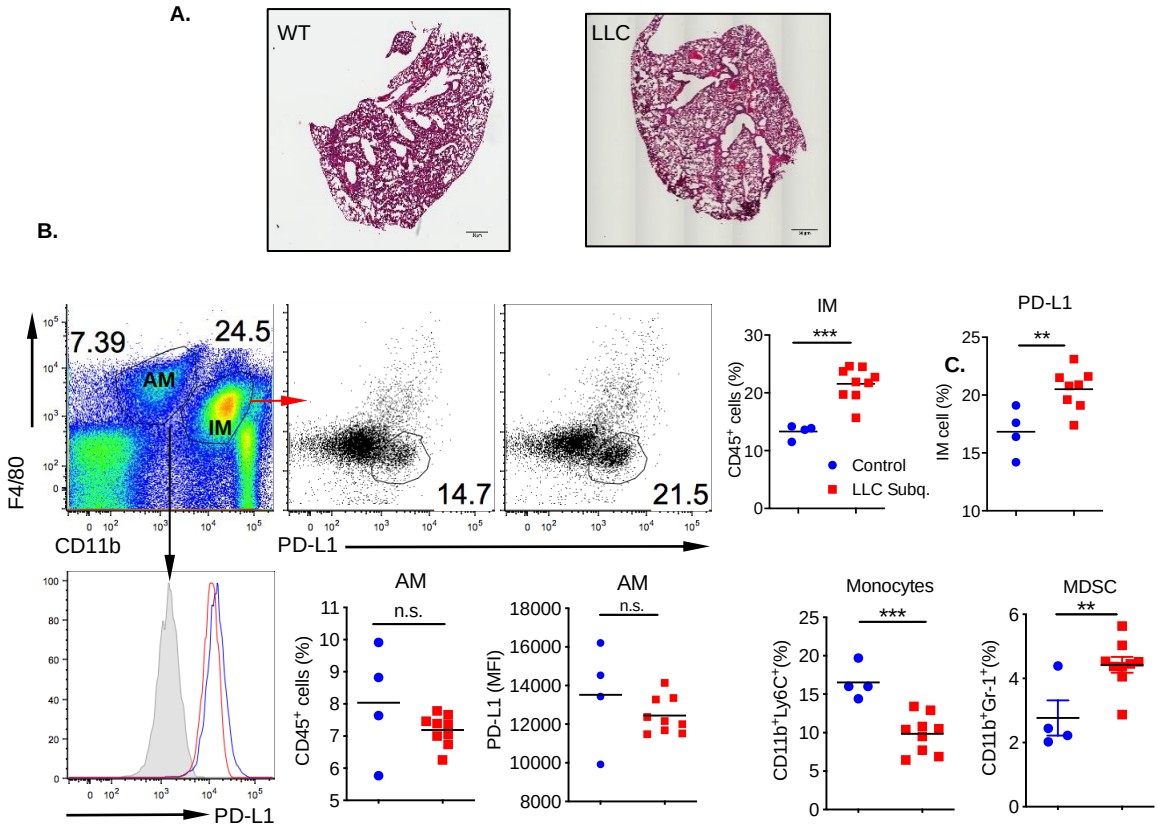

Figure 10. TDE augment tumor growth and metastasis (A) H&E section of naive (top) and LLC subcutaneous tumor bearing (bottom) lungs. Scale bar, 50μm. **(B)** Percentage of F4/80^{+}CD11b^{+} IM and representative PD-L1 expression plots in control versus LLC tumor bearing mice (top panels). F4/80^{+}CD11c^{+} AM percentage and overall PD-L1 expression in the lungs of control and LLC tumor bearing mice (bottom panels). control n=4; LLC tumor n=9. **(C)** Recruitment of circulating monocytes (CD11b^{+}Ly6C^{+}) and myeloid-derived suppressor cells (CD11b^{+}Gr-1^{+}) in the lungs of control versus tumor bearing mice. The data are shown as mean ± SEM. **p<0.01,

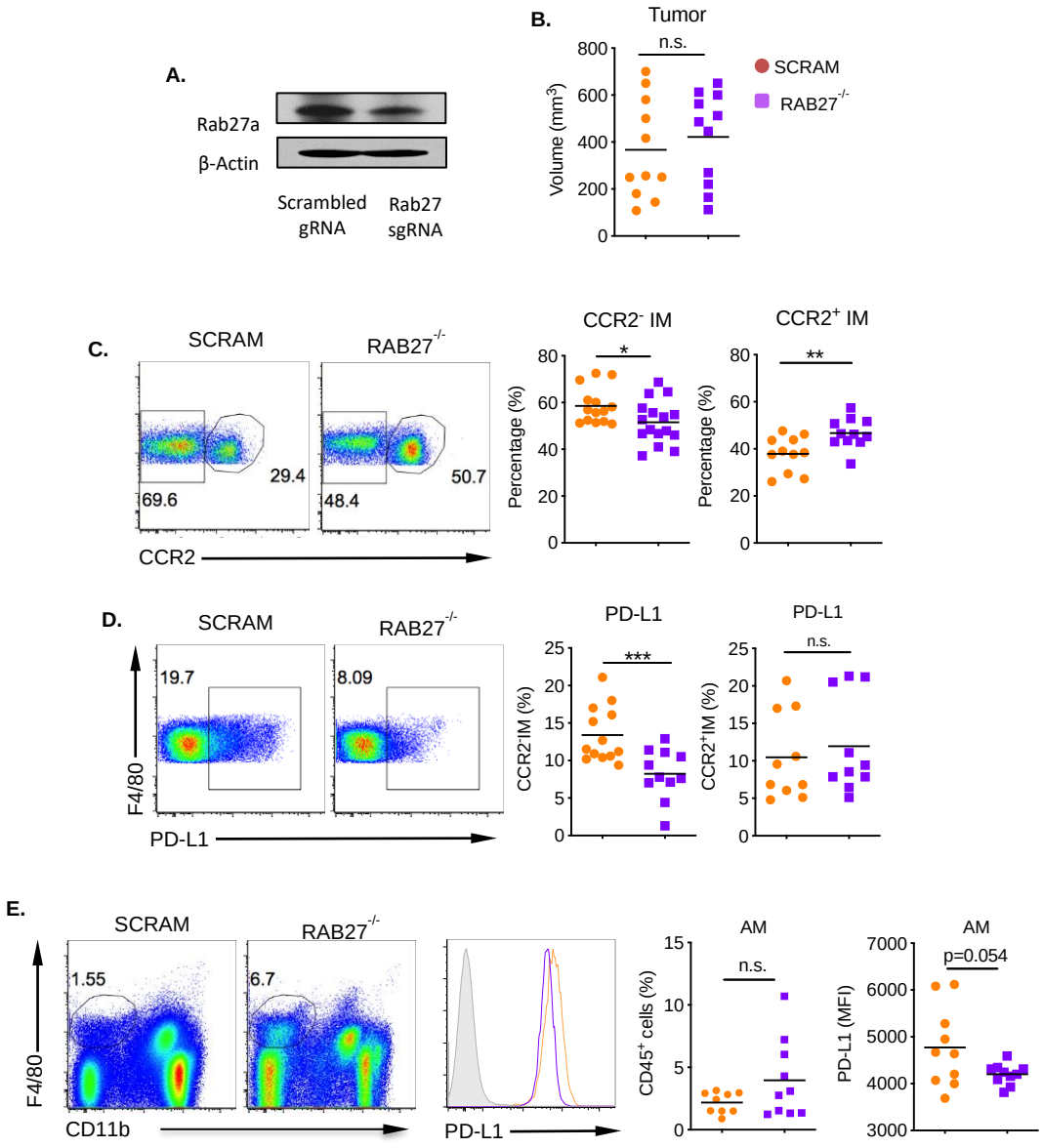

Figure. 11 *In vivo* assessment of TDE influence on myeloid PD-L1 (A) Representative WB for Rab27a protein expression in CRISPR/CAS9 generated Rab27a$^{-/-}$ 4T-1 tumor cells **(B)** Primary tumor volume 28 days post injection with 1.2x10^{6} SCRAM or Rab27a$^{-/-}$ 4T-1 tumor cells (n=11 per group). **(C-D)** CCR2 and PD-L1 expression on CD11b^{+} IM in the lungs of SCRAM versus RAB27$^{-/-}$ tumor bearing mice. n=12 per group. **(E)** Percentage and PD-L1 expression on F4/80^{+}CD11c^{+} AM in the lungs of SCRAM versus RAB27$^{-/-}$ tumor bearing mice. The data are shown as mean ± SEM. *p<0.05, **p<0.01, ***p<0.001 (unpaired student's t test).

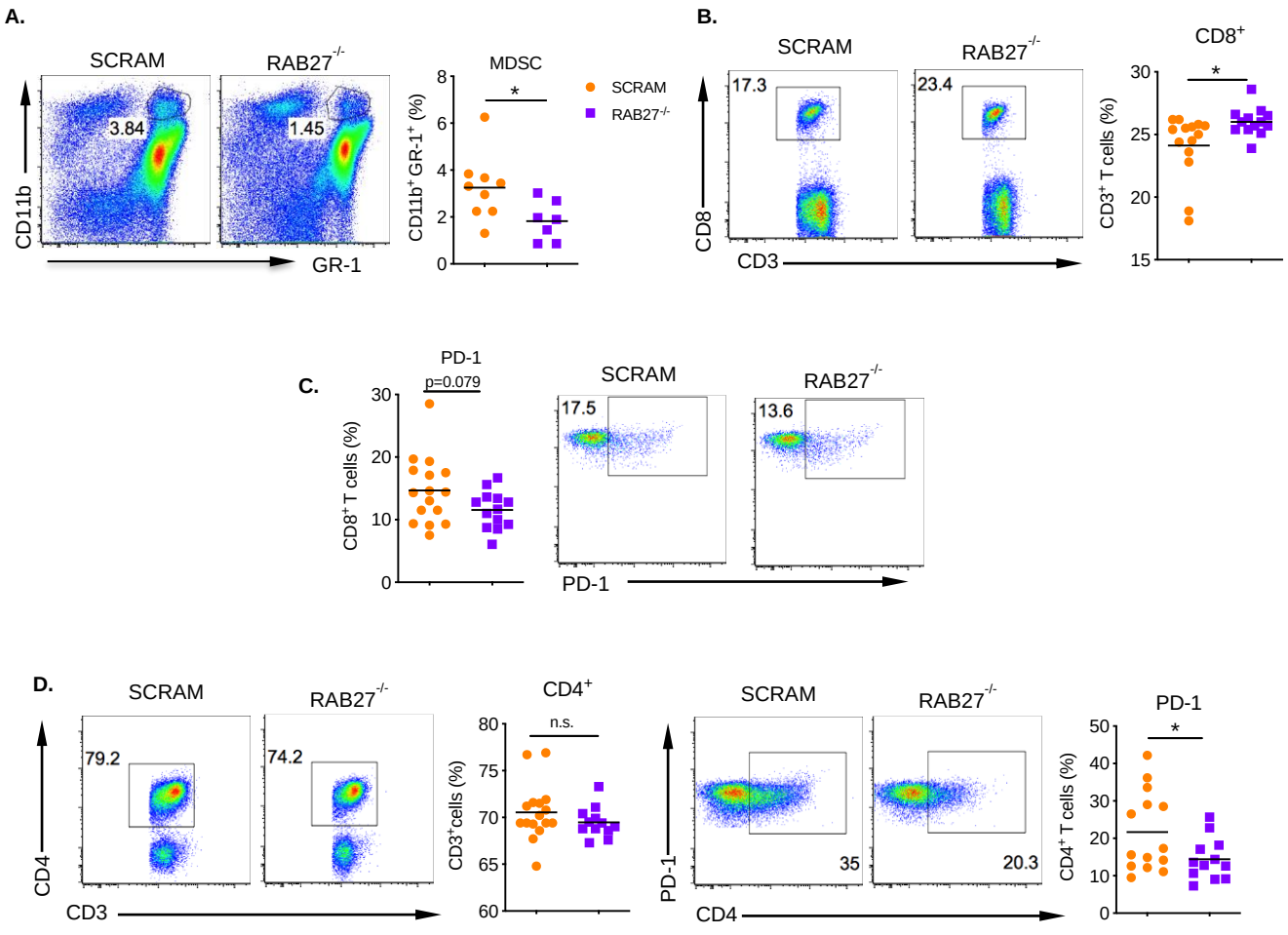

Figure. 12 *In vivo* assessment of TDE influence on immune compartment (A) Recruitment of MDSCs ($CD11b^{+}Gr\text{-}1^{+}$) into the lungs of SCRAM or $Rab27^{-/-}$ tumor bearing mice. Scram n=9; $Rab27^{-/-}$ n=7. **(B-C)** Percentage of $CD8^{+}$ T cells and PD-1 expression in the lung of SCRAM versus $RAB27^{-/-}$ tumor bearing mice **(D)** Percentage and PD-1 expression of $CD4^{+}$ T cells in the lung of SCRAM versus $RAB27^{-/-}$ tumor bearing mice. Representative dot plots and summarized data are shown. The data are shown as mean ± SEM. *p<0.05 (unpaired student's t test).

2.3.7 TDE polarize human $CD14^+$ cells to an immunosuppressive phenotype

To ascertain the clinical relevance of our findings, we examined if we could recapitulate the phenotype using exosomes derived from human tumor cells. As shown in Figure 13A, exosomes isolated from the human NSCLC A549 cell line but not the control human bronchial epithelial cell line (HBEC) significantly increased PD-L1 expression on $CD14^+$ monocytes. Co-culture of these treated $CD14^+$ cells with autologous $CD3^+$ T cells in the presence of plate bound anti-CD3 mAbs demonstrated that A549 TDE polarized $CD14^+$ cells drastically inhibited both CD4 and CD8 T cell proliferation as well as IFN-γ production from $CD8^+$ T cells (Figure 13B). Stimulation with recombinant human HMGB-1 increased PD-L1 expression in $CD14^+$ cells suggesting a least a partial role for HMGB-1 induced TLR2 activation (Figure 13C). Addition of TLR2-blocking antibody dramatically decreased PD-L1 expression indicating human exosomes also signal through TLR2 to drive PD-L1 expression (Figure 13D).

To further examine how our pre-clinical model could correlate with clinical outcomes, we obtained draining lymph node (dLN) samples from NSCLC patients that were negative for tumor cell infiltration to best mimic a pre-metastatic niche (Table 1). We compared those LNs to the LNs from lung transplant donors, which were considered to be healthy donors in this case. Overall analysis of surface marker expression within the myeloid cell compartment indicated increased levels of $CD16^+$, $CD33^+$, $CD63^+$, $CD68^+$, and $CD206^+$, suggesting an overall activated, classic M2 phenotype in cells from patient samples compared to those of healthy donors (Figure 14A). Furthermore, when specifically looking at CD206 and PD-L1 co-expression in the $CD68^+$ macrophages, there was roughly double the expression in the NSCLC cohort compared to healthy controls (Figure 14B). Notably, macrophage CD206/PD-L1 co-expression positively correlated with PD-1 expression on the $CD8^+$ T cells within the dLN (Figure 14C). viSNE

analysis of the $CD4^+$ T cell population also demonstrated increased PD-1 expression compared to healthy controls and a positive trending correlation with the macrophage CD206/PD-L1 expression (Figure 14D). Taking the immune phenotype markers together, principal component analysis (PCA) of the myeloid and T cell populations within the LNs demonstrated a significant difference in mean expression pattern between NSCLC patients and healthy donors (Figure 14E). Linear regression analysis of PC1 demonstrated the significance of disease state in accounting for variance within this profiling.

To determine whether the immunological changes within the dLN were associated with exosomal phenotype, we turned to the TCGA dataset to see if we could find any correlation between exosome release genes and nodal metastasis. We divided patients into two groups based on nodal staging, NX/N0 were considered negative whereas N1-N3 were considered positive for metastasis. Our screening revealed that two exosome released genes, YKT6 (Figure 15A) and TSG101 (Figure 15B), had higher expression in the primary tumor of lung adenocarcinoma patients with positive nodal metastasis compared to nodal negative. A similar phenotype for YKT6 was also seen in patients with colon adenocarcinoma (Figure 15C). Furthermore, the top quartile of lung adenocarcinoma patients expressing YKT6 demonstrated significantly poorer survival outcomes when compared to the bottom quartile of YKT6 expressing patients (Figure 15D).

We then turned to our own NSCLC patient cohort to substantiate the TCGA dataset results. We found that $CD45^-$ tumor cells displayed increased expression of YKT6 (Figure 15E) and TSG101 (Figure 15F) as compared to $CD45^+$ cells sorted from primary tumor. Furthermore, there was a trending positive correlation between YKT6 expression in the primary tumor cells and PD-L1 expression in the dLN (Figure 15G). TSG101 also

showed a trending positive correlation though not as robustly as YKT6 (Figure 15H). Grouping the NSCLC patients into cohorts based on their PD-L1 expression level (high >10% $CD68^{+}CD206^{+}PD\text{-}L^{+}$ and low <10% $CD68^{+}CD206^{+}PD\text{-}L^{+}$ expression), demonstrated a significantly increased YKT6 mRNA level in the $PD\text{-}L1^{high}$ cohort over the $PD\text{-}L1^{low}$ (Figure 15I). These results suggest at least a positive association in our NSCLC patient cohort between release of primary tumor derived exosomes and the immunosuppressive landscape of the myeloid and T cells in the dLN.

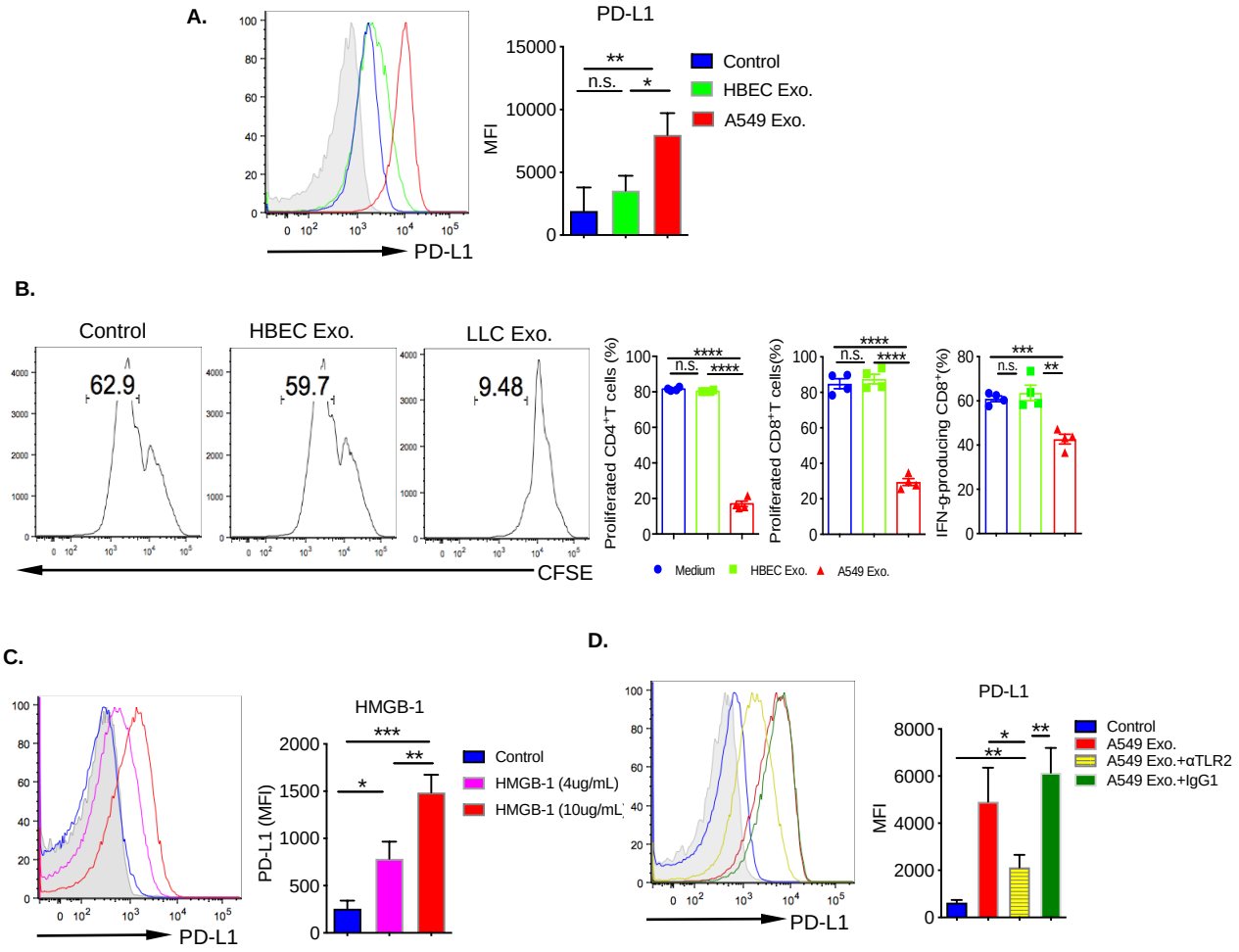

Figure 13. The effect of human TDE on human macrophages. **(A)** CD14⁺ myeloid cells were sorted from peripheral blood of healthy donors and stimulated with 40μg/mL of control human bronchial epithelial cell (HBEC) or A549 lung adenocarcinoma (A549) exosomes for 16 hours. PD-L1 expression was determined by flow cytometry (n=3 separate PBMC donors). Representative histogram and summarized data are shown. **(B)** Proliferation of autologous CD4⁺ and CD8⁺ T cells stimulated with plate bound anti-CD3 Abs in the presence of CD14⁺ cells previously cultured with A549 or HBEC exosomes (40μg/mL) for 48 hours. Data are representative from n=3 independent experiments. Representative dot plots and summarized data are shown **(C)** Sorted CD14⁺ cells were stimulated with the indicated dose of human recombinant HMGB-1 protein for 16 hours prior to flow cyotmetric analysis of PD-L1 expression. Representative histograms and summarized data are shown. n=4 healthy donors. **(D)** Sorted CD14⁺ cells were stimulated with 40μg/mL A549 exosomes with or without the addition of αTLR2 (40μg/mL) or IgG_1 blocking antibody. Representative histogram and summarized data are shown. The data are shown as mean ± SEM. *p<0.05, **p<0.01, ***p<0.001, ****p<0.0001 (one-way ANOVA with multiple comparisons).

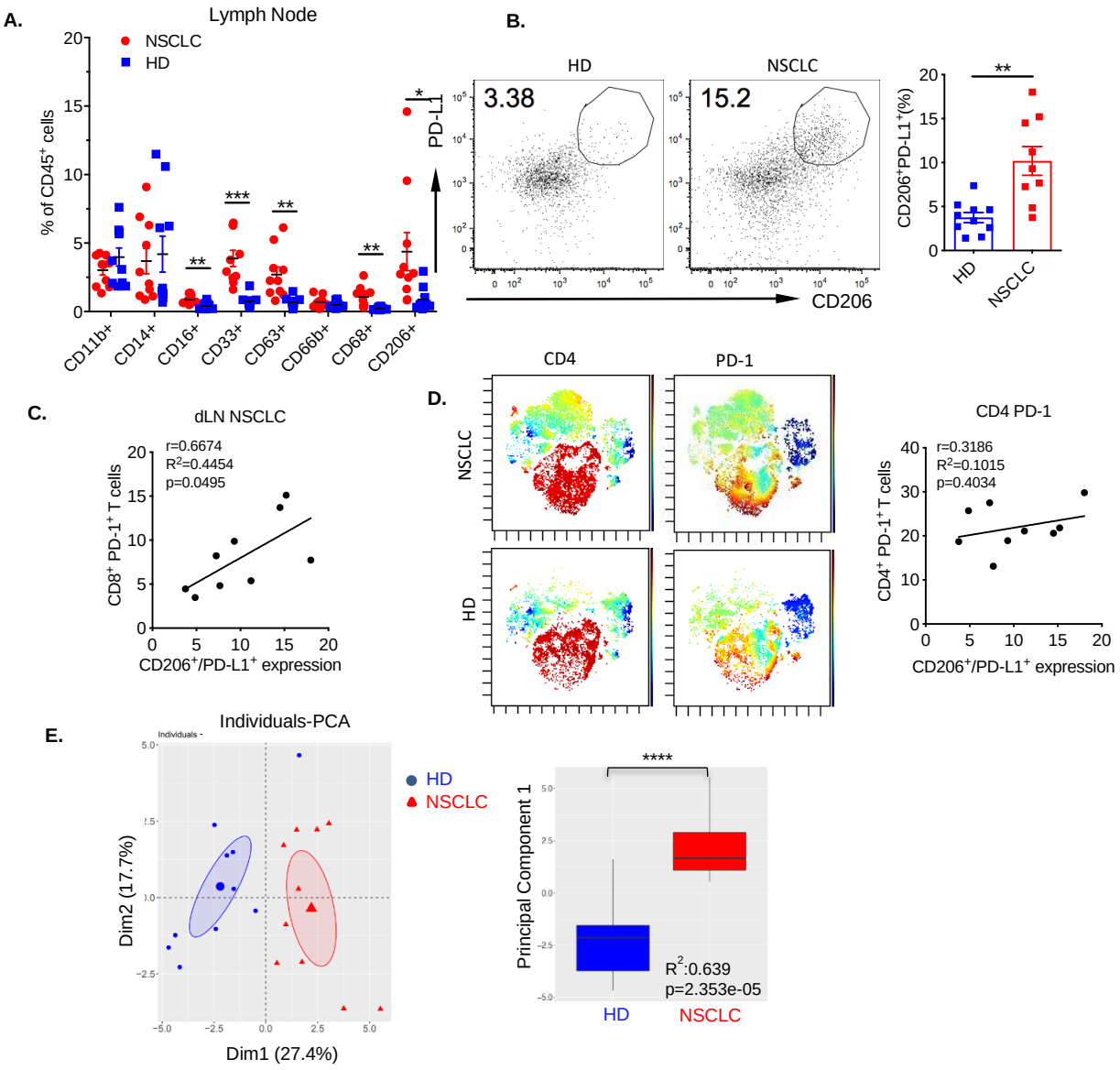

Figure 14. Immune phenotyping in dLN of NSCLC patients. **(A)** The expression of myeloid associated markers in lymph nodes of non-cancerous lung transplants (10 healthy donors) versus T1-3N0 NSCLC patients (n=9). **(B)** The expression of CD206 and PD-L1 on CD68+ macrophages in the draining lymph nodes of non-cancerous lung transplants (10 healthy donors) versus T1-3N0 NSCLC patients (n=9). **(C)** Pearson correlation between CD206/PD-L1^{+} macrophages and CD8^{+} PD-1^{+} T cells within the dLN. **(D)** Expression levels of CD4 and PD-1 across CD45^{+} cells from dLN of healthy donors and NSCLC patients illustrated in t-SNE plots. **(E)** Pearson correlation between PD-1 expression on CD4^{+} T cells and CD206/PD-L1 expression on CD68^{+} myeloid cells in dLN of NSCLC patients. **(F)** PCA plot of the first two principal components ("Dim1" and "Dim2"), depicting the relationships of NSCLC (red triangles) and HD (blue circles) subjects. The percent variance explained by each principal component is indicated in parentheses. The 95% confidence ellipses and centroids (enlarged symbols) for each group of samples (NSCLC and HD) are also shown (left). Boxplot depicting the values for the first principal component, partitioned by disease state (NSCLC vs. HD), as determined by PCA (right). ****p<0.0001 generated by linear regression. The data are shown as mean ± SEM. *p<0.05, **p<0.01, ***p<0.001(unpaired student's t test).

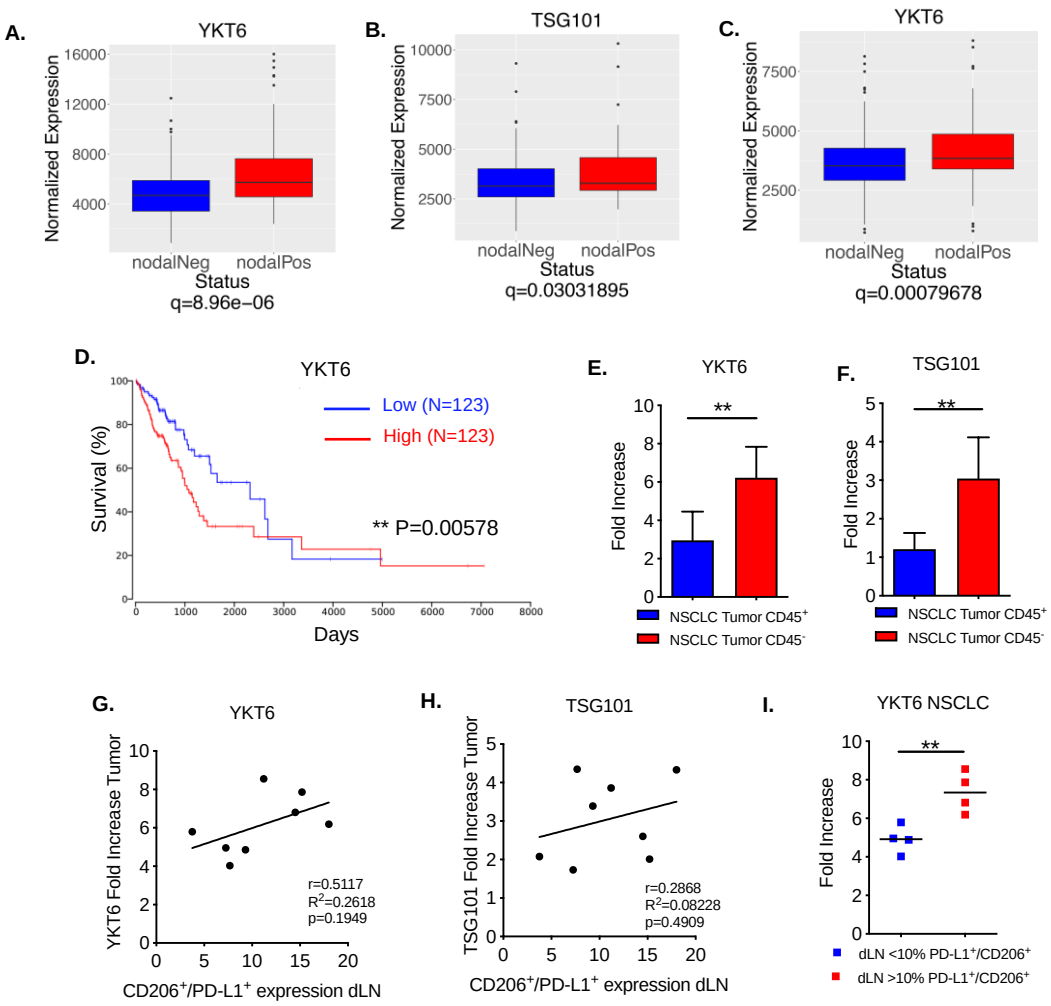

Figure 15. Correlation between TDE release and pre-metastatic niche. **(A)** Boxplot showing YKT6 expression in patients with negative nodal staging (N0) compared to positive nodal staging (N1-N3) in lung adenocarcinoma (LUAD) patients from the TCGA database. Plots were made with Deseq2's function plotCounts with count normalized to library size. Positive (N1-N3) n=85, Negative (NX/N0) n=156 **(B)** Boxplot depicting TSG101 expression in patients with negative nodal staging (N0) compared to positive nodal staging (N1-N3) in lung adenocarcinoma (LUAD). Plots were made with Deseq2's function plotCounts with count normalized to library size. Positive (N1-N3) n=85, Negative (NX/N0) n=156 **(C)** Boxplot depicting YKT6 expression in patients with negative nodal staging (N0) compared to positive nodal staging (N1-N3) in colon adenocarcinoma (COAD). Positive (N1-N3) n=193, Negative (NX/N0) n=283. **(D)** Kaplan-Meier survival curve generated by Oncolnc for TCGA dataset LUAD patients based on expression profile (High= top 25%) and (low=bottom 25%) of YKT6. n=123 per group. **p<0.01 (log rank test). **(E)** YKT6 expression in $CD45^+$ versus $CD45^-$ cells in primary tumor from NSCLC patients. n=8. **(F)** TSG101 expression in $CD45^+$ versus $CD45^-$ cells in primary tumor from NSCLC patients. n=8. **(G)** Pearson correlation between YKT6 expression in NSCLC tumor $CD45^-$ cells and CD206/PD-L1 expression on $CD68^+$ myeloid cells in dLN n=8. **(H)** Pearson correlation between TSG101 expression in NSCLC tumor $CD45^-$ cells and CD206/PD-L1 expression on $CD68^+$ myeloid cells in dLN. n=8. **(I)** YKT6 mRNA expression levels in NSCLC patient primary tumors grouped by CD206/PD-L1 expression level (high >10% $CD68^+CD206^+PD\text{-}L^+$ and low <10% $CD68^+CD206^+PD\text{-}L^+$ expression) in $CD68^+$ macrophages within the dLN. n=4 patients per group. The data are shown as mean ± SEM. *p<0.05, **p<0.01 (unpaired student's t test).

2.4 DISCUSSION

Discussion

The formation of a pre-metastatic niche is a cornerstone for cancer metastasis. Without a favorable local microenvironment, circulating cancer cells will not be able to engraft and grow. Immune suppression is one of the defining characteristics of a pre-metastatic niche and it is believed that one of the key modulators of this phenotype are macrophages [35]. However, how macrophages acquire their immunosuppressive characteristics within the pre-metastatic niche has yet to be clearly elucidated. In this study, we demonstrate that TDE polarize tissue resident macrophages towards an immunosuppressive phenotype through NF-kB-dependent signaling.

Immune checkpoint blockade (ICB) therapy using either PD-1 or PD-L1 antibodies has demonstrated significant clinical benefit with the overall response rate for NSCLC hovering between 17-21% [87]. While it was originally thought tumor cells were the main source of PD-L1-mediated suppression, recent studies have indicated that PD-L1 expression on antigen presenting cells (APCs) such as dendritic cells or macrophages play a more dominant role in determining efficacy of PD-1 ICB therapy [46, 88]. Given the importance of PD-L1 on myeloid cells, it is paramount to determine what drives expression of PD-L1. PD-L1 expression on exosomes themselves has been credited to induce an overall immunosuppressed phenotype in both mice and humans [62]. In our study, elimination of exosome secretion from the primary tumor decreased expression of PD-L1 on lung resident F4/80^{+}CD11b^{+}CCR2^{-} IM and decreased recruitment of MDSCs, while increasing effector T cell infiltration. *In vitro* analysis demonstrated that exosomes

from tumor cells alone increased the *de novo* synthesis of PD-L1 in macrophages. We conclude that PD-L1 expression on macrophages induced by TDE is not dependent on exosomal PD-L1 transfer. Several lines of evidence support this conclusion including increased PD-L1 mRNA levels and a complete dependence on TLR2 and MyD88 signaling. In an attempt to determine what exosomal factor(s) elicits the TLR2 activation, we assayed for the effect of known metastasis-associated protein and TLR2 ligand, HMGB-1 on driving PD-L1 expression. UVB radiation of melanoma cells previously has been shown to increase their expression of PD-L1 in an HMGB-1 dependent manner [84]. While they found tumor secreted HMGB-1 signals through RAGE, here we demonstrate that exosomal HMGB-1 signals through TLR2 to increase expression of PD-L1 on myeloid cells in both mice and humans. Elimination of HMGB1 in primary subcutaneous tumors decreased the number of metastatic lesions in the lung pointing towards a causative role in tumor metastasis.

One caveat to mention regarding our studies focuses on the heterogeneity of the exosomal pool. Recent studies have shown that there are different subtypes and subpopulations of exosomes released from the same parent cell[89, 90]. Our experiments used a single pool of exosomes isolated from cancer or normal tissue cell lines. Therefore, going forward, it would be interesting to investigate whether there are subpopulations of exosomes within our isolate and how those impact on our phenotype. Specifically, are there necessary or identifiable characteristics of a particular exosomal subtype that drive PD-L1 expression in myeloid cells?

In an effort to determine if exosomes contribute to pre-metastatic niche formation in human cancer patients, we used dLN samples from cadaveric lung transplant organs as healthy controls and compared them to dLN from NSCLC patients. Specifically, we chose LN samples from patients with T1N0-T3N0 staging to investigate the immune

landscape of LNs that at least by current practices in staging are negative for tumor cell infiltration and could best mimic a pre-metastatic niche in humans[91]. Assuming the staging is correct, the patient dLN display an already increased proportion of $CD206^{+}PD\text{-}L1^{+}$ macrophages, particularly for some patients, as compared to healthy donor controls. Macrophage PD-L1 expression positively correlated with PD-1 expression on $CD8^{+}$ T cells. Taken together these findings point towards an altered immune profile despite negative nodal staging.

To demonstrate a link between nodal metastasis and exosomes from primary tumors, we found that out of the 20 known exosome release genes, two in particular, YKT6 and TSG101 correlated with positive metastatic nodal staging in the LUAD patient cohort within the TCGA database [92]. We were able to substantiate this data using dLN and primary tumor samples from our own NSCLC patient cohort. Specifically, there was a trending correlation between YKT6 expression in the primary tumor cells and PD-L1 expression on macrophages in the dLN. The lack of significance is most likely due to the limited size of the patient samples. Nevertheless, grouping the 8 patients into cohorts based on their PD-L1 expression level (high >10% $CD68^{+}CD206^{+}PD\text{-}L^{+}$ and low <10% $CD68^{+}CD206^{+}PD\text{-}L^{+}$ expression), YKT6 mRNA levels were significantly increased in the high cohort over the low. Collectively, these results suggest that primary tumors capable of secreting high amounts of TDE have an increased likelihood of metastasis due to the ability of TDE to reprogram the immune landscape within the pre-metastatic site towards an immunosuppressive $PD\text{-}L1^{+}$ phenotype on macrophages.

A recent study profiling immune activation and evasion throughout the developmental stages of carcinogenesis in human lung squamous cell carcinoma found an increased abundance of M1 macrophages in high grade lesions and early carcinoma as compared to low grade lesions clearly demonstrating the M1 phenotype is not solely

pro-inflammatory in nature but could be pro-carcinogenic as well [93]. Further analysis of these high-grade lesions showed enrichment for CD80, PD-L1, IL-10, and IL-6, an immunomodulatory profile that bears a striking resemblance to our TDE-stimulated "non-classical M1" macrophages. Additional studies in early stage lung cancer have also shown that M1 macrophages exhibit the highest expression level of PD-L1 and CD80 compared to TAM and classical M2 [77]. Collectively, these data emphasize the potential clinical relevance of our study. The presence of PD-L1^{+}, "non-classical M1" macrophages along with other tumor promoting characteristics could be used as an immune biomarker to indicate early primary carcinogenesis or, as we propose, pre-metastatic niche formation. Analysis of the composition within the sentinel lymph nodes for PD-L1 expression on macrophages could be useful in assessing the metastatic potential of that site. It is also important to consider the potential of targeting pathogenic exsomal release genes like YKT6. NSCLC patients with high YKT6 expression have previously been shown to have increased plasma concentrations of exosomes and worse survival outcomes [94]. Within our own NSCLC patient cohort, YKT6 was shown to be increased in primary tumors and positively correlated with an immunosuppressive phenotype within the dLN. The development of new therapeutics aimed at these targets could decrease the prevalence of immunosuppressive PD-L1^{+} macrophages in a pre-metastatic niche and lower the overall potential of primary tumor metastasis.

In summary, we discover that TDE polarize tissue-resident macrophages towards an immunosuppressive phenotype in a pre-metastatic niche. This immunosuppressive "non-classical M1" phenotype is characterized by: 1) increased *de novo* synthesis of PD-L1, 2) expression of Arg-1 and iNOS and 3) inhibition of T cell effector functioning. Our findings provide novel insight into how TDE orchestrate a pro-metastatic phenotype by reprogramming tissue resident macrophages. Pro-tumoral factors like IL-10, G-CSF, and

MCP-1 secreted from these “non-classical M1” macrophages further add to the downstream inflammatory milieu that ultimately characterizes a fully formed pre-metastatic niche. Notably in the future, it would be interesting to investigate whether disruption to this pathway could provide benefit in decreasing primary tumor metastasis or could improve the efficacy of immunotherapies currently failing due to exosomal induced PD-L1 expression.

3. TUMOR DERIVED EXOSOMES DRIVE PD-L1 EXPRESSION THROUGH METABOLIC REPROGRAMMING

3.1 Introduction

3.1.1 M1 versus M2 macrophage metabolism

The macrophage compartment is a diverse and plastic lineage. While certain subsets of macrophages, like tissue resident, are seeded in early development, others are polarized towards a specific functionality by environmental factors[43]. As a consequence of these different polarization mechanisms, the resulting macrophages often have specific characteristics that are associated with each particular type. Currently, the widely accepted paradigm is that there are two overarching classes of macrophages: M1-like macrophages which are pro-inflammatory in nature can be polarized by Th1 related cytokines while M2-like macrophages are influenced by Th2 related cytokines like IL-4 and are considered more immune dampening[95].

The idea of the M1 versus M2 macrophages activation spectrum originally came from experiments focused on the differential T lymphocyte responses to *Leishmania major* infection in resistant C57BL/6 versus susceptible BALB/c mice. T lymphocytes in C57BL/6 mice responded to the infection by producing large amounts of the macrophage activating cytokine, IFNγ. Consequently, macrophages in these mice had high expression of inducible nitric oxide synthase (iNOS) and generated large amount of nitric oxide (NO) to kill the pathogen. Conversely, macrophages from the BALB/c mice had increased expression of arginase and stimulated production of TGF-β rather than IFNγ from associated T cells. These seminal experiments established key identifying characteristics that are still used today to classify M1

versus M2 macrophages. Specifically, M1 macrophages are considered to express high levels of iNOS and produce inflammatory cytokines like TNFα and IL-1β whereas M2 macrophages have high arginine expression and secrete immune modulating cytokines like TGF-β, and IL-10[56, 96]. While there is only on class of M1 macrophages, M2 macrophages can be further broken down into M2a, M2b, M2c, and M2d, based on their polarization stimuli[97].

In addition to cytokine profile, one of the more common ways to distinguish macrophage subtype is through metabolic profiling. The dynamic changes in macrophage phenotype are also associated with characteristic signatures in cell metabolism. M1 macrophages mainly rely on glycolysis for energy production while M2 macrophages are more dependent on the citric acid cycle (TCA) and mitochondrial oxidative phosphorylation (Schematic 1) [98]. Since glycolysis is one of the simplest ways to produce energy in the cell, it is logical that this is the preferential mechanism of energy production in inflammatory macrophages which are first responders in the context of injury or infection[97]. Overall, in glycolysis, two molecules of ATP are generated for each unit of glucose converted into pyruvate. Other intermediate molecules are also generated during this process that can also be used for amino acid and fatty acid synthesis.

Following an immune response, infiltration of anti-inflammatory M2-like macrophages is necessary to prevent excess damage to host tissues. Therefore, their metabolic phenotype needs to mimic and support this function. M2-like macrophages mainly rely on increased expression of arginase to shuttle arginine into ornithine rather than NO[97]. Ornithine has been shown to increase cell growth and aid in wound healing. Additionally, other intermediates within the TCA cycle, like itaconate and α-ketoglutarate, have also been shown to perpetuate anti-inflammatory properties[99]. Relying on this mechanism of energy production not only produces 36 molecules of

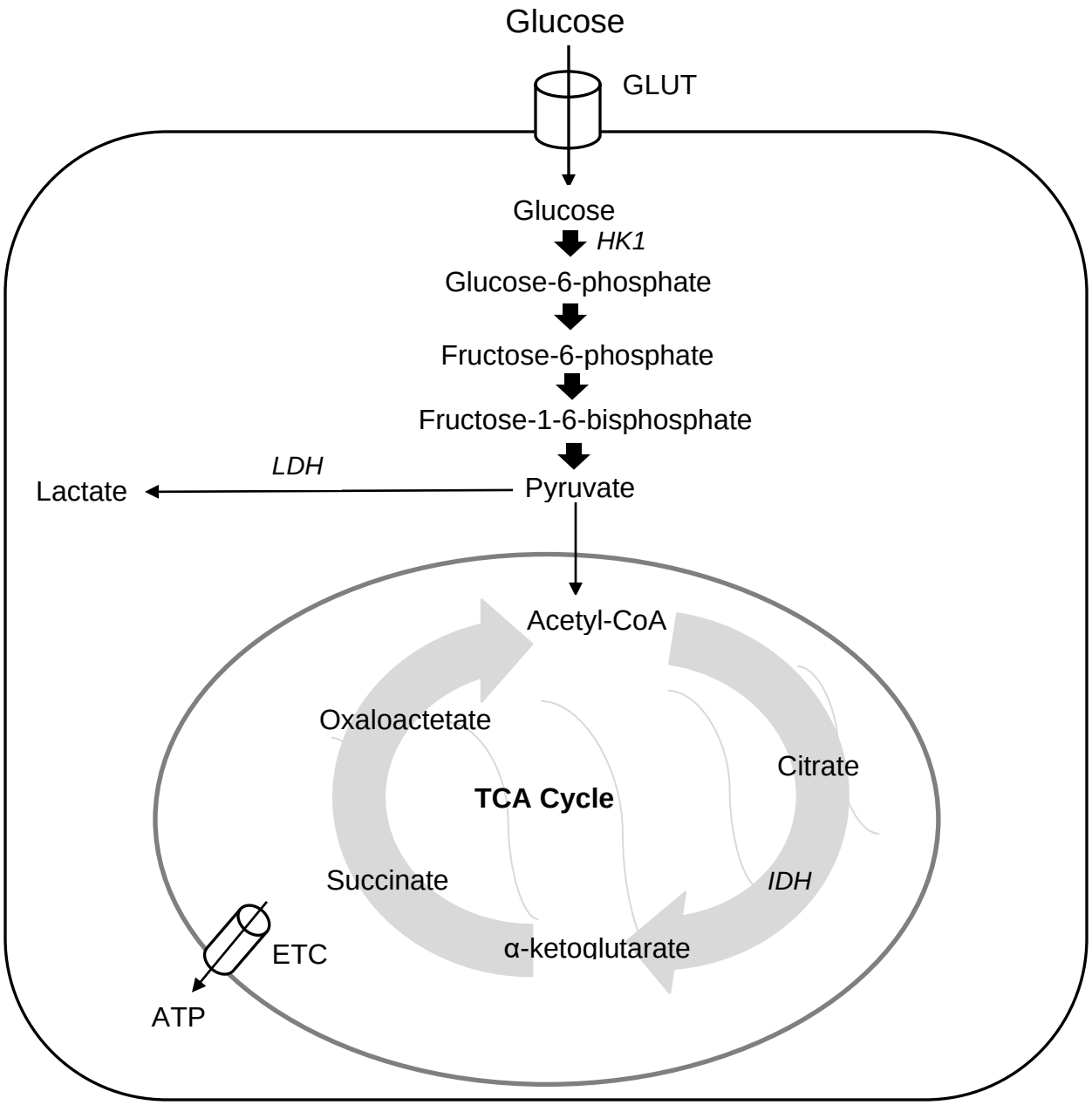

Schematic 1. Overview of glycolytic and oxidative metabolism. Generalized overview showing the different fates of glucose. HK1-hexokinase-1, LDH-lactate dehydrogenase, IDH-isocitrate dehydrogenase, ETC- electron transport chain

ATP for one unit of glucose, but the metabolic intermediates generated are also beneficial to M2 macrophages in functionally controlling inflammation.

3.1.2 Warburg Metabolism

In the context of cancer, TAMs are considered a subgroup of M2-like macrophages, specifically M2d[97]. They are polarized by TLR ligands, secrete immunosuppressive cytokines like IL-10, express characteristic surface markers of CD206, CD163, and like most M2's, have increased expression of Arginase-1 and indoleamine 2,3-dioxygenase (IDO-1). The immunosuppressive "M2-like" phenotype of TAMs is often credited to promote tumor angiogenesis, growth, and metastasis[100]. Classically then, it was thought that TAMs metabolic signature would be similar to the other counterparts in the subgroup, namely oxidative phosphorylation. Isolation of macrophages from a variety of tumors did indeed show dependence on mitochondrial respiration and increased oxygen consumption[101, 102, 103]. However, more recent reports seemingly suggest that the TAM metabolic phenotype is closely linked to time and tumor staging[104].

Transcriptomic studies conducted on early tumors demonstrate a pronounced glycolytic phenotype in macrophages that display characteristic M2 associated markers such as Arg-1, CD206 and CD163[105]. Overtime, as the tumor microenvironment becomes more hypoxic as the diffusion gradient of oxygen decreases due to increasing tumor size, TAMs began to switch to a less glycolytic and more oxidative phenotype[106]. Macrophages isolated from pancreatic ductal adenocarcinoma (PDAC) lesions demonstrated marked increased in extracellular acidification rate (ECAR) and decreases in oxygen consumption[107]. Interestingly, these macrophages were shown to help tumor cells undergo EMT and extravasate through a mock endothelial lumen. Inhibition of glycolysis using 2-DG blunted the pro-

metastatic capabilities of the TAMs. This phenomenon of preferentially using glycolysis despite normoxic conditions is called the Warburg Effect[108].

The Warburg effect was first described in the 1920's by Otto Warburg and his colleagues who noticed that tumor cells were utilizing more moles of glucose than the surrounding tissue[109]. Today, this is the basis for Fluoro-deoxyglucose Positron Emission Tomography (FDG-PET) that is used clinically to image and visualize growing tumors in the body. There have been many different speculations as to why tumor cells would choose to forgo quantity of ATP over rate of ATP production including increased utilization of a limited resource, enhanced disruption to tissue architecture and immune cell evasion, and promotion of flux into biosynthetic pathways[109]. While these questions remain the topic of further investigation in the field, one fact regarding Warburg Metabolism is consistent, the production of the metabolic by-product lactate.

3.1.3 Lactate

Lactate is normally produced under anaerobic conditions such as during a strenuous workout regimen in which the oxygen demands of the muscles surpasses the oxygen concentration in the tissue resulting the generation of the lactate[110]. However, while the exact mechanism is unknown, cancer cells choose to convert the majority of their glucose into lactate despite both normoxic conditions and incurred deficit of ATP production. One proposed hypothesis is that aerobic glycolysis and lactate production is an immunological defense mechanism[111]. Glucose is an essential nutrient to immune cells while lactate is not. Therefore, by consuming the essential resource for localized immune cells, particularly lymphocytes, tumors are able to starve out and neutralize the immunological threat. Additionally, lactate has directly been shown to inhibit proliferation and effector function of cytotoxic T cells[112, 113].

Acidification of the local microenvironment by lactate also results in decreased lymphocyte viability and functionality[108].

While lactate is detrimental to immune cells, multiple studies have shown lactate to be a beneficial metabolite to tumor cells. Lactate promotes tumor cell growth and expansion[114, 115]. Additionally, while lactate kills off the cytotoxic lymphocytes, it is also capable of reprogramming infiltrating macrophages to a pro-tumoral phenotype[116]. A recent seminal study determined that lactate is capable of inducing a novel epigenetic modification on macrophage histones called lactylation[117]. In the context of M1 polarizing stimuli, M1 macrophages generate copious amount of both intracellular and extracellular lactate. This pool of lactate results in lacytlation of exposed histone lysine residues triggering the “lactate clock”. Overtime, as lacytlation levels increase, homeostatic genes like Arg-1 are activated. These results support the claim that in the context of cancer, TAMs start as glycolytic Warburg like M1s but then overtime transition to the classical M2 phenotype.

3.1.4 Summary and Findings

The purpose of this study was to determine the mechanism by which TDE polarize tissue resident macrophages within a pre-metastatic site towards an immunosuppressive phenotype. Overall, with this study, we uncover a novel link between exosomes, metabolism, and glycolytic metabolism. Specifically, we show that TDE through NF-κB signaling, drive a highly glycolytic phenotype reminiscent of Warburg metabolism in stimulated macrophages. These cells are shunted down the glycolytic path by increases in nitric oxide which directly inhibit oxidative phosphorylation. As a consequence of increased glycolysis, there is a marked increase in secretion of lactate from these cells. We found that this increased pool of lactate feeds back on the cells and promotes PD-L1 upregulation. Inhibition of glycolysis via 2-deoyxglucose or inhibition of lactate production

with oxamate, dramatically reduced the glycolytic capacity, and PD-L1 expression. A similar phenotype was seen with exosomes isolated from human NSCLC cell lines. Additionally, in the dLN of NSCLC patients, PD-L1 expression positively correlated with GLUT-1 expression on resident macrophages. Taken together, our findings support the idea that TDE drive primary tumor metastasis through NF-κB mediated reshaping of macrophage glycolytic metabolism resulting in an immunosuppressive phenotype characterized by increased PD-L1 expression and lactate secretion.

3.2 MATERIALS AND METHODS

3.2.1 Mice

C57BL/6 mice were purchased from commercially available vendors. LysM-cre;HIF1-$\alpha^{fl/fl}$ mice were generated by crossing LysM$^{Cre/wt}$ and HIF-1$\alpha^{f/f}$ mice both which were purchased from Jackson Laboratory (Bar Harbor, ME). LysM$^{wt/wt}$ x HIF-1$\alpha^{f/f}$ mice were used as controls. LysM-cre;Raptor$^{fl/fl}$ and LysM-cre;Rictor$^{fl/fl}$ mice were generated in a similar manner. All animals were housed and treated in accordance with institutional guidelines and approved by the Institutional Animal Care and Use Committee at the University of Louisville, Louisville, KY.

3.2.2 NF-κB Phosphoflow studies

For intracellular phosphorylation studies, peritoneal macrophages were seeded in a 24 well plate ($0.5x10^6$/well). Cells were then stimulated with sodium L-lactate 20mM for the indicated time. Cells were then harvested from the plate and pelleted by centrifugation. They were then stained for viability. Cells were washed, pelleted, and resuspended in 100µl of 4% formaldehyde per 1 million cells and fixed for 15 minutes at room temperature. Cells were then washed with PBS. Ice cold methanol (2mL) was then added to the cells while gently vortexing to a make a final concentration of 90%

methanol. Cells were permeabilized on ice for 10 minutes. Cells were then washed in excess PBS twice to remove methanol. Primary phospho-NF-κB p65 (Ser536) (93H1) (1:1600) and F4/80-APC was then added and incubated at RT for 1 hour. Cells were then washed in PBS twice. 100µl (0.625:100) secondary donkey anti-rabbit IgG Alexa Fluor 555 (Biolegend) was added and incubated at RT for 30 minutes in the dark. Cells were washed with PBS and ran on the BD FACS Canto (BD Biosciences).

3.2.3 NF-κB Confocal Translocation

For NF-κB translocation studies, peritoneal macrophages were plated on a glass cover slip in a 24 well dish and stimulated with sodium L-lactate for the indicated time. Cells were then washed with PBS, permeabilized with 0.3% Triton 100x, and stained with primary antibody NF-κB p65 (D14E12) (1:100) overnight at 4°C, washed with PBC and stained with secondary donkey anti-rabbit IgG Alexa Fluor 555 (Biolegend) (1:100) for 1 hour at room temperature. Fluorescent images were obtained using a Nikon confocal microscope A1R with appropriate lasers.

3.2.4. Quantitative PCR

Total RNA was extracted using TRizol (Invitrogen) and isolated according to manufacturer's instructions. cDNA was generated using the iScript cDNA Synthesis Kit (Bio-Rad). mRNA expression analysis was carried out using iQ SYBR Green (Bio-Rad). RNA concentration was quantified using NanoDrop RNA 6000 nano-assays and analyzed using the CFX Connect PCR Machine (Bio-Rad). See Table S2 for the primer sequences.

3.2.5 Seahorse Extracellular Flux Assay

An XF96e Analyzer (Agilent Technologies, Santa Clara, CA) was used to measure bioenergetic function in isolated peritoneal macrophages. Prior to the run, sorted peritoneal macrophages were plated at a concentration of $0.6x10^5$cells/ well. Cells were stimulated with MLE-12 or LLC exosomes (40 µg/mL) overnight. For all bioenergetic measurements, the culture media was changed 1 h prior to the assay run to unbuffered Dulbecco's Modified Eagle Medium (DMEM, pH 7.4) supplemented with 11 mM D-Glucose (Sigma cat. G7528), 2 mM L-glutamine (Mediatech cat. 61-030-RM), and 100 µM L-carnitine (Sigma cat. C0283). The final concentrations of oligomycin (port A), FCCP (port B), and antimycin A/rotenone (port C) were 2 µg/ml, 2.5 µM and 10 µM/1 µM, respectively. Three basal OCR measurements were recorded prior to injection of oligomycin. After recording the oligomycin-sensitive OCR, FCCP-sensitive rates were recorded. Finally, antimycin A/rotenone was injected to inhibit electron flow through the electron transport system. As a secondary measurement, extracellular acidification rate (ECAR) was also recorded, and 2-deoxyglucose was injected at final concentration of 250 µM (port D) to interrogate the contribution of glycolysis to ECAR.

3.2.6 Mitochondria Staining

Cells were washed with PBS and resuspended in pre-warmed 0.1% BSA solution. Following Fc blocking, cells were stained with Mitotracker Red (20nM) and MitoTracker Green (80nM) for 30 minutes at 37°C. Cells were then stained for surface markers. For DCFDA staining, 100µL of 40µM DCFDA (abcam) was added to 100µL of cells ($1x10^6$) and incubated in the dark at 37°C for 30 minutes. Cells were then washed with PBS and stained for flow cytometry like normal.

3.2.7 *In vitro* metabolism assays

2-NBDG (100μM, BioVision) was added to peritoneal macrophages previously cultured in glucose free RPMI for 2 hours. The following concentrations of metabolic inhibitors or substrates were used for 16 hour cell culture: 2-deoxy-D-glucose (1mM, Sigma), Sodium oxamate (10mM, Sigma), SEITU (1mM-5mM, Cayman Chemical), Dimethyl-2-oxoglutarate (1mM-5mM, Sigma), Sodium-L-Lactate (20mM, Sigma). Levels of L-lactate in the supernatants were measured by L-Lactate Assay Kit I (Eton Bioscience, San Diego, CA) according to manufacturer's instructions.

3.2.8 In vivo ^{18}FDG uptake experiment

8-10 week old C57BL/6 mice were injected i.v. with LLC exosomes (10μg, in 100μl PBS) every 3 days for 2 weeks. Mice were fasted for 12 hours prior to intraperitoneal injection with ^{18}FDG. One hour after injection, the mice were euthanized, lungs were harvested and measured on a Biodex Atomlab™ 500 for radioactivity. Lung tissue was enzymatically digested (collagenase (5g/L), Hyaluronidase(0.4g/L), DNAse I (0.15g/L)) for 20 minutes with rotation at 37°C. Following digestion, RBC's were lysed using ACK. Cells were stained with primary Biotin anti-mouse CD19 (Biolegend,115504), secondary Streptavidin MicroBeads (Miltenyl Biotec,130-048-101), CD8a (Ly-2) MicroBeads (Miltenyl Biotec,130-049-401), CD4 (L3T4) (Miltenyl Biotec,130-049-201) for 15 minutes. Cells were then magnetically separated on an autoMACS Pro separator (Miltenyl Biotec) using the positive selection protocol. The negative fraction was then collected and read on a Biodex Atomlab™ 500 for radioactivity. Cells were then resuspended in Trizol and saved in the -80°C for RT-PCR.

3.2.9 Human metabolism Studies-*In vitro* culture

Sorted $CD14^+$ cells were pre-incubated with BAY-11-7082 (0.2μg/mL) for 1 hour prior to 16 hour stimulation with A549 exosomes. Metabolic assays were conducted using the same concentrations and procedures as the mouse protocols.

3.2.10 Human NSCLC Samples

Samples were obtained as approved by the University of Louisville Institutional Review Board. Draining LN were obtained from lung transplant donors during lung resection and from cancer patients during tumor resection and/or biopsy. Patient information was summarized in Table S1. Lymph node samples were analyzed via flow cytometry using Viability Dye-APC-Cy7, CD68-PercP, CD206-PE, PD-L1-Pe-Cy7, and GLUT-1-primary (R&D, Clone 202915), secondary (R&D,α-mouse IgG-APC).

3.3.1 TDE stimulation augments glycolytic phenotype in macrophages

Macrophages can undergo polarized activation depending on different environmental cues[99]. The binary M1/M2 macrophage paradigm previously proposed considers M1 macrophages to be pro-inflammatory, relying on glycolytic metabolism, while M2 are pro-tumor, oxidative phosphorylation dependent [98]. This dichotomy is now being challenged by the idea of an overlapping macrophage spectrum with cells capable of exhibiting both anti-tumoral and pro-tumoral characteristics depending on environmental context [96]. Nevertheless, macrophage phenotype and polarization are closely associated with metabolic reprogramming. To first explore if metabolic alterations drive TDE-mediated macrophage polarization, glucose-deprived macrophages were co-cultured with 2-NBDG to assay glucose consumption. TDE-stimulated macrophages had significantly increased glucose uptake over control macrophages (Figure 16A). To determine if glucose metabolism was directly impacting the PD-L1 expression, peritoneal macrophages were cultured with 2-deoxyglucose (2-DG) with or without TDE treatment. 2-DG mediated

disruption to glycolytic metabolism significantly downregulated PD-L1 expression following TDE stimulation suggesting a role for glycolysis in driving PD-L1 expression (Figure 16B). Further analysis of metabolic enzymes showed increases in glucose transporter-1 (GLUT-1), hypoxia inducible factor-1α (HIF1-α), and lactose dehydrogenase A (LDHA) expression (Figure 16C). Pyruvate dehydrogenase kinase 1 (PDK1), inhibitor of the pyruvate dehydrogenase complex was also increased but in both of the exosome-stimulated groups. Analysis of hexokinase-1 (HK1) and isocitrate

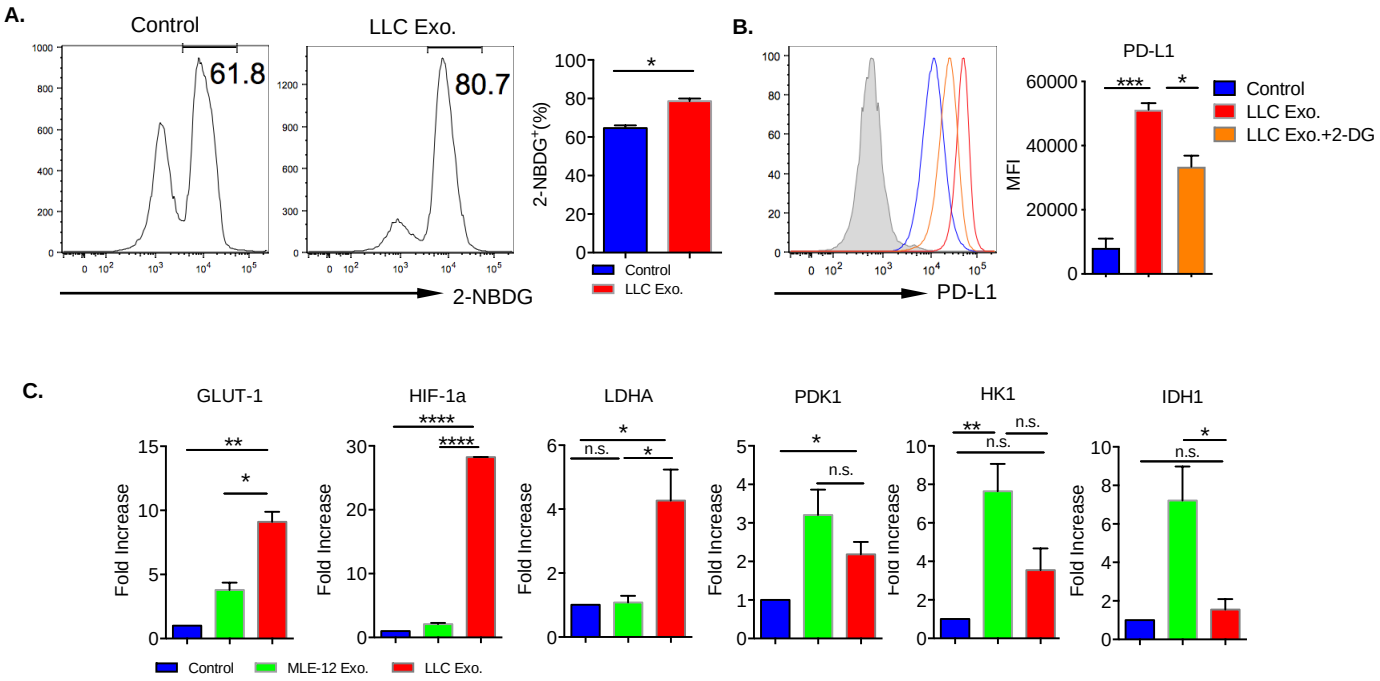

Figure 16. Metabolic phenotyping in TDE stimulated macrophages. **(A**) Peritoneal macrophages were pre-cultured in glucose depleted RPMI-1640 for 2 hours prior addition of 100μM 2-NBDG for 16 hours. Representative histograms and summarized data are shown. n=3. *p<0.05 (unpaired student's t test). **(B)** Peritoneal macrophages were cultured with or without LLC exosome (40μg/mL) in the presence or absence of 1mM 2-DG for 16 hours. PD-L1 expression was determined by flow cytometry. Representative histogram and summarized data are shown. n=3. **(C)** Peritoneal macrophages were stimulated with MLE-12 or LLC exosomes for 6 hours prior to quantification of glucose transporter-1 (GLUT-1), Hypoxia inducible factor-1α (HIF-1α), lactate dehydrogenase (LDHA), pyruvate dehydrogenase kinase 1 (PDK1), Hexokinase-1 (HK-1), and Isocitrate dehydrogenase-1 (IDH1), by RT-PCR. Data normalized to control expression level. n=3 mice per group. The data are shown as mean ± SEM. *p<0.05, **p<0.01, ***p<0.001, ****p<0.0001 (one-way ANOVA with multiple comparisons).

dehydrogenase-1 (IDH1) demonstrated no considerable differences in TDE-stimulated macrophages compared to control.

Increased glucose uptake coupled to increased GLUT-1, HIF-1α, and LDHA expression suggest that TDE stimulated macrophages favor a highly glycolytic metabolic profile despite being in normoxic conditions. To confirm this hypothesis, we performed a Seahorse assay which measures both the extracellular acidification rate (ECAR) and oxygen consumption rate (OCR) in stimulated cells. As shown in Figure 17A, LLC exosome stimulated macrophages had an increased ECAR as compared to the controls. Interestingly, as shown in the OCR, the LLC exosome-stimulated macrophages were unresponsive to mitochondrial inhibitors, oligomycin and FCCP. This effect was not due to an excessive TDE treatment (Figure 17B). The bioenergetic profile showed a dramatic decrease in ATP-linked energy production in the TDE group, indicating a defect in mitochondrial respiration (Figure 17C). We evaluated the mitochondrial status of TDE-stimulated macrophages using Mitotracker Green and Mitotracker Red staining that can distinguish between respiring mitochondria (MitoTracker Red^{+}) and dysfunctional mitochondria (MitoTracker Green$^{+/high}$, MitoTracker Red$^{+/low}$) [118]. Contrary to the media alone and MLE-12 exosome controls, LLC exosome-stimulated macrophages had a decreased proportion of solely Mitotracker Green^{+} cells and an increased number of Mitotracker Red^{+} cells (Figure 17D), indicating more respiring mitochondria.

3.3.2 TDE inhibit oxidative phosphorylation via nitric oxide

The bioenergetic profile also showed a high level of non-mitochondrial oxygen consumption in the TDE treated macrophages signifying another mechanism outside of mitochondrial ATP generation was utilizing the oxygen (Figure 17C). DCFDA staining showed TDE-stimulated macrophages generated less reactive oxygen species (ROS)

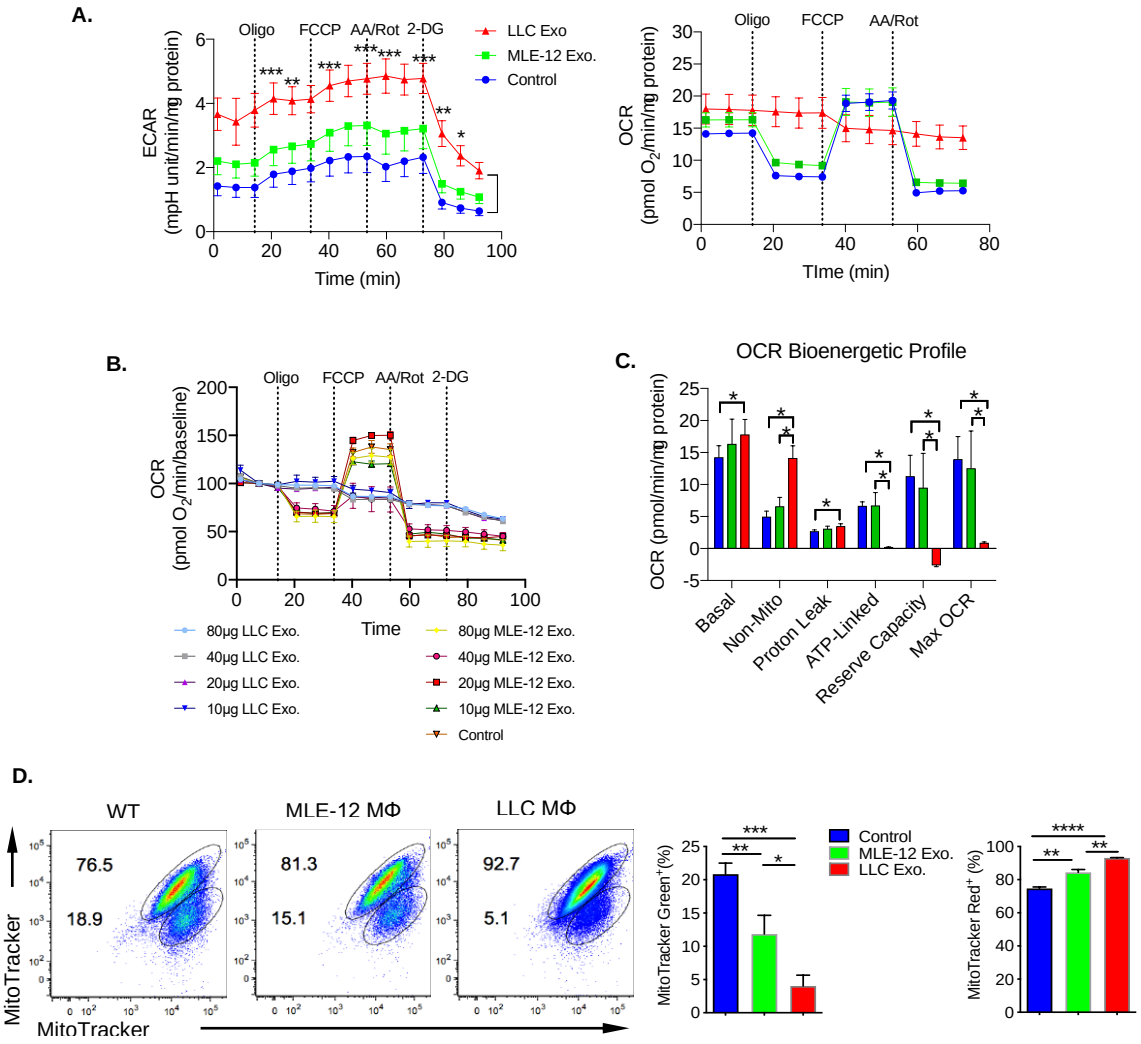

Figure 17. Glycolytic Phenotype in TDE stimulated macrophages. **(A)** ECAR (left) and OCR (right) of F4/80^{+} peritoneal macrophages were sorted from peritoneal lavage and seeded in Seahorse XF-96 cell culture microplates (0.6x10^{5} cells/well). The cells were then pre-treated with MLE-12 or LLC exosomes (40µg/mL) for 16 hours, followed by sequential treatment with Oligomycin, FCCP, and antimycin A plus rotenone. Data are representative for n=4 independent experiments. **B)** F4/80^{+} peritoneal macrophages were sorted and seeded in Seahorse XF-96 cell culture microplates (0.6x10^{5} cells/well). The cells were then pre-treated with indicated concentrations of MLE-12 or LLC exosomes for 16 hours, followed by sequential treatment with Oligomycin, FCCP, and antimycin A plus rotenone. Data are representative for n=2 independent experiments **(C)** OCR Bioenergetic profiling showing relative values of parameters for representative Seahorse assay. **(D)** Peritoneal macrophages stimulated with control or TDE exosomes (40µg/mL) for 16 hours were stained with MitoTracker Red (20nM) and MitoTracker Green (80nM). Cells were assayed for mitochondrial functionality via flow cytometry. Representative flow plots and summarized data are shown. The data are shown as mean ± SEM. *p<0.05, **p<0.01, ***p<0.001, ****p<0.0001 (one-way ANOVA with multiple comparisons).

than the two control groups eliminating this as the potential source of oxygen consumption (Figure 18A). Another molecule often found within the tumor microenvironment that utilizes oxygen is nitric oxide (NO) [119]. In addition to consuming free oxygen, NO can inhibit the electron transport chain via interfering with proper functioning of complexes III and IV within actively respiring mitochondria (Figure 18B)[120]. To test if NO mediated mitochondrial inhibition was occurring, we measured intracellular NOS2 expression following LLC exosome stimulation and indeed found increased expression (Figure 18C), which agrees with the previously shown mRNA iNOS data (Figure 5C). Addition of the NOS2 inhibitor, S-ethylisothiourea hydrobromide (SEITU) completely rescued the oxidative respiration capacity of the macrophages (Figure 18D). The bioenergetic profile demonstrated properly restored ATP synthesis in a dose dependent manner, indicating that NO is indeed responsible for inhibiting oxidative respiration (Figure 18E). Furthermore, stimulation of peritoneal macrophages with TDE in the presence of SEITU decreased PD-L1 expression suggesting that the PD-L1 is directly tied to glycolytic and not oxidative metabolism (Figure 18F). NOS2 expression in TDE stimulated macrophages was dependent on MyD88 signaling (Figure 18G) but independent of HIF1-α (Figure 18H) indicating that NOS2 and HIF-1α influence glycolysis through two separate mechanisms.

3.3.3 HIF-1α is downstream of NF-κB in the TDE signaling cascade

Further investigation into HIF-1α's role in TDE metabolic reprogramming revealed that deficiency in HIF-1α results in decreased GLUT-1 expression and a marginal decrease in PD-L1 expression following TDE stimulation (Figure 19A). TDE stimulation in MyD88$^{-/-}$ macrophages dramatically decreased both HIF-1α and GLUT-1 expression indicating that these factors are indeed downstream of TLR2 signaling and are mediated by exosome ligation (Figure 19B). Interestingly, inhibition of NF-κB via BAY also

decreased HIF-1α expression indicating HIF-1α activation lies downstream of NF-κB (Figure 19C). Collectively, these data demonstrate that TDE polarize macrophages to increase PD-L1 expression through metabolic reprogramming. Specifically, NF-κB is the master transcription factor that activates HIF-1α/GLUT-1 to bring more glucose into macrophages and NOS2/NO to inhibit mitochondrial oxidative phosphorylation shunting pyruvate into lactate. Stimulation with oxidative metabolite, α-ketoglutarate, completely abolished PD-L1 expression in TDE stimulated macrophages (Figure 19D), further strengthening the causative relationship between glycolysis and PD-L1 expression.

3.3.4 Glycolytic metabolism fuels lactate production and PD-L1 expression

One of the classic hallmarks of Warburg metabolism is not only glycolysis in normoxic conditions but also the shunting of pyruvate away from Acetyl-CoA and into lactate. Having demonstrated that TDE polarize macrophages towards a highly glycolytic phenotype reminiscent of Warburg metabolism, we hypothesized that lactate production may be enhanced in TDE-treated macrophages and lactate may act as the critical metabolite to induce PD-L1 expression. To test these hypotheses, we first measured the concentration of lactate in the supernatant from macrophage culture. As compared to the other controls, stimulation with TDE augmented lactate secretion (Figure 20A). Increasing numbers of macrophages expectedly increased the concentration of secreted lactate following TDE stimulation (Figure 20B). The increased lactate was a result of exosomal ligation and signaling through the MyD-88 pathway (Figure 20C). Inhibition of NF-κB also decreased lactate production following TDE stimulation (Figure 20D). HIF-1α deficiency notably abrogated the amount of secreted lactate but not back to baseline providing further evidence for the contribution of the NOS2 pathway to lactate secretion (Figure 20E). In addition, the mRNA expression of lactate exporter, monocarboxylate

transporter-4 (MCT4) was increased, which may account for the increased ability of these cells to secrete lactate into the supernatant (Figure 20F). We next sought to determine if lactate was the ultimate downstream metabolite of augmented glycolysis that was responsible for driving increased PD-L1 expression. Stimulation of peritoneal macrophages with lactate did increase PD-L1 expression (Figure 21A). Furthermore, Phosflow assay revealed that lactate induced phosphorylation of NF-κBp65 at 15 and 30-minutes (Figure 21B). These results were verified using a confocal microscopy that demonstrated peak NF-kBp65 translocation into the nucleus at 30 minutes following lactate stimulation and regression to the cytoplasm by one hour (Figure 21C). Flow cytometric analysis further confirmed lactate indeed induced PD-L1 expression in an NF-κB-dependent manner (Figure 21D). RT-PCR results recapitulated this finding (Figure 21E). RT-PCR analysis also showed an increase in lactate importer monocarboxylate transporter-1 (MCT-1) following TDE stimulation suggesting extracellular as well as intracellular lactate can be driving this phenotype (Figure 21F).

Having shown that TDE stimulation increases the secretion of lactate and that lactate is indeed capable of upregulating PD-L1, we next validated this conclusion by inhibiting lactate synthesis following TDE stimulation using the LDHA inhibitor oxamate (OXA). As shown in Figure 21G, stimulation of macrophages with TDE in the presence of OXA decreased the expression of PD-L1 thus supporting our hypothesis that lactate is indeed the downstream effector metabolite that can drive autocrine PD-L1 expression through NF-κB activation. Together, these data show a novel role for lactate in driving PD-L1 expression. Specifically, we propose in our model that TDE signaling activates NF-κB and its downstream effectors NOS2 and HIF-1α, to augment glycolytic metabolism and shunt pyruvate into lactate (Figure 21H). The newly synthesized lactate is able to

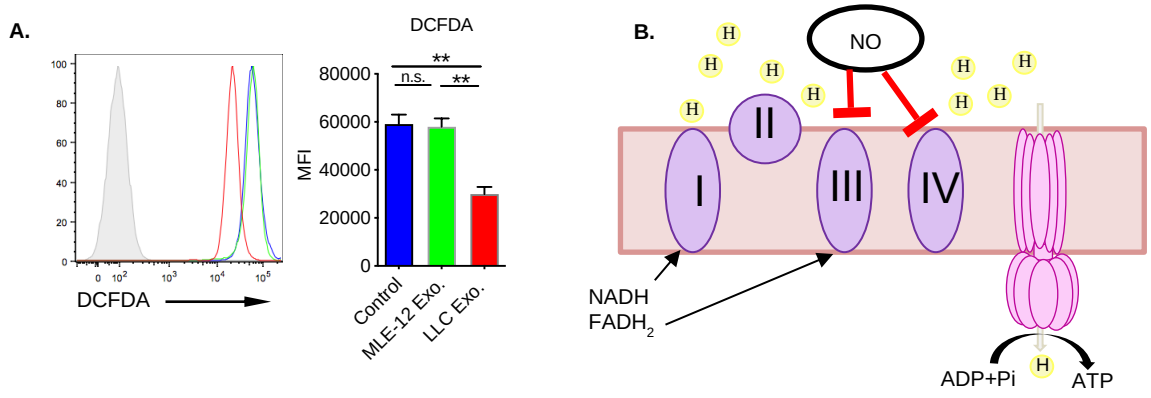
A.
DCFDA
MFI
n.s.
Control
MLE-12 Exo.
LLC Exo.
B.
NO
H
I
II
III
IV
NADH
FADH2
ADP+Pi
ATP

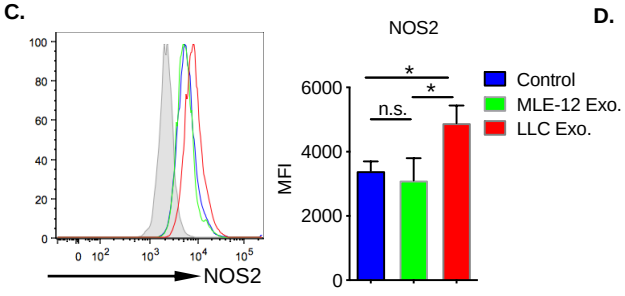
C.
NOS2
MFI
n.s.
Control
MLE-12 Exo.
LLC Exo.

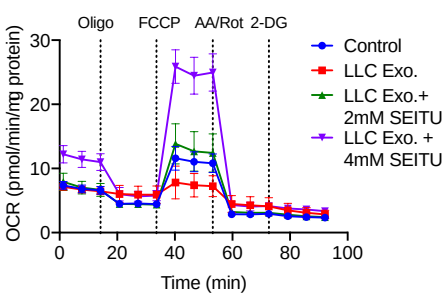
D.
Oligo
FCCP
AA/Rot
2-DG
OCR (pmol/min/mg protein)
Time (min)
Control
LLC Exo.
LLC Exo.+ 2mM SEITU
LLC Exo. + 4mM SEITU

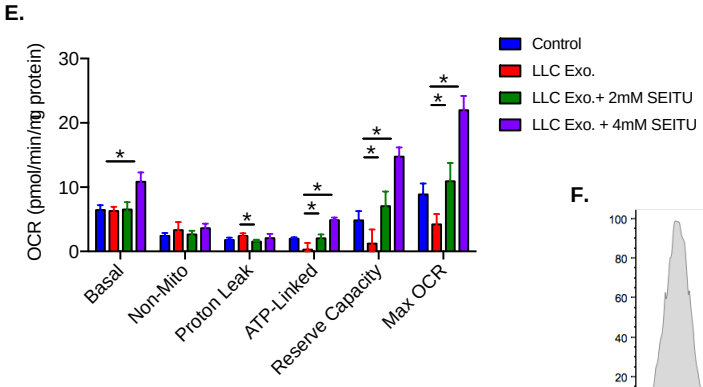
E.
OCR (pmol/min/mg protein)
Basal
Non-Mito
Proton Leak
ATP-Linked
Reserve Capacity
Max OCR
Control
LLC Exo.
LLC Exo.+ 2mM SEITU
LLC Exo. + 4mM SEITU

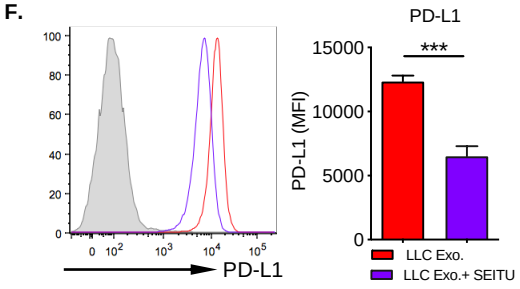
F.
PD-L1
PD-L1 (MFI)
LLC Exo.
LLC Exo.+ SEITU

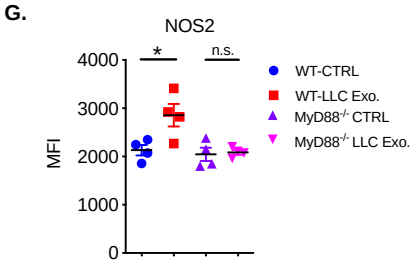
G.
NOS2
MFI
n.s.
WT-CTRL
WT-LLC Exo.
MyD88-/- CTRL
MyD88-/- LLC Exo.

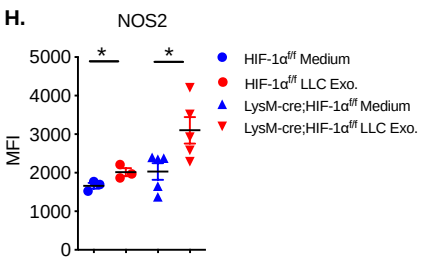
H.
NOS2
MFI
HIF-1α f/f Medium
HIF-1α f/f LLC Exo.
LysM-cre;HIF-1α f/f Medium
LysM-cre;HIF-1α f/f LLC Exo.

Figure 18. Nitric Oxide drives glycolytic phenotype. **(A)** DCFDA/Reactive Oxygen species content (20μM) analyzed by flow cytometry in macrophages stimulated with control or TDE (40μg/mL) for 16 hours. Representative histograms and summarized data are shown. (n=3). **(B)** Schematic diagram depicting the electron transport chain (ETC) and NO mediated inhibition. **(C)**. Intracellular NOS2 expression in peritoneal macrophages stimulated with MLE-12 or LLC exosomes for 16 hours. Representative histogram and summarized data are shown (n=3). **(D)** $F4/80^{+}$ peritoneal macrophages were sorted and seeded in a Seahorse XF-96 cell culture microplate ($0.6x10^{5}$ cells/well), stimulated with or without LLC exosomes (40μg/mL) for 16 hours in the presence of 2mM or 4mM SEITU and real-time OCR was determined at basal level and in response to sequential treatments of oligomycin, FCCP, antimycina/rotenone, and 2-DG. Data are representative of two independent experiments with similar results. **(E)** OCR bioenergetic profiling showing relative values of parameters for representative Seahorse Assay where peritoneal macrophages were treated with NOS2 inhibitor, SEITU. **(F)** Expression of PD-L1 in peritoneal macrophages treated with TDE with or without SEITU. (4mM) for 16 hours. Representative histogram and summarized MFI data are shown. n=3. ***p<0.001 (unpaired student's t test). **(G)** Intracellular NOS2 expression of WT or $MyD88^{-/-}$ peritoneal macrophages stimulated with LLC exosomes (40μg/mL) for 16 hours assessed by flow cytometry. n=4 mice per group. **(H)** Intracellular NOS2 expression in $HIF\text{-}1\alpha^{f/f}$ and LysM-cre;$HIF\text{-}1\alpha^{f/f}$ peritoneal macrophages following 16 hour stimulation with LLC exosomes. n=3 mice per $HIF\text{-}1\alpha^{f/f}$ control group; n=4 mice per LysM-cre;$HIF\text{-}1\alpha^{f/f}$ group. The data are shown as mean ± SEM. *p<0.05, **p<0.01, ***p<0.00, ****p<0.0001 (one-way ANOVA with multiple comparisons).

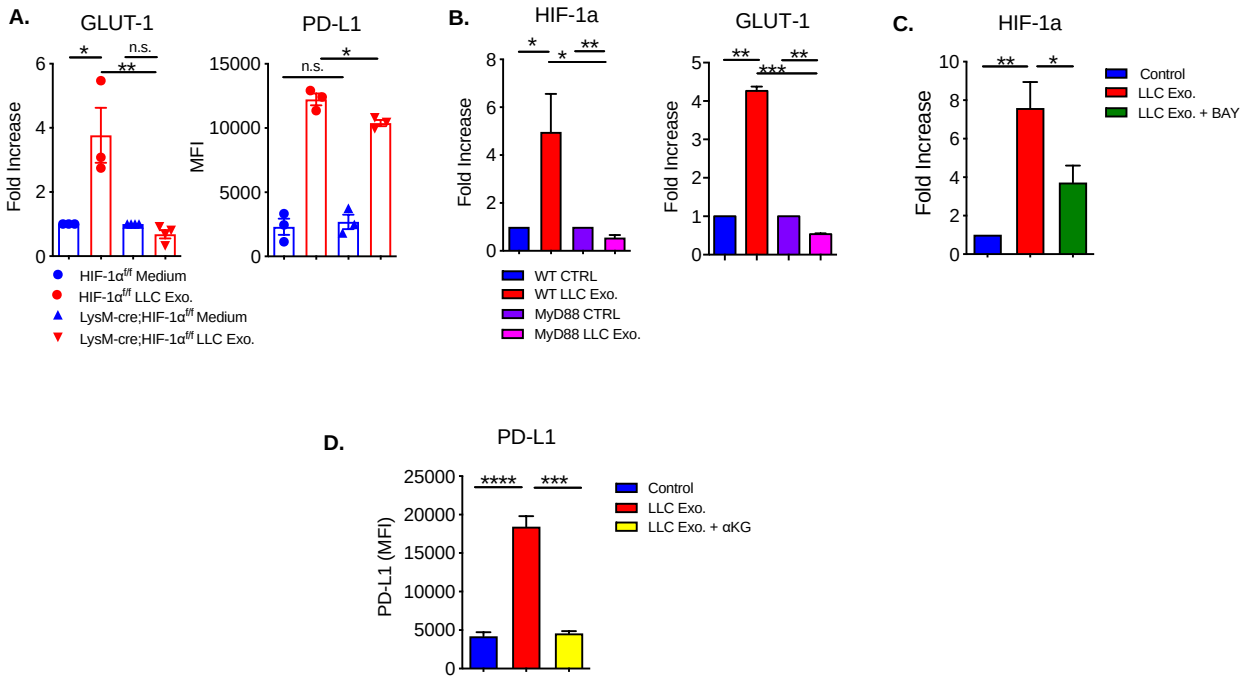

Figure 19. The role of HIF-1α in the TDE signaling cascade (A) RT-PCR analysis of GLUT-1 mRNA (left) and PD-L1 surface (right) expression in HIF-1α$^{fl/fl}$ and LysM-cre; HIF-1α$^{fl/fl}$ peritoneal macrophages treated for 6 hours and 16 hours, respectively, with LLC exosomes **(B)** The mRNA expression levels of HIF-1α and GLUT-1 expression in wild type or MyD88$^{-/-}$ peritoneal macrophages stimulated with LLC exosomes (40μg/mL) for 6 hours. n=4 mice per group. **(C)** The mRNA expression levels of HIF-1α in peritoneal macrophages pre-treated with the NF-κB inhibitor, BAY-11-7082 (0.2μg/mL) for 1 hour prior to 6 hour LLC exo. stimulation. n=3. **(D)** PD-L1 expression in peritoneal macrophages co-cultured with LLC exosomes and dimethyl-α-Ketoglutarate for 16 hours n=3. The data are shown as mean ± SEM. *p<0.05, **p<0.01, ***p<0.001 (one-way ANOVA with multiple comparisons).

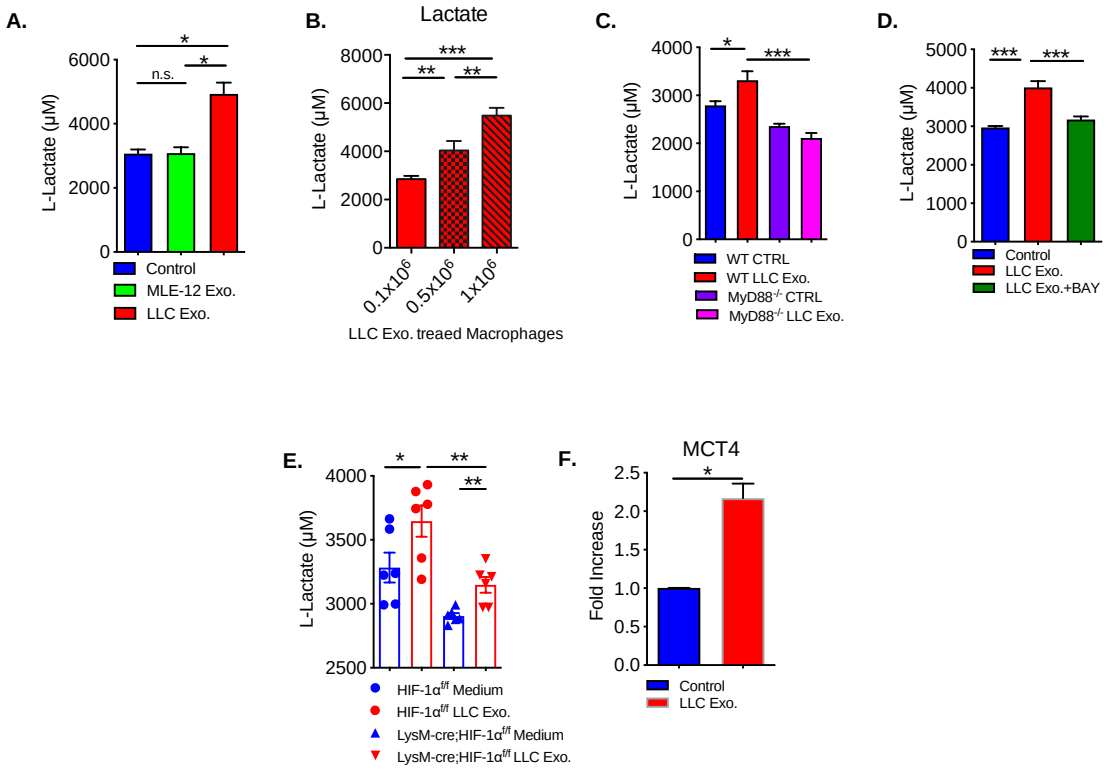

Figure 20. Glycolytic metabolism fuels lactate production (A) Supernatants from peritoneal macrophages treated with MLE-12 or LLC exosomes (40μg/mL) for 16 hours were collected. Levels of L-lactate in the supernatants were determined by lactate assay kit. n=3. **(B)** Concentration of L-lactate in the supernatant of increasing numbers of peritoneal macrophages treated with LLC exosomes. n= 3 mice per group. **(C)** Level of L-lactate in the supernatant of WT or MyD88$^{-/-}$ macrophages stimulated with TDE exosomes for 16 hours. n=3. **(D)** L-lactate levels in the supernatant of peritoneal macrophages pre-treated with 0.2μg/mL BAY-11-7082 for 1 hour prior to 16 hour stimulated with TDE. n=3. **(E)** Supernatants from HIF-1α$^{f/f}$ and LysM-cre;HIF-1α$^{f/f}$ peritoneal macrophages treated with LLC exosomes (16 hours) were collected and L-lactate concentration was determined. **(F)** The mRNA expression levels of monocarboxylate transporter-4 (MCT-4) on peritoneal macrophages treated with TDE for 6 hours. n=3. Expression levels were normalized to the control. *p<0.05 (unpaired student's t test). The data are shown as mean ± SEM. *p<0.05, **p<0.01, ***p<0.00, ****p<0.0001 (one-way ANOVA with multiple comparisons).

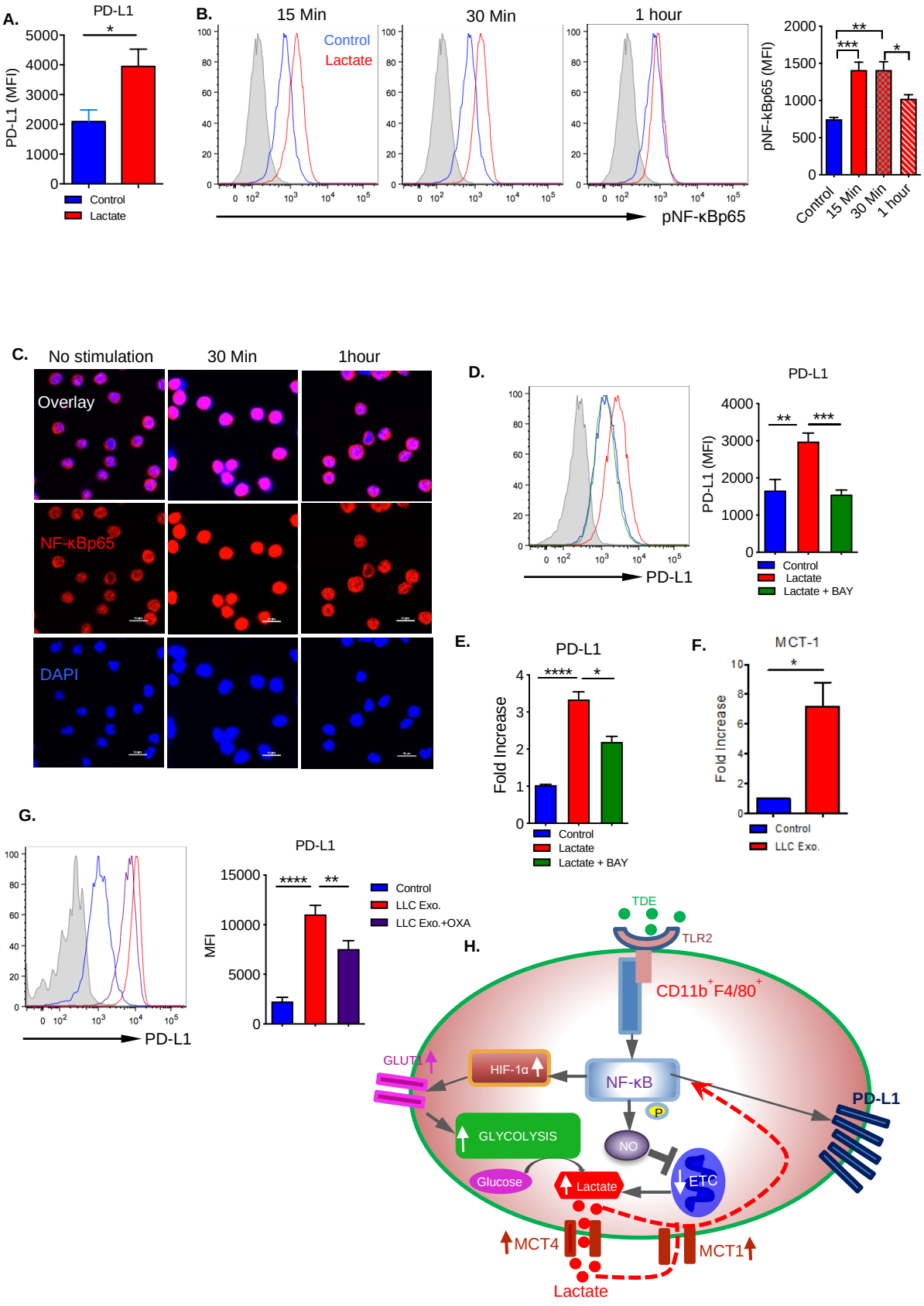
A.
PD-L1
PD-L1 (MFI)
Control
Lactate
B.
15 Min
30 Min
1 hour
Control
Lactate
pNF-κBp65
pNF-κBp65 (MFI)
Control
15 Min
30 Min
1 hour
C.
No stimulation
30 Min
1hour
Overlay
NF-κBp65
DAPI
D.
PD-L1
PD-L1 (MFI)
Control
Lactate
Lactate + BAY
E.
PD-L1
Fold Increase
Control
Lactate
Lactate + BAY
F.
MCT-1
Fold Increase
Control
LLC Exo.
G.
PD-L1
MFI
Control
LLC Exo.
LLC Exo.+OXA
H.
TDE
TLR2
CD11b+F4/80+
GLUT1
HIF-1α
NF-κB
P
PD-L1
GLYCOLYSIS
NO
Glucose
Lactate
ETC
MCT4
MCT1
Lactate

Figure 21. Lactate upregulates PD-L1 in an NF-κB dependent manner (A) Summarized PD-L1 expression in peritoneal macrophages stimulated with 20mM L-lactate for 16 hours in glucose depleted RPMI-1640 culture medium (n=3). *p<0.05 (unpaired student's t test). **(B)** Intracellular phosphorylated NF-κBp65 expression (pNF-κBp65) expression assessed by flow cytometry following stimulation with L-Lactate (20mM) for indicated time. Representative histograms and summary MFI data are shown (n=3). **(C)** Confocal translocation assay demonstrating increased co-localization of NF-κBp65 to the nucleus following 30 minutes stimulation with 20mM L-lactate. Scale bar = 10μm. **(D)** PD-L1 expression in peritoneal macrophages pretreated for 1 hour with BAY prior to 16 hour stimulation with 20mM sodium L-lactate. Representative histogram and summarized MFI data are shown. n=3. **(E)** mRNA levels of PD-L1 in peritoneal macrophages pretreated for 1 hour with BAY prior to 6 hour stimulation with 20mM sodium L-lactate.**(F)** mRNA expression level of monocarboxylate transporter-1 (MCT-1) in peritoneal macrophages treated with LLC exosomes for 6 hours. Data normalized to control. n=3. *p<0.05 (unpaired student's t test)**. (G)** PD-L1 expression in peritoneal macrophages treated with TDE for 16 hours with or without the presence of Oxamate (10mM). Representative histograms and summarized data are shown. n=3. **(H)** Schema depicting TDE-induced PD-L1 expression via direct NF-κB transcription and NF-κB mediated glycolytic metabolism. The data are shown as mean ± SEM. *p<0.05, **p<0.01, ***p<0.001 (one-way ANOVA with multiple comparisons).

feedback on NF-κB, further increasing PD-L1 expression and maintaining the enhanced glycolytic phenotype.

3.3.5 *In vivo* assessment of TDE induced glycolytic and PD-L1 phenotype

Our *in vitro* results indicate that TDE drive glycolytic metabolism in macrophages through NF-κB mediated induction of HIF-1α and NOS2. Next, we wanted to confirm that tissue resident macrophages *in vivo* also display this augmented glycolytic phenotype following TDE stimulation. To achieve this, we injected C57BL/6 mice with LLC or MLE-12 exosomes intravenously every 3 days for 2 weeks (Figure 22A). The day after the final treatment, mice were intraperitoneally injected with ^{18}F-fluorodeoxyglucose (FDG). Clinically, ^{18}F-fluorodeoxyglucose positron emission tomography/ computed tomography is an essential imaging modality for NSCLC lesions with increased uptake often correlating with increased tumor PD-L1 expression[121]. In our study, one hour after injection of ^{18}FDG, the mice were euthanized and whole lung radioactivity was measured which demonstrated no significant difference between the two treatment groups (Figure 22B). However, the macrophage enriched population isolated from the lungs of TDE treated mice had a marked increase in ^{18}FDG uptake as compared to the control group (Figure 22C). Furthermore, the macrophage enriched population from the TDE group also demonstrated increased expression of PD-L1, HIF-1α, and MCT-4, as compared to the control group (Figure 22D). Taken together, these results validate our *in vitro* findings that TDE stimulation results in enhanced glycolytic metabolic reprogramming of tissue resident macrophages which drives upregulation of PD-L1.

3.3.6 Human TDE induced metabolic phenotype

Next, we wanted to determine if metabolic alterations similarly influenced human PD-L1 expression on CD14^{+} macrophages. Inhibition of glycolysis via 2-DG significantly

decreased PD-L1 expression following A549 exosome treatment (Figure 23A). Flow cytometric analysis of GLUT-1 showed increased expression following TDE stimulation compared to the controls (Figure 23B). Investigation into the lactate compartment of these cells reveled, as expected, a TLR2 dependent increase in lactate secretion into the supernatant upon TDE stimulation (Figure 23C). Likewise, stimulation with exogenous lactate increased PD-L1 through NF-κB (Figure 23D). Overall, these data suggest that human TDE metabolically reprogram $CD14^{+}$ monocytes via the same metabolic mechanism elucidated in mouse models.

Understanding that human TDE also influence the metabolic phenotype of macrophages, we wanted to correlate PD-L1 expression to metabolism in a human pre-metastatic niche. We split the $CD68^{+}$ macrophages within the dlN into two groups, $CD206^{hi}PD\text{-}L1^{hi}$ and $CD206^{lo}PD\text{-}L1^{lo}$, and then measured GLUT-1 expression using flow cytometry. The $CD206^{hi}PD\text{-}L1^{hi}$ group demonstrated an increased GLUT-1 expression compared to the $CD206^{lo}PD\text{-}L1^{lo}$ (Figure 23E). Strikingly, given the small sample size, the GLUT-1 expression on the $CD68^{+}$ cells positively and significantly correlated with their CD206/PD-L1 expression (Figure 23F). Taken together, these results suggest that despite the negative LN staging, dynamic changes in the metabolism of local myeloid populations have been made, possibly readying the tissue for metastatic tumor cell arrival.

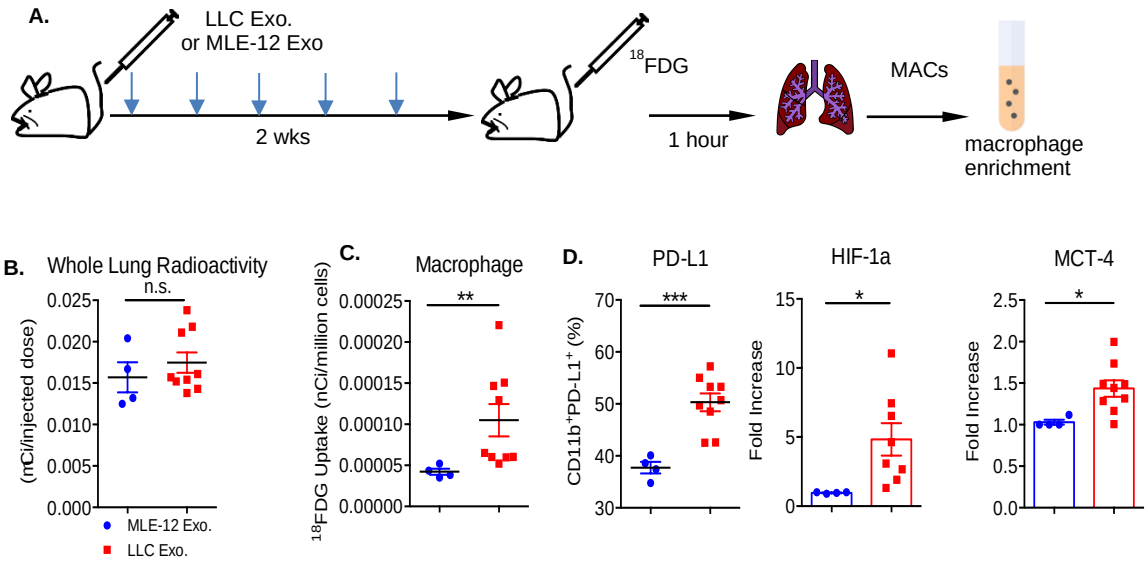

Figure 22. *In vivo* assessment of glucose uptake in TDE primed macrophages (A) Schematic for experimental design (B-D). **(B)** Radioactivity measured by Biodex Atomlab™ 500 following intraperitoneal injection of ^{18}fluordeoxyglucose (^{18}FDG) in the lungs of C57BL/6 mice treated i.v. every 3 days for 2 weeks with control MLE-12 exo. or LLC exo (10μg/mouse). n=4 per MLE-12 exo group; n=9 per LLC exo group. **(C)** ^{18}FDG uptake in the macrophage population enriched via magnetic cell isolation from the lungs of MLE-12 exo or LLC exo treated mice. **p<0.01 via Mann-Whitney U test. **(D)** mRNA expression of PD-L1, HIF-1α, and MCT-4 in the macrophage enriched population in MLE-12 exo versus LLC Exo treated mice. n=3. Representative dot plots and summarized data are shown. The data are shown as mean ± SEM. *p<0.05, **p<0.01, ***p<0.001 (unpaired student's t test).

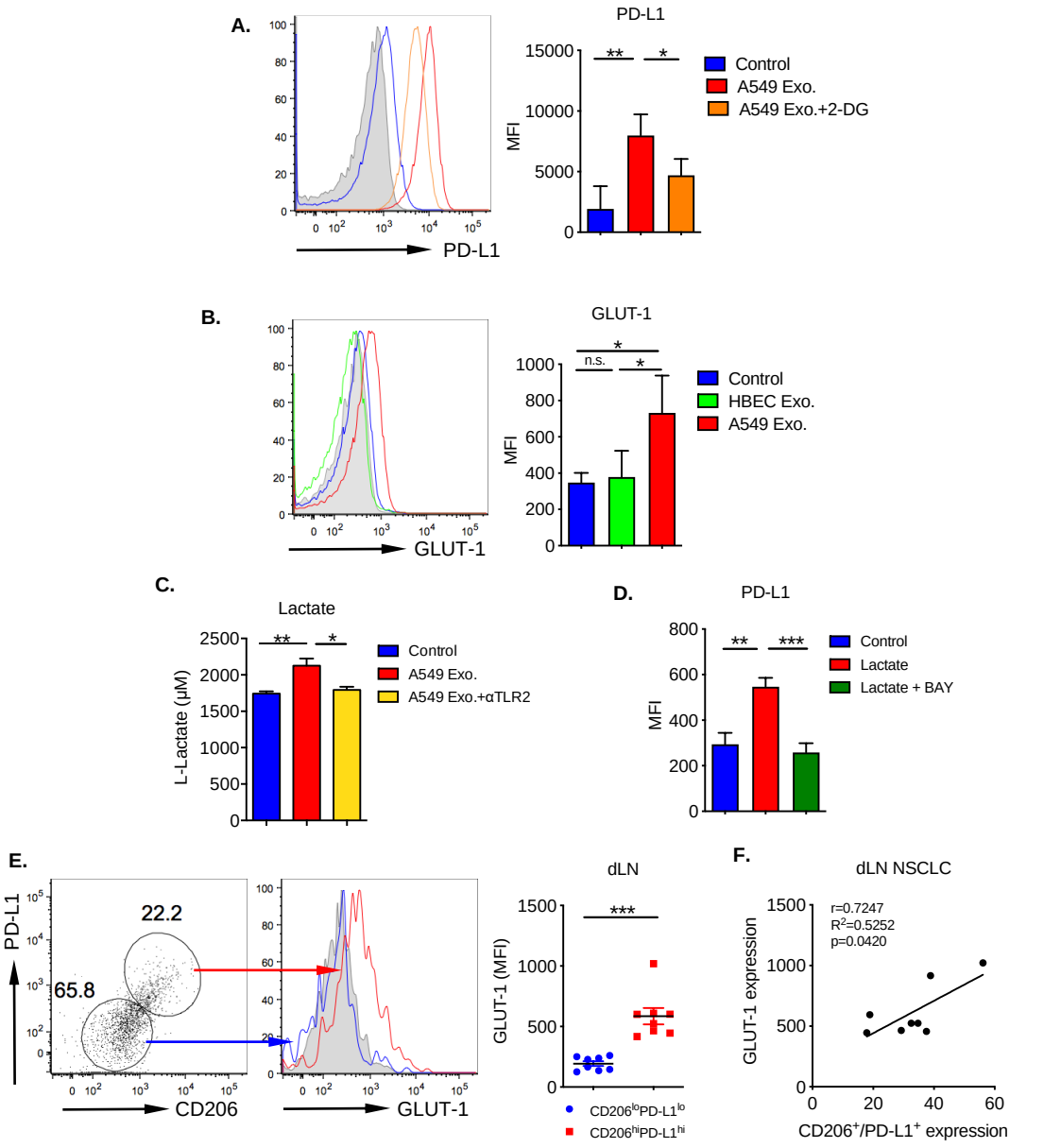

Figure 23. Human TDE drive PD-L1 expression through metabolic reprogramming. (A) Sorted CD14⁺ cells were stimulated with A549 exosome with or without 2-DG (1mM) for 16 hours. n=3. **(B)** GLUT-1 expression measured by flow cytometry following HBEC or A549 exosome stimulation for 16 hours. n=4. **(C)** Levels of L-lactate in the supernatants of sorted CD14⁺ cells pre-treated with 0.2μg/mL BAY for 1 hour prior to A549 exosome stimulation. **(D)** PD-L1 expression in CD14⁺ cells following 16 hour stimulation with lactate (20mM) with or without 1 hour pretreatment with BAY-11-7082. **(E)** GLUT-1 expression in $CD206^{hi}PD\text{-}L1^{hi}$ versus $CD206^{lo}PD\text{-}L1^{lo}$ $CD68^{+}$ macrophages. ***p<0.001 (unpaired student's t test). **(F)** Pearson correlation between CD206/PD-L1 and GLUT-1 expression in $CD68^{+}$ macrophages in NSCLC dLN. The data are shown as mean ± SEM. *p<0.05, **p<0.01, ***p<0.001 (one-way ANOVA with multiple comparisons).

3.4 DISCUSSION

One of the defining characteristics of a pre-metastatic niche is immunosuppression. Without dampening or neutralization of cytotoxic immune responses, circulating tumors cells would not be able to engraft and grow in a secondary site following extravasation from the blood vessel. While many pro-tumoral cell types have been identified within the pre-metastatic niche, the most well characterized is the macrophage. Due to their inherent plasticity, these cells have been shown to alter their metabolic phenotype and functioning towards a tumor promoting phenotype when placed in proximity to malignant cells.

In macrophages biology, metabolic phenotype is closely tied to function. Macrophage classification is often associated with particular metabolic signatures. In cancer, macrophages are often classified as the tumor-promoting, “M2” subtype, indicated by their increased Arg-1 expression and reliance on mitochondrial oxidative metabolism. This paradigm was recently challenged when human monocytes were cultured with conditioned media from pancreatic ductal adenocarcinoma (PDAC) and demonstrated a pronounced glycolytic signature reminiscent of the Warburg effect [107]. The increased rate of glycolysis in tumor cells ultimately drives an increased production of lactate, a pro-tumoral metabolite capable of increasing KRAS driven tumor growth and reducing anti-tumor T cell expansion [112, 122]. Recently, intracellular lactate was found to induce a new type of epigenetic modification called lactylation that drove M2 gene expression within a classic M1 polarized macrophage [117]. Here, we demonstrate another novel mechanism by which macrophages acquire a “non-classical M1” phenotype characterized by PD-L1

mediated immunosuppression and enhanced glycolytic metabolism. While lactate has previously been associated with an immunosuppressive TAM phenotype (42), we discover, for the first time, a role for lactate in driving PD-L1 expression in an autocrine manner in “non-classical M1” macrophages. Any inhibitory perturbations to our proposed glycolytic pathway significantly decreased PD-L1 expression due to blunted lactate production. Furthermore, addition of an oxidative metabolite like α-ketoglutarate completely blocked TDE driven PD-L1 upregulation again strengthening the important relationship between glycolysis, lactate and PD-L1.

We demonstrate that NF-kB pathway directly regulates this “non-classical M1” phenotype. In addition to directly facilitating PD-L1 expression by binding to the promoter [81], we report here a novel mechanism by which NF-κB regulates PD-L1 expression through metabolic alterations. Following signaling from TLR2/MyD88 TDE ligation, NF-κB activates two distinct pathways that independently augment glycolysis. First, HIF-1α activation leads to an increased expression of GLUT-1 resulting in a higher rate of influx of glucose into macrophages. Secondly, activated NOS2 increases the production of NO which in turn inhibits complexes III and IV of the electron transport chain thus effectively shunting pyruvate into lactate. Therefore, akin to Warburg metabolism, TDE stimulated macrophages are preferentially using glycolysis in normoxic conditions because the mitochondrial oxidative phosphorylation pathway has effectively been eliminated by NO. Inhibition of NO by SEITU completely restored normal oxidative metabolism further supporting this notion. The enhanced glycolysis eventually leads to more lactate production and subsequent PD-L1 expression on macrophages. We demonstrate that lactate directly activates NF-kB leading to PD-L1 expression on macrophages. Interestingly, previous studies have shown that lactate stimulates NF-kB activation in

endothelial cells [123] and cancer-associated fibroblasts [124] to drive tumor angiogenesis and adaptive resistance to targeted therapies.

Clinically, the concept of Warburg metabolism seen in tumors lead to the utilization of FDG-PET scans to visualize growing tumors within the body. We aimed to use a similar concept in our studies to demonstrate that macrophages using Warburg metabolism display an increased capacity for glucose uptake. Results from our *in vivo* studies demonstrate the indeed macrophages within the lungs of mice primed with TDE have increased glucose uptake compared to control. The macrophages with increased FDG uptake also had increased expression of PD-L1, HIF-1α, and MCT4. Going forward, these data seemingly call into question the role macrophages within tumors play in FDG-PET glucose uptake. Could these cells be the main consumers of FDG-glucose rather than the tumor cells? Additionally, could glucose tracing be a viable way to identify a potential site of metastasis? The results of our study suggest that within the dLN of NSCLC patients, $CD68^+$ macrophages that have increased co-expression of PD-L1 and GLUT-1. While this is just correlative data, it does suggest that macrophages within a pre-metastatic site could potentially be identified using a form of labeled glucose tracing.

Overall, our findings provide mechanistic insight as to how TDE polarize tissue resident macrophages towards a $PD\text{-}L1^+$ immunosuppressive phenotype through metabolic reprogramming. Specifically, we found that TDE stimulation augments glycolytic metabolism in both mice and humans through NF-κB mediated conversion of pyruvate into lactate with subsequent lactate driven PD-L1 expression. Additionally, data from our own NSCLC patient cohort demonstrated a notable correlation between PD-L1 and GLUT-1 expression within a pre-metastatic site. Therefore, going forward, it would be interesting to further explore whether inhibiting immunosuppressive metabolites like

lactate could increase the efficacy of immune checkpoint therapy and whether increased glucose uptake could be used clinically as a marker for pre-metastatic niche formation.

4. CONCLUDING REMARKS AND FUTURE DIRECTIONS

The overall aim of this study was to determine if tumor derived exosomes contribute to the earliest precipitating events in pre-metastatic niche formation leading to the characteristic overt immunosuppressive phenotype. Our findings suggest that indeed TDE do polarize tissue resident macrophages towards a “non-classical M1” immunosuppressive phenotype characterized by increased PD-L1 expression and lactate secretion. Given these results, we probed further to identify the mechanism that drove this phenotype. Since metabolism is often linked with macrophage function, we hypothesized that TDE simulation alters macrophage metabolism. While we originally anticipated TDE to skew metabolism towards an M2-like phenotype due to the apparent similarities in Arginase-1 and IL-10 expression, pivotal experiments demonstrated a distinct glycolytic, M1-like phenotype. Overall, we found that NF-κB acts as a master regulator of NOS2 and HIF-1α that causes shunting of glucose into lactate via NO mediated inhibition of oxidative phosphorylation. The increased secretion of lactate feeds back and drives further PD-L1 expression. Additionally, using a small cohort of NSCLC patients, we found that even within metastasis negative dLNs, macrophages already demonstrate increased PD-L1 and CD206 expression. Correlation with GLUT-1 seemingly suggests to implicate increased glycolysis as one proposed mechanism driving the PD-L1 expression. Patients that had the highest PD-L1 expression also had an increase in exosomal release genes, YKT6 and TSG101.

There are two important ancillary questions raised by the findings in our study. First, given these data, how does TDE-induced PD-L1 contribute to immune checkpoint

therapy failure? Specifically, we found exosomes drive increased PD-L1 expression on macrophages, does this excess source of PD-L1 sequester anti-PD-L1 antibody allowing tumor derived PD-L1 to inhibit effector T cell function? Would inhibition of exosome release from primary tumors using targeted siRNA to YKT6 decrease macrophage PD-L1 expression and rescue immune checkpoint therapy? Would it decrease the rate of primary tumor metastasis? Additionally, based on our study, deeper inquiry is needed into the role lactate plays in antagonizing immune checkpoint therapy. Do T cells that have escaped PD-L1 mediated inhibition ultimately fail due to excessive lactate production within the tumor or pre-metastatic environment? Further investigation into strategies that can neutralize these factors is important to improving overall survival rates for patients treated with immune checkpoint therapies.

Secondly, our study indicates that macrophages like tumor cells, have an increased glycolytic capacity that can be identified via glucose tracing. Current protocols for screening axillary draining lymph nodes during breast cancer surgery involves utilization of a blue colloid dye or a radiocolloid isotope tracer. Lymph nodes that are either “hot” and/or “blue” are considered to be the sentinel lymph node from the tumor and removed[125]. If the sentinel lymph node contains metastatic tumor cells, additional lymph nodes are removed. However, while this process called sentinel lymph node biopsy and axillary lymph node dissection has improved outcomes for patients by decreasing risk of metastasis, it often results in the serious complication of lymphedema. In one study, hot sentinel lymph nodes were identified and excised in 97% of patients[125]. However, only 20% were actually malignant. Therefore, there is a clinical need for improved screening techniques with increased sensitivity and specificity to correctly identify metastatic nodes or those with a high metastatic potential versus healthy tissue. Given the results of this study, I believe that adopting a modified form of localized glucose tracing could be useful in identifying, in real time, the metastatic potential of a lymph node.

In conclusion, this study expands upon the current knowledge in the field regarding primary tumor metastasis. It also unveils a novel connection between exosomes, metabolism, and metastasis that could serve as a future target in the field of immunotherapy.

Table S1. Patient Characteristics

Patient Number	Gender	Age	Race	Subtype of NSCLC	Stage	Grade	Smoking Status
020	Female	60	White	Squamous Cell carcinoma	pT1b NO	Not reported	Yes
022	Male	69	White	Adenocarcinoma -NOS	pT3NO	G3	Yes
026	Female	66	African American	Adenocarcinoma -NOS	pT2N0	G2	No
043	Female	80	White	Adenocarcinoma -NOS	pT1bN0	G1	No
044	Male	57	White	Squamous Cell Carcinoma	pT2aN0	G2	Yes
049	Male	59	White	Squamous Cell Carcinoma (Clear cell variant)	pT2bN0	G3	N/A
050	Female	66	White	Adenocarcinoma	pT2aN0	G2	Yes
056	Male	60	White	Adenocarcinoma	pT2aN0	G2	Yes
058	Female	64	African American	Squamous Cell Carcinoma	pT1bN0	G2	Yes

Table S2. Primer sequences for real-time PCR analysis

Gene Name	Forward Primer qPCR	Reverse Primer qPCR
HIF-1α	AACGTGGAAGGTGCTTCACT	GAGCGGCCCAAAAGTTCTTC
GLUT1	CAGGCTGTGCTGTGCTCAT	TTCAAAGAAGGCCACAAGC
ARG-1	TTTTAGGGTTACGGCCGGTG	CCTCGAGGCTGTCCTTTTGA
PD-L1	GGAATTGTCTCAGAATGGTC	GTAGTTGCTTCTAGGAAGGAG
LDHA	GCAGACTTGGCTGAGAGCAT	TGGGACACTGAGGAAGACATC
IDH1	GCTAGTGACAGGCTGGGTAA	ACACCACCACCTTCTTCAAA
IDH2	GACAGTCACCCGCCATTACC	GCGTCTGTGCAAACCTGATAA
VEGF	TTACTGCTGTACCTCCACC	ACAGGACGGCTTGAAGATG
HK1	CTGCTCACCAGGGCTACTG	CCCTTTTCTGAGCCGTCCG
PDK1	TCCTTAGAGGGCTACGGGAC	ACACAGGGAGTCTCTCGACG
iNOS	GGGACTGAGCTGTTAGAGACAC	CCAAATCCAACGTTCTCCGT
MCT1	ATGATCGCTGGTGGTTGTCT	CAAGTTGAAAGCAAGCCCAA
MCT4	GCCACCTCAACGCCTGCTA	TGTCGGGTACACCCATATCCTTA
BV8	GCATGTGCTGTGCTGTCAGT	TCTTTCCTGCCTTCCATTTG
MMP8	TTCGCGTGGATAAGGAGTTC	GGAAACTCACACGCCAGAAG
S100a8	GGAGTTCCTTGCGATGGTGAT	GTAGACATATCCAGGGACCCAGC
S100a9	AGCATAACCACCATCATCGACAC	TGTGCTTCCACCATTTGTCTGA
YKT6 (human)	GGAGTCTCTGTTACAGCGAGGTG	GAGTTTTGTTTCCGGGCAGTT
TSG101 (human)	GCCAGCTCAAGAAAATGGTGT	AGGCACAGGGATTGTTCCAG

Table S3. Full Antibody Reference List

Reagent	Source	Identifier
Fixable Viability Dye eFluor 780	eBioscience	Cat# 65-0865-18
Anti-Human CD45 Alexa Fluor 700 (Clone 2D1)	Biolegend	Cat# 368513
Anti-Human CD11b Biotin (Clone ICRF44)	Biolegend	Cat# 301304
Anti-Human CD14 PE (Clone HCD14)	Biolegend	Cat# 325606
Anti-Human CD16 FITC (Clone 3G8)	Biolegend	Cat# 302005
Anti-Human CD68 PerCP-Cy5.5 (Clone Y1/82A)	Biolegend	Cat# 333813
Anti-Human CD66b PE/Dazzle 594 (Clone G10F5)	Biolegend	Cat# 305121
Anti-Human HLA-DR APC (Clone L243)	Biolegend	Cat# 307610
Anti-Human PD-L1 (CD274) Pe-Cy7 (Clone 29E.2A3)	Biolegend	Cat# 329718
Anti-Human CD33 Brilliant Violet 605 (Clone P67.6)	Biolegend	Cat# 366611
Anti-Human CD63 Brilliant Violet 650 (Clone H5C6)	Biolegend	Cat# 344723
Anti-Human CD206 Brilliant Violet 421 (Clone 15-2)	Biolegend	Cat# 321125
Anti-Human TIM-3 (CD366) Biotin (Clone F38-2E2)	Biolegend	Cat# 345046
Anti-Human CD8 PE (Clone HIT8a)	Biolegend	Cat# 300908
Anti-Human CD45RO FITC (Clone UCHL1)	Biolegend	Cat# 304204
Anti-Human CD3 PerCP-Cy5.5 (Clone HIT3a)	Biolegend	Cat# 300328
Anti-Human GLUT-1 (Clone 202915)	R&D	Cat# MAB1418
Anti-Human γδ TCR APC	MACS	Lot# 5171009649
Anti-Human PD-1 (CD279) Pe-Cy7 (Clone EH112.2H7)	Biolegend	Cat# 329918
Anti-Human CD4 Brilliant Violet 605 (Clone Sk3)	Biolegend	Cat# 344645
Anti-Human PD-L1 (CD274) APC (Clone 29E.2A3)	Biolegend	Cat# 329918
Anti-Human CD45RA Brilliant Violet 421 (Clone HI100)	Biolegend	Cat# 304129

Reagent	Source	Identifier
Anti-Mouse F4/80 Pe-Cy7 (Clone BM8)	Biolegend	Cat# 123116
Anti-Mouse PD-L1 (CD274) (Clone 10F.9G2)	Biolegend	Cat# 124306
Anti-Mouse CD45 PerCP (Clone 30-F11)	Biolegend	Cat# 103132
Anti-Mouse CD11b FITC (Clone M1/70)	Biolegend	Cat# 101206
Anti-Mouse CCR2 APC	R&D Biosystems	Cat# FAB5538A
Anti-Mouse Ly6C PerCP (Clone HK1.4)	Biolegend	Cat# 128012
Anti-Mouse Ly6G PE (Clone 1A8)	Biolegend	Cat# 127608
Anti-Mouse PD-L1 (CD274) APC (Clone 10F.9G2)	Biolegend	Cat# 124312
Anti-Mouse CD3 PerCP (Clone 17A2)	Biolegend	Cat# 100218
Anti-Mouse CD4 APC (Clone GK1.5)	Biolegend	Cat# 100412
Anti-Mouse CD8 Pe-Cy7 (Clone 53-6.7)	Biolegend	Cat# 100722
Anti-Mouse PD-1 (CD279) PE (Clone 29F.1a12)	Biolegend	Cat# 135206
Anti-Mouse GR-1 PE (Clone RB6-8C5)	Biolegend	Cat# 108408
Anti-Mouse IFNγ (XM91.2)	Biolegend	Cat# 505808

REFERENCES

1. Parham, P. *The Immune System*, Second Edition edn. Garland Sciences: New York, NY, 2005.

2. Cooper, M.D. & Alder, M.N. The evolution of adaptive immune systems. *Cell* **124**, 815-822 (2006).

3. Parkin, J. & Cohen, B. An overview of the immune system. *Lancet (London, England)* **357**, 1777-1789 (2001).

4. Artis, D. & Spits, H. The biology of innate lymphoid cells. *Nature* **517**, 293-301 (2015).

5. Klein, L., Kyewski, B., Allen, P.M. & Hogquist, K.A. Positive and negative selection of the T cell repertoire: what thymocytes see (and don't see). *Nature reviews. Immunology* **14**, 377-391 (2014).

6. Enouz, S., Carrié, L., Merkler, D., Bevan, M.J. & Zehn, D. Autoreactive T cells bypass negative selection and respond to self-antigen stimulation during infection. *J Exp Med* **209**, 1769-1779 (2012).

7. Kelly, J.T. & Busse, W.W. Host immune responses to rhinovirus: mechanisms in asthma. *J Allergy Clin Immunol* **122**, 671-682 (2008).

8. Ratajczak, W., Niedźwiedzka-Rystwej, P., Tokarz-Deptuła, B. & Deptuła, W. Immunological memory cells. *Cent Eur J Immunol* **43**, 194-203 (2018).

9. Strassburg, M.A. The global eradication of smallpox. *American journal of infection control* **10**, 53-59 (1982).

10. Dunn, G.P., Old, L.J. & Schreiber, R.D. The three Es of cancer immunoediting. *Annual review of immunology* **22**, 329-360 (2004).

11. Boffetta, P. & Islami, F. The contribution of molecular epidemiology to the identification of human carcinogens: current status and future perspectives. *Annals of oncology : official journal of the European Society for Medical Oncology* **24**, 901-908 (2013).

12. Dunn, G.P., Old, L.J. & Schreiber, R.D. The immunobiology of cancer immunosurveillance and immunoediting. *Immunity* **21**, 137-148 (2004).

13. Penn, I. Transmission of cancer from organ donors. *Annals of transplantation* **2**, 7-12 (1997).

14. Huang, S. *et al.* Outcomes of Organ Transplantation from Donors with a Cancer History. *Med Sci Monit* **24**, 997-1007 (2018).

15. Rodríguez, P.C., Zea, A.H. & Ochoa, A.C. Mechanisms of tumor evasion from the immune response. *Cancer chemotherapy and biological response modifiers* **21**, 351-364 (2003).

16. Dobosz, P. & Dzieciątkowski, T. The Intriguing History of Cancer Immunotherapy. *Front Immunol* **10**, 2965-2965 (2019).

17. Graeber, C. *The Breakthrough: immunotherapy and the race to cure cancer*. Scribe Publications, 2019.

18. McCarthy, E.F. The toxins of William B. Coley and the treatment of bone and soft-tissue sarcomas. *The Iowa orthopaedic journal* **26**, 154-158 (2006).

19. Hunter, P. The fourth pillar: Despite some setbacks in the clinic, immunotherapy has made notable progress toward becoming an additional therapeutic option against cancer. *EMBO Rep* **18**, 1889-1892 (2017).

20. Smyth, M.J. & Teng, M.W. 2018 Nobel Prize in physiology or medicine. *Clin Transl Immunology* **7**, e1041-e1041 (2018).

21. de Miranda, N.F.C.C. & Trajanoski, Z. Advancing cancer immunotherapy: a vision for the field. *Genome Medicine* **11**, 51 (2019).

22. Larkin, J. *et al.* Five-Year Survival with Combined Nivolumab and Ipilimumab in Advanced Melanoma. *N Engl J Med* **381**, 1535-1546 (2019).

23. Institute, C.R. Timeline of Progress. 2020 [cited 2020 May 29]Available from: https://www.cancerresearch.org/immunotherapy/timeline-of-progress

24. Wolchok, J. How is Immunotherapy for Melanoma Changing the Outlook for Patients? 2020 [cited 2020 May 29]Available from: https://www.cancerresearch.org/immunotherapy/cancer-types/melanoma

25. Herbst, R.S., Morgensztern, D. & Boshoff, C. The biology and management of non-small cell lung cancer. *Nature* **553**, 446 (2018).

26. Institute, N.C. Non-Small Cell Lung Cancer Treatment (PDQ®)–Health Professional Version. 2020 [cited 2020 May 29]Available from: https://www.cancer.gov/types/lung/hp/non-small-cell-lung-treatment-pdq

27. Arbour, K.C. & Riely, G.J. Systemic Therapy for Locally Advanced and Metastatic Non-Small Cell Lung Cancer: A Review. *Jama* **322**, 764-774 (2019).

28. Society, C.C. Lung metastases. 2020 [cited 2020 May 29]Available from: https://www.cancer.ca/en/cancer-information/cancer-type/metastatic-cancer/lung-metastases/?region=on

29. Seo, J.B., Im, J.G., Goo, J.M., Chung, M.J. & Kim, M.Y. Atypical pulmonary metastases: spectrum of radiologic findings. *Radiographics : a review publication of the Radiological Society of North America, Inc* **21**, 403-417 (2001).

30. Siegel, R.L., Miller, K.D. & Jemal, A. Cancer Statistics, 2017. *CA: a cancer journal for clinicians* **67**, 7-30 (2017).

31. Drug, U.S.F. FDA expands pembrolizumab indication for first line treatment of NSCLC. 2019 [cited 2020 May 29]Available from: https://www.fda.gov/drugs/fda-expands-pembrolizumab-indication-first-line-treatment-nsclc-tps-1

32. Paz-Ares, L. *et al.* Pembrolizumab plus Chemotherapy for Squamous Non-Small-Cell Lung Cancer. *N Engl J Med* **379**, 2040-2051 (2018).

33. Costantini, A. *et al.* Efficacy of next treatment received after nivolumab progression in patients with advanced nonsmall cell lung cancer. *ERJ Open Res* **4** (2018).

34. Fidler, I.J. The pathogenesis of cancer metastasis: the 'seed and soil' hypothesis revisited. *Nat Rev Cancer* **3**, 453-458 (2003).

35. Liu, Y. & Cao, X. Characteristics and Significance of the Pre-metastatic Niche. *Cancer cell* **30**, 668-681 (2016).

36. Quail, D.F. & Joyce, J.A. Microenvironmental regulation of tumor progression and metastasis. *Nat Med* **19**, 1423-1437 (2013).

37. Gay, L.J. & Felding-Habermann, B. Contribution of platelets to tumour metastasis. *Nature reviews. Cancer* **11**, 123-134 (2011).

38. Strilic, B. & Offermanns, S. Intravascular Survival and Extravasation of Tumor Cells. *Cancer cell* **32**, 282-293 (2017).

39. Tormoen, G.W., Crittenden, M.R. & Gough, M.J. Role of the immunosuppressive microenvironment in immunotherapy. *Adv Radiat Oncol* **3**, 520-526 (2018).

40. Guan, Q., Xiao, C. & Zhang, M. Immune Regulatory Cells in Inflammation, Infection, Tumor, Metabolism, and Other Diseases. *Mediators Inflamm* **2018**, 4170780-4170780 (2018).

41. Chin, A.R. & Wang, S.E. Cancer Tills the Premetastatic Field: Mechanistic Basis and Clinical Implications. *Clinical cancer research : an official journal of the American Association for Cancer Research* **22**, 3725-3733 (2016).

42. Binnewies, M. *et al.* Understanding the tumor immune microenvironment (TIME) for effective therapy. *Nat Med* **24**, 541-550 (2018).

43. Mantovani, A., Sozzani, S., Locati, M., Allavena, P. & Sica, A. Macrophage polarization: tumor-associated macrophages as a paradigm for polarized M2 mononuclear phagocytes. *Trends Immunol* **23**, 549-555 (2002).

44. Bader, J.E. *et al.* Macrophage depletion using clodronate liposomes decreases tumorigenesis and alters gut microbiota in the AOM/DSS mouse model of colon cancer. *Am J Physiol Gastrointest Liver Physiol* **314**, G22-G31 (2018).

45. Linde, N. *et al.* Macrophages orchestrate breast cancer early dissemination and metastasis. *Nature communications* **9**, 21 (2018).

46. Lin, H. *et al.* Host expression of PD-L1 determines efficacy of PD-L1 pathway blockade-mediated tumor regression. *J Clin Invest* **128**, 805-815 (2018).

47. McAndrews, K.M. & Kalluri, R. Mechanisms associated with biogenesis of exosomes in cancer. *Molecular cancer* **18**, 52 (2019).

48. Hoshino, A. *et al.* Tumour exosome integrins determine organotropic metastasis. *Nature* **527**, 329-335 (2015).

49. Boukouris, S. & Mathivanan, S. Exosomes in bodily fluids are a highly stable resource of disease biomarkers. *Proteomics Clin Appl* **9**, 358-367 (2015).

50. Feng, W., Dean, D.C., Hornicek, F.J., Shi, H. & Duan, Z. Exosomes promote pre-metastatic niche formation in ovarian cancer. *Molecular cancer* **18**, 124 (2019).

51. Lässer, C. Identification and analysis of circulating exosomal microRNA in human body fluids. *Methods in molecular biology (Clifton, N.J.)* **1024**, 109-128 (2013).

52. Ludwig, S. *et al.* Suppression of Lymphocyte Functions by Plasma Exosomes Correlates with Disease Activity in Patients with Head and Neck Cancer. *Clinical cancer research : an official journal of the American Association for Cancer Research* **23**, 4843-4854 (2017).

53. Li, I. & Nabet, B.Y. Exosomes in the tumor microenvironment as mediators of cancer therapy resistance. *Molecular cancer* **18**, 32 (2019).

54. Liu, Y. *et al.* Tumor Exosomal RNAs Promote Lung Pre-metastatic Niche Formation by Activating Alveolar Epithelial TLR3 to Recruit Neutrophils. *Cancer cell* **30**, 243-256 (2016).

55. Yang, H. *et al.* Exosome-Derived miR-130a Activates Angiogenesis in Gastric Cancer by Targeting C-MYB in Vascular Endothelial Cells. *Molecular therapy : the journal of the American Society of Gene Therapy* **26**, 2466-2475 (2018).

56. Bardi, G.T., Smith, M.A. & Hood, J.L. Melanoma exosomes promote mixed M1 and M2 macrophage polarization. *Cytokine* **105**, 63-72 (2018).

57. Bretz, N.P. *et al.* Body fluid exosomes promote secretion of inflammatory cytokines in monocytic cells via Toll-like receptor signaling. *J Biol Chem* **288**, 36691-36702 (2013).

58. Yang, Y. *et al.* Exosomal PD-L1 harbors active defense function to suppress T cell killing of breast cancer cells and promote tumor growth. *Cell research* **28**, 862-864 (2018).

59. Nishida-Aoki, N. *et al.* Disruption of Circulating Extracellular Vesicles as a Novel Therapeutic Strategy against Cancer Metastasis. *Molecular therapy : the journal of the American Society of Gene Therapy* **25**, 181-191 (2017).

60. Poggio, M. *et al.* Suppression of Exosomal PD-L1 Induces Systemic Anti-tumor Immunity and Memory. *Cell* **177**, 414-427 e413 (2019).

61. Kim, D.H. *et al.* Exosomal PD-L1 promotes tumor growth through immune escape in non-small cell lung cancer. *Experimental & molecular medicine* **51**, 94 (2019).

62. Chen, G. *et al.* Exosomal PD-L1 contributes to immunosuppression and is associated with anti-PD-1 response. *Nature* **560**, 382-386 (2018).

63. Cordonnier, M. *et al.* Tracking the evolution of circulating exosomal-PD-L1 to monitor melanoma patients. *Journal of Extracellular Vesicles* **9**, 1710899 (2020).

64. Theodoraki, M.N. *et al.* Circulating exosomes measure responses to therapy in head and neck cancer patients treated with cetuximab, ipilimumab, and IMRT. *Oncoimmunology* **8**, 1593805 (2019).

65. Theodoraki, M.N., Yerneni, S.S., Hoffmann, T.K., Gooding, W.E. & Whiteside, T.L. Clinical Significance of PD-L1(+) Exosomes in Plasma of Head and Neck Cancer Patients. *Clinical cancer research : an official journal of the American Association for Cancer Research* **24**, 896-905 (2018).

66. Ricklefs, F.L. *et al.* Immune evasion mediated by PD-L1 on glioblastoma-derived extracellular vesicles. *Science advances* **4**, eaar2766 (2018).

67. Ludwig, N. & Whiteside, T.L. Potential roles of tumor-derived exosomes in angiogenesis. *Expert opinion on therapeutic targets* **22**, 409-417 (2018).

68. Lux, A., Kahlert, C., Grutzmann, R. & Pilarsky, C. c-Met and PD-L1 on Circulating Exosomes as Diagnostic and Prognostic Markers for Pancreatic Cancer. *International journal of molecular sciences* **20** (2019).

69. Peinado, H. *et al.* Melanoma exosomes educate bone marrow progenitor cells toward a pro-metastatic phenotype through MET. *Nature medicine* **18**, 883-891 (2012).

70. Wen, S.W. *et al.* The Biodistribution and Immune Suppressive Effects of Breast Cancer-Derived Exosomes. *Cancer research* **76**, 6816-6827 (2016).

71. Morrissey, S.M. & Yan, J. Exosomal PD-L1: Roles in Tumor Progression and Immunotherapy. *Trends in cancer* (2020).

72. Gabrusiewicz, K. *et al.* Glioblastoma stem cell-derived exosomes induce M2 macrophages and PD-L1 expression on human monocytes. *Oncoimmunology* **7**, e1412909 (2018).

73. Thery, C., Amigorena, S., Raposo, G. & Clayton, A. Isolation and characterization of exosomes from cell culture supernatants and biological fluids. *Current protocols in cell biology* **Chapter 3**, Unit 3 22 (2006).

74. Gupta, S. *et al.* An improvised one-step sucrose cushion ultracentrifugation method for exosome isolation from culture supernatants of mesenchymal stem cells. *Stem Cell Res Ther* **9**, 180-180 (2018).

75. Ray, A. & Dittel, B.N. Isolation of mouse peritoneal cavity cells. *J Vis Exp* (2010).

76. Peinado, H. *et al.* Melanoma exosomes educate bone marrow progenitor cells toward a pro-metastatic phenotype through MET. *Nature medicine* **18**, 883-891 (2012).

77. Singhal, S. *et al.* Human tumor-associated monocytes/macrophages and their regulation of T cell responses in early-stage lung cancer. *Science Translational Medicine* **11**, eaat1500 (2019).

78. Xiang, X. *et al.* TLR2-mediated expansion of MDSCs is dependent on the source of tumor exosomes. *Am J Pathol* **177**, 1606-1610 (2010).

79. Zhang, X. *et al.* PD-L1 induced by IFN-gamma from tumor-associated macrophages via the JAK/STAT3 and PI3K/AKT signaling pathways promoted progression of lung cancer. *International journal of clinical oncology* **22**, 1026-1033 (2017).

80. Mantovani, A., Allavena, P., Sica, A. & Balkwill, F. Cancer-related inflammation. *Nature* **454**, 436-444 (2008).

81. Asgarova, A. *et al.* PD-L1 expression is regulated by both DNA methylation and NF-kB during EMT signaling in non-small cell lung carcinoma. *Oncoimmunology* **7**, e1423170-e1423170 (2018).

82. Lastwika, K.J. *et al.* Control of PD-L1 Expression by Oncogenic Activation of the AKT-mTOR Pathway in Non-Small Cell Lung Cancer. *Cancer research* **76**, 227-238 (2016).

83. Wu, L. & Yang, L. The function and mechanism of HMGB1 in lung cancer and its potential therapeutic implications. *Oncol Lett* **15**, 6799-6805 (2018).

84. Wang, W. *et al.* Upregulation of PD-L1 via HMGB1-activated IRF3 and NF-kB contributes to UV radiation-induced immune suppression. *Cancer research*, canres.3134.2018 (2019).

85. Zhang, X. *et al.* Tumor-derived exosomes induce N2 polarization of neutrophils to promote gastric cancer cell migration. *Molecular cancer* **17**, 146 (2018).

86. van Niel, G., D'Angelo, G. & Raposo, G. Shedding light on the cell biology of extracellular vesicles. *Nature reviews. Molecular cell biology* **19**, 213-228 (2018).

87. Borghaei, H. *et al.* Nivolumab versus Docetaxel in Advanced Nonsquamous Non-Small-Cell Lung Cancer. *The New England journal of medicine* **373**, 1627-1639 (2015).

88. Tang, H. *et al.* PD-L1 on host cells is essential for PD-L1 blockade-mediated tumor regression. *J Clin Invest* **128**, 580-588 (2018).

89. Willms, E. *et al.* Cells release subpopulations of exosomes with distinct molecular and biological properties. *Scientific reports* **6**, 22519 (2016).

90. Willms, E., Cabañas, C., Mäger, I., Wood, M.J.A. & Vader, P. Extracellular Vesicle Heterogeneity: Subpopulations, Isolation Techniques, and Diverse Functions in Cancer Progression. *Front Immunol* **9**, 738-738 (2018).

91. Silvestri, G.A. *et al.* Methods for staging non-small cell lung cancer: Diagnosis and management of lung cancer, 3rd ed: American College of Chest Physicians evidence-based clinical practice guidelines. *Chest* **143**, e211S-e250S (2013).

92. Hessvik, N.P. & Llorente, A. Current knowledge on exosome biogenesis and release. *Cell Mol Life Sci* **75**, 193-208 (2018).

93. Mascaux, C. *et al.* Immune evasion before tumour invasion in early lung squamous carcinogenesis. *Nature* (2019).

94. Ruiz-Martinez, M. *et al.* YKT6 expression, exosome release, and survival in non-small cell lung cancer. *Oncotarget* **7**, 51515-51524 (2016).

95. Mills, C.D., Kincaid, K., Alt, J.M., Heilman, M.J. & Hill, A.M. M-1/M-2 macrophages and the Th1/Th2 paradigm. *Journal of immunology (Baltimore, Md. : 1950)* **164**, 6166-6173 (2000).

96. Sica, A. & Mantovani, A. Macrophage plasticity and polarization: in vivo veritas. *J Clin Invest* **122**, 787-795 (2012).

97. Viola, A., Munari, F., Sánchez-Rodríguez, R., Scolaro, T. & Castegna, A. The Metabolic Signature of Macrophage Responses. *Front Immunol* **10**, 1462 (2019).

98. Jablonski, K.A. *et al.* Novel Markers to Delineate Murine M1 and M2 Macrophages. *PloS one* **10**, e0145342 (2015).

99. Noe, J.T. & Mitchell, R.A. Tricarboxylic acid cycle metabolites in the control of macrophage activation and effector phenotypes. *Journal of leukocyte biology* **106**, 359-367 (2019).

100. Chittezhath, M. *et al.* Molecular Profiling Reveals a Tumor-Promoting Phenotype of Monocytes and Macrophages in Human Cancer Progression. *Immunity* **41**, 815-829 (2014).

101. Carmona-Fontaine, C. *et al.* Metabolic origins of spatial organization in the tumor microenvironment. *Proceedings of the National Academy of Sciences of the United States of America* **114**, 2934-2939 (2017).

102. Liu, P.S. *et al.* alpha-ketoglutarate orchestrates macrophage activation through metabolic and epigenetic reprogramming. *Nature immunology* **18**, 985-994 (2017).

103. Vats, D. *et al.* Oxidative metabolism and PGC-1beta attenuate macrophage-mediated inflammation. *Cell metabolism* **4**, 13-24 (2006).

104. Biswas, S.K., Sica, A. & Lewis, C.E. Plasticity of macrophage function during tumor progression: regulation by distinct molecular mechanisms. *Journal of immunology (Baltimore, Md. : 1950)* **180**, 2011-2017 (2008).

105. Jeong, H. *et al.* Tumor-Associated Macrophages Enhance Tumor Hypoxia and Aerobic Glycolysis. *Cancer research* **79**, 795-806 (2019).

106. Vitale, I., Manic, G., Coussens, L.M., Kroemer, G. & Galluzzi, L. Macrophages and Metabolism in the Tumor Microenvironment. *Cell metabolism* **30**, 36-50 (2019).

107. Penny, H.L. *et al.* Warburg metabolism in tumor-conditioned macrophages promotes metastasis in human pancreatic ductal adenocarcinoma. *Oncoimmunology* **5**, e1191731 (2016).

108. Wegiel, B., Vuerich, M., Daneshmandi, S. & Seth, P. Metabolic Switch in the Tumor Microenvironment Determines Immune Responses to Anti-cancer Therapy. *Frontiers in oncology* **8**, 284-284 (2018).

109. Liberti, M.V. & Locasale, J.W. The Warburg Effect: How Does it Benefit Cancer Cells? *Trends Biochem Sci* **41**, 211-218 (2016).

110. Astrand, P.O., Hultman, E., Juhlin-Dannfelt, A. & Reynolds, G. Disposal of lactate during and after strenuous exercise in humans. *Journal of applied physiology (Bethesda, Md. : 1985)* **61**, 338-343 (1986).

111. Domblides, C., Lartigue, L. & Faustin, B. Control of the Antitumor Immune Response by Cancer Metabolism. *Cells* **8**, 104 (2019).

112. Fischer, K. *et al.* Inhibitory effect of tumor cell-derived lactic acid on human T cells. *Blood* **109**, 3812-3819 (2007).

113. Mendler, A.N. *et al.* Tumor lactic acidosis suppresses CTL function by inhibition of p38 and JNK/c-Jun activation. *Int J Cancer* **131**, 633-640 (2012).

114. Seth, P. *et al.* Deletion of Lactate Dehydrogenase-A in Myeloid Cells Triggers Antitumor Immunity. *Cancer research* **77**, 3632-3643 (2017).

115. de la Cruz-López, K.G., Castro-Muñoz, L.J., Reyes-Hernández, D.O., García-Carrancá, A. & Manzo-Merino, J. Lactate in the Regulation of Tumor Microenvironment and Therapeutic Approaches. *Frontiers in oncology* **9**, 1143-1143 (2019).

116. Colegio, O.R. *et al.* Functional polarization of tumour-associated macrophages by tumour-derived lactic acid. *Nature* **513**, 559-563 (2014).

117. Zhang, D. *et al.* Metabolic regulation of gene expression by histone lactylation. *Nature* **574**, 575-580 (2019).

118. Ip, W.K.E., Hoshi, N., Shouval, D.S., Snapper, S. & Medzhitov, R. Anti-inflammatory effect of IL-10 mediated by metabolic reprogramming of macrophages. *Science* **356**, 513-519 (2017).

119. Salimian Rizi, B., Achreja, A. & Nagrath, D. Nitric Oxide: The Forgotten Child of Tumor Metabolism. *Trends in cancer* **3**, 659-672 (2017).

120. Everts, B. *et al.* Commitment to glycolysis sustains survival of NO-producing inflammatory dendritic cells. *Blood* **120**, 1422-1431 (2012).

121. Takada, K. *et al.* 18F-FDG uptake in PET/CT is a potential predictive biomarker of response to anti-PD-1 antibody therapy in non-small cell lung cancer. *Scientific reports* **9**, 13362 (2019).

122. Colegio, O.R. *et al.* Functional polarization of tumour-associated macrophages by tumour-derived lactic acid. *Nature* **513**, 559-563 (2014).

123. Vegran, F., Boidot, R., Michiels, C., Sonveaux, P. & Feron, O. Lactate influx through the endothelial cell monocarboxylate transporter MCT1 supports an NF-kappaB/IL-8 pathway that drives tumor angiogenesis. *Cancer Res* **71**, 2550-2560 (2011).

124. Apicella, M. *et al.* Increased Lactate Secretion by Cancer Cells Sustains Non-cell-autonomous Adaptive Resistance to MET and EGFR Targeted Therapies. *Cell metabolism* **28**, 848-865 e846 (2018).

125. Boneti, C. *et al.* Axillary Reverse Mapping: Mapping and Preserving Arm Lymphatics May Be Important in Preventing Lymphedema During Sentinel Lymph Node Biopsy. *Journal of the American College of Surgeons* **206**, 1038-1042 (2008).

CURRICULUM VITA

NAME: Samantha Megan Morrissey

ADDRESS: 1234 Texas Ave
Louisville, KY 40204

DOB: Evanston, IL October 12, 1990

EDUCATION
& TRAINING: B.A., Biology- University of Pennsylvania
2009-2013

AWARDS: 2019 Best Graduate Poster, Second Place, Research! Louisvile

2017 Best Graduate Poster Presentation, First Place
Southeastern Medical Scientist Symposia

PROFESSIONAL SOCIETY:

2020 Phi Kappa Phi Honor Society

PUBLICATIONS:

1. Chen, X., Morrissey, S., Chen, F. & Yan, J. Novel Insight Into the Molecular and Metabolic Mechanisms Orchestrating IL-17 Production in γδ T Cells. *Front Immunol* **10**, 2828 (2019).

2. Fleming, C. *et al.* Microbiota-activated CD103(+) DCs stemming from microbiota adaptation specifically drive γδT17 proliferation and activation. *Microbiome* **5**, 46 (2017).

3. Fleming, C., Morrissey, S., Cai, Y. & Yan, J. γδ T Cells: Unexpected Regulators of Cancer Development and Progression. *Trends in cancer* **3**, 561-570 (2017).

4. Lou, Y. *et al.* Critical roles of TIPE2 protein in murine experimental colitis. *Journal of immunology (Baltimore, Md. : 1950)* **193**, 1064-1070 (2014).

5. Morrissey, S.M. & Yan, J. Exosomal PD-L1: Roles in Tumor Progression and Immunotherapy. *Trends in cancer* **6**, 550-558 (2020).

6. Sun, H. *et al.* Exacerbated experimental colitis in TNFAIP8-deficient mice. *Journal of immunology (Baltimore, Md. : 1950)* **194**, 5736-5742 (2015).

7. Whaley, J.T. *et al.* Use of postexcision preirradiation mammography in patients with ductal carcinoma in situ of the breast treated with breast-conserving therapy. *Practical radiation oncology* **3**, e107-e112 (2013).

NATIONAL PRESENTATIONS:

2020 American Society of Clincians/ American Association of Physicians Travel Awardee

2019 Keystone Symposia Travel Awardee